This document has been approved for public release and sale; its distribution is unlimited.

DEPARTMENT OF THE AIR FORCE

AIR UNIVERSITY

AIR FORCE INSTITUTE OF TECHNOLOGY

Wright-Patterson Air Force Base, Ohio

AFIT/DS/ENP/94-01

THE EXCITATION MECHANISM OF PRASEODYMIUM-DOPED SEMICONDUCTORS

DISSERTATION

Paul L. Thee, Major, USAF

AFIT/DS/ENP/94-01

Approved for public release; distribution unlimited

AFIT/DS/ENP/94-01

THE EXCITATION MECHANISM OF PRASEODYMIUM-DOPED SEMICONDUCTORS

DISSERTATION

Presented to the Faculty of the Graduate School of Engineering

of the Air Force Institute of Technology

Air University

In Partial Fulfillment of the

Requirements for the Degree of

Doctor of Philosophy

Paul L. Thee, B.S., M.S.

Major, USAF

June 1994

AFIT/DS/ENP/94-01

THE EXCITATION MECHANISM OF PRASEODYMIUM-DOPED SEMICONDUCTORS

Paul L. Thee, B.S., M.S.
Major, USAF

Approved:

Yung Kee Yeo — 5/12/94
Yung Kee Yeo
Chairman, Advisory Committee

Robert L. Hengehold — 12 May 94
Robert L. Hengehold
Member, Advisory Committee

Mark E. Oxley — 12 May 94
Mark E. Oxley
Member, Advisory Committee

Donald C. Reynolds — 5/12/94
Donald C. Reynolds
Dean's Representative

Accepted:

Robert A. Calico, Jr.
Dean, Graduate School of Engineering

Preface

Blessed is the man who finds wisdom, the man who gains understanding, Wisdom is supreme; therefore get wisdom. Though it cost all you have, get understanding. How much better to get wisdom than gold, to choose understanding rather than silver!

The Bible (NIV), Prov. 3:13, 4:7, 16:16

"Don't try to win the Nobel Prize, Paul. Just do some good research...and be sure to get the Department Head on your committee."

Col. Jay Sherman, HQ AFTAC/CV, May 91

AFIT requires a great deal of sacrifice from its students, but no less from the families and I indeed thank my wife Sonji for her sacrifices this *second* time through AFIT. I am deeply grateful to Dr. Yung Kee Yeo for his tireless devotion to physics, scientific advice and motivation. Dr. Yeo always took time to help me whether it was a problem in my lab or advice on my career. I also greatly appreciate Dr. Robert Hengehold for his pragmatism and encouragement over my time here at AFIT. Greg Smith and Belinda Johnson were invaluable for without their technical assistance to keep my laboratory running I could not have done this. The consistent encouragement from my parents and their confidence also meant a great deal to me. Finally, I truly thank God for the strength to endure this program.

Paul L. Thee

Dedicated to my son Brandon

Table of Contents

List of Figures

List of Tables

List of Abbreviations

Å	Ångstrom (10^{-10} meters)
$Al_xGa_{1-x}As$	Aluminum Gallium Arsenide, x=Al mole fraction
BE	Bound Exciton
C	Carbon
°C	Celsius degrees
CB	Conduction Band
CL	Cathodoluminescence
DAP	Donor-Acceptor Pair
DLTS	Deep Level Transient Spectroscopy
EL	Electroluminescence
EPR	Electron Paramagnetic Resonance
Er	Erbium
ESR	Electron Spin Resonance
eV	Electron-volt
F	Fluorine
FB	Free-to-Bound
GaAs	Gallium Arsenide
GaP	Gallium Phosphide
InP	Indium Phosphide
K	Kelvin
LED	Light Emitting Diode
LPE	Liquid Phase Epitaxy
μ	Micron (10^{-6} meters)
MBE	Molecular Beam Epitaxy
meV	Millielectron-volt
MOCVD	Metalorganic Chemical Vapor Deposition
N	Nitrogen
Nd	Neodymium
nm	Nanometer (10^{-9} meters)
O	Oxygen
PC	Personal Computer
PL	Photoluminescence
PL(T)	Photoluminescence, Temperature-dependent
PLE	Photoluminescence Excitation (same as SEL)
Pr	Praseodymium
RBS	Rutherford Backscattering Spectroscopy
RE	Rare Earth(s)
SEL	Selective Excitation Luminescence
SEM	Scanning Electron Microscope
Si	Silicon
SIMS	Secondary Ion Mass Spectrometry
TDH	Temperature-dependent Hall Measurement
TEM	Transmission Electron Microscope
Tm	Thulium
VB	Valence Band
VPE	Vapor Phase Epitaxy
Yb	Ytterbium

Abstract

Rare earth (RE) elements in semiconductors are interesting because their main luminescence emissions are essentially temperature and host independent. Additionally, some of these emissions occur in technologically valuable regions of the infrared (IR) spectrum, but luminescence intensities obtained from RE-doped semiconductors have been very weak. This study on praseodymium (Pr) luminescence in $Al_xGa_{1-x}As$ was designed to enhance the understanding of the excitation mechanism.

Pr was implanted at 390 keV with doses from 5×10^{12} to $5\times10^{13}/cm^2$ into GaAs and $Al_xGa_{1-x}As$ ($x=0.15$ to 0.50) wafers which were annealed using the rapid thermal annealing (RTA) method. Low temperature photoluminescence (PL) was conducted using an Ar-ion laser and Ge detector. PL emissions of Pr from all hosts include peaks near 1.3 and 1.6 μm which are assigned to the intra-4f transitions of $^1G_4\rightarrow{}^3H_5$ and $^3F_3\rightarrow{}^3H_4$, respectively. For differing hosts the optimal RTA temperature varied from 725 to 775 °C and optimal ion dose varied between $10^{13}/cm^2$ and $5\times10^{13}/cm^2$.

The intensity of PL emissions depends strongly on the Al mole fraction. For GaAs, the 1.3 μm emissions are strongest, whereas for all AlGaAs, the 1.6 μm emissions are by far the strongest. Selective excitation luminescence (SEL) experiments revealed that, in general, the Pr-related PL intensity is quenched when the excitation laser energy is decreased below the value of the host free exciton energy. Temperature dependent PL studies revealed activation energies of Pr-related traps. Coimplantation of Pr with Er or lighter elements including B, C, N, O, and F all proved to quench the Pr luminescence.

An excitation model proposes that Pr luminescence can occur when the Pr can successfully trap free carriers and form bound excitons. When the bound exciton recombination energy is well-matched to the 4f energy levels either in combination or singly with Auger process assistance, strong Pr emissions can occur.

THE EXCITATION MECHANISM OF PRASEODYMIUM-DOPED SEMICONDUCTORS

I. Introduction

For over a decade, researchers have pursued the goal of efficiently producing light from semiconductors doped with rare earth (RE) elements. Motivated by the possibility of fabricating RE-based LEDs and lasers operating at technologically valuable wavelengths, they have explored the luminescent properties of REs and proposed excitation models to explain the results. However, the goal of a practical RE-based LED still eludes completion. Therefore, this research continues and expands the understanding of RE behavior in semiconductors.

Motivation

REs represent a potentially valuable technology, because their emissions are very insensitive to the host type and temperature, and many of these emissions occur near the important wavelengths of minimum attenuation and dispersion in silica-based fiber optics. Semiconductors are the choice as host material since, as injection mode diodes, they can electrically pump RE luminescence.

Researchers have worked primarily on the REs erbium (Er), ytterbium (Yb), and neodymium (Nd), but praseodymium (Pr) has received comparatively little attention even though it has shown promising luminescent characteristics. This experimental investigation is thus centered around increasing the understanding of the excitation mechanism of praseodymium in semiconductors.

A primary technological motivation for the effort proposed in this work is that some infrared emissions from REs coincide with absorption minima for silica-based fiber optics. In a 1979 paper, Miya and others described the transmission loss in silica-based optical fibers (Miya *et al.*, 1979:106). The minimum transmission loss is attained at wavelengths near 1.55 microns while other lesser minimums occur at 1.2 and 1.3 microns. In addition, the minimum dispersion in silica-based fibers is at 1.3 microns (Pomrenke *et al.*, 1991b:415). The interest in certain RE elements is derived from these optical fiber characteristics. Erbium has been shown to emit at about 1.54 microns in several semiconductors (Pomrenke *et al.*, 1989:339; Ennen *et al.*, 1983:943; Pomrenke *et al.*, 1991b:415), while neodymium has an emission line at 1.1 microns in GaP and GaAs (Muller *et al.*, 1986:2210). Praseodymium has 1.1, 1.3, and 1.6 micron emission lines in GaAs and 1.3 micron lines in InP (Pomrenke *et al.*, 1991a:159). Thus efficient electro-optical RE-based luminescent devices operating at these wavelengths would be ideally suited for systems using fiber optics.

The use of RE-doped semiconductors can then open up many opportunities for new optoelectronic device applications. Light-emitting diodes (LEDs) and lasers based on REs as the active media could be integrated directly onto electronic chips as near-perfect optical fiber communications emitter sources. Optical fibers could then serve as connections between these thermally robust devices. Light-emitting diodes operating at these wavelengths have been fabricated for several semiconductor/rare earth combinations and growth methods, however the reported efficiencies are far below that required for device applications (Dmitriev *et al.*, 1983:1201; Roland *et al.*, 1988:956; Klein *et al.*, 1990:1299; Whitney *et al.*, 1988a:740).

The application of this basic research is directed toward the long range development of device technology for various optoelectronic and photonic devices in AF avionics and other electronics. The temperature independence of RE emissions is

important in devices subject to thermal cycling or higher temperature environments, while the narrow linewidth afforded by RE luminescence allows high bandwidth modulation. These effects demonstrate the desirability of narrow RE emission lines in AF electronics and communications.

Problem Statement

An important task on the way to efficient RE-doped semiconductor devices is the optimization of the luminescent efficiency. In order to optimize luminescent efficiency in these materials, a correct understanding of the mechanisms by which the energy is transferred from the lattice material to the rare earth impurities is needed. In order to understand this excitation mechanism, basic research into the energy dynamics of the rare earth luminescence in semiconductors is required. This effort consists of basic research into the nature of the rare earth element praseodymium in semiconductors. The ultimate goal is to understand the excitation mechanism sufficiently well to selectively and significantly enhance the luminescent efficiency.

Approach

The main objective for this research was to expand the number of RE elements explored in-depth. All efforts were pointed toward a better understanding of the RE excitation mechanisms. Specifically, praseodymium was investigated in a manner closely paralleling earlier erbium research. This parallel research allowed direct comparison of results and excitation theories which will hopefully benefit both RE research paths. Comparisons revealed common characteristics which may provide a framework for further research.

In order to examine Pr, experimental data was gathered from Pr implanted into several different types of semiconductor hosts. Much information was gleaned by comparing and contrasting the behavior of Pr in these different host lattices.

Praseodymium was incorporated into 3 main host semiconductor materials including gallium arsenide (GaAs), several variants of aluminum gallium arsenide (AlGaAs), and silicon (Si). The Pr luminescence characteristics were studied based on anneal temperature, Pr implant dose, host type, host carrier type, sample temperature, and excitation energy. These results were analyzed, compared to previous work in REs, and used to formulate a consistent excitation mechanism for Pr.

Outline

This dissertation is organized into several parts which sequentially present a review of the background and previous work on rare earths and the results and conclusions of this effort. First, the background of solid state physics related to this work is reviewed in chapter II. Chapter III summarizes the previous work done on the rare earths Er and Pr in semiconductors. The methods for growth, preparation, and characterization of the samples are discussed in chapters IV and V. The results of this present effort are documented in chapter VI, while the conclusions and recommendations are detailed in the final chapter.

II. BACKGROUND

The important properties of semiconductors are not entirely based in their native characteristics, but on the dramatic effects brought on by impurities in the semiconductor lattices. It is important then to briefly outline the nature of these impurity effects.

Semiconductor Energy Bands and Impurities

The electronic structure of a perfect, pure crystalline solid consists of allowed energy bands (a group of nearly continuous energy levels) separated by forbidden energy gaps. The distribution of electrons in these bands is described by the Fermi-Dirac distribution and the density of allowed states function (Pankove, 1971:6-7). The valence band (VB) and conduction band (CB) play the critical role in determining the characteristics of semiconductors. Separating the VB and CB from each other is the fundamental energy gap or bandgap. In an idealized semiconductor at temperatures very near 0 K, electrons completely fill all VB states while the CB is empty allowing no conduction of electrons in the crystal.

In Figure 1, energy band diagrams for an insulator, a semiconductor, and a metal are compared. In this figure, the atomic-like core bands are shown, E_g is the bandgap, and ε_f is the Fermi Energy level. Semiconductors have a bandgap small enough for some VB electrons to jump to the CB with reasonable thermal energy while insulator bandgaps are so large as to pose an effective barrier between the bands. In a metal, conduction of electrons takes place in the partially filled CB.

In a perfect semiconductor crystal, defects in the lattice or the introduction of impurities (atoms different from the host) break the perfect lattice periodicity and introduce localized states which decay quickly with distance outside a limited set of neighboring lattice atoms. These localized impurity states manifest themselves as

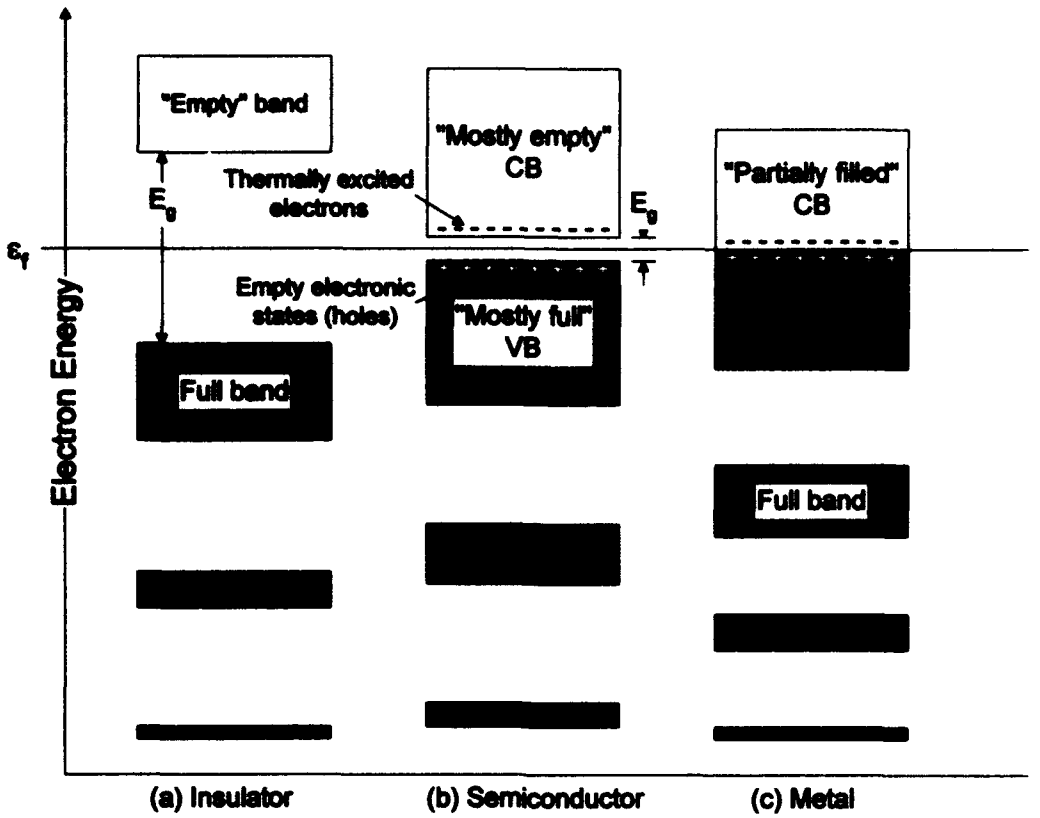

Figure 1. Energy Band Diagrams for an (a) Insulator, (b) Semiconductor, and (c) Metal (after McKelvey, 1984:246)

allowed energy states within the 'forbidden' energy gap, intermediate between the CB and VB of the host crystal. These energy states profoundly affect the electrical and optical characteristics of the semiconductor.

Single impurities themselves may be classified according to their physical position in the lattice. A substitutional impurity atom replaces a host atom at its original site while an interstitial impurity atom is situated between the sites of the host lattice possibly disrupting the native atom bondings and local crystal structure. The substitutional impurities can be further classified by their electron configuration relative to the replaced host atom. Impurity atoms from the same column of the periodic table as the host atoms are isovalent or isoelectronic impurities (having the same number of

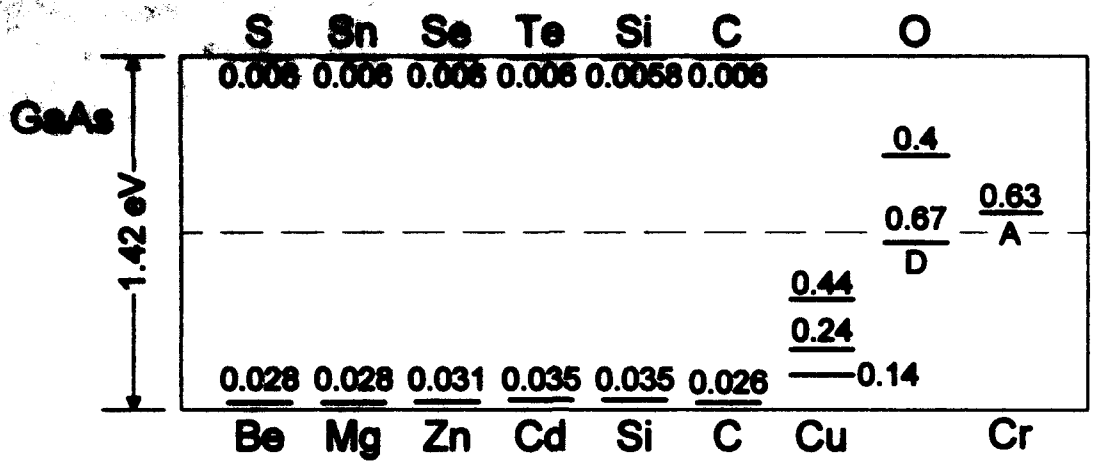

Figure 2. Donor and Acceptor Energy Levels in GaAs (after Sze, 1985:23)

valence electrons as the replaced host atom). Non-isovalent impurity atoms have more or less valence electrons than required to fulfill local bonding requirements. If the substitutional impurity has more electrons than necessary for bonding, it is called a donor since ionized electrons are donated to the CB. Fewer electrons than required by bonding makes an impurity an acceptor, that is, it can accept electrons from the VB. Impurities which radiate light are typically referred to as radiative centers.

The energy levels of substitutional impurities in the lattice are defined by their ionization energies compared to the band-edge. The conventional positions of these donor and acceptor levels for various impurities in GaAs are shown in Figure 2. If the neutral impurity is a donor, it is ionized by releasing its loosely bound electron to the conduction band. Similarly, the acceptor ionization corresponds to the emission of a hole to the VB (or, equivalently, the capture of a VB electron by the impurity) forming a negative ion state. In both cases, the ionization energy defines the energy level of the substitutional donor or acceptor in the energy gap of the host lattice. Donor energy levels are placed below the CB by the amount of their ionization energy, while acceptor levels are above the VB by their ionization energy.

Radiative and Non-Radiative Transitions

The transitions of electrons between allowed energy states in the lattice may be radiative (producing a photon) or non-radiative (releasing the energy in some form other than light). Radiative transitions can take place via a variety of paths, typically across the energy gap or to impurity states within the energy gap. These transitions may be CB to VB, CB to acceptor, or just about any shift of an electron between energy levels in the lattice. Several texts extensively document the many possible emissive transitions and the associated energies (Boer, 1990:1008-1038; Pankove, 1971:107-155).

Excitons deserve special mention because they represent a particularly important process, especially with respect to RE luminescence. When a lattice absorbs energy sufficient to push electrons from the VB to the CB, free CB electrons and their associated VB holes are created. Excitons consist of an electron and a hole paired off by coulomb interaction in which the electron and hole orbit around their center of mass. Free excitons can wander through the crystal until captured, dissociated, or recombined. When excitons are captured by impurities (becoming bound excitons), they can recombine to preferentially pump energy into lattice impurities. This is a main mechanism theorized for rare earth excitation in semiconductors.

An electron can drop to an available hole state by other than radiative means. These non-radiative processes can sometimes dominate radiative processes making them of critical interest to semiconductor luminescence studies. Major non-radiative processes include Auger processes, transitions through localized states, and multi-phonon processes.

In the Auger effect, the energy from the electron-hole recombination can be absorbed by a different electron and then dissipated through phonon emission. A great

variety of Auger processes are possible, and the previously mentioned radiative transitions may couple to phonons through a secondary electron temporarily elevated in energy in its band (Pankove, 1971:161).

Non-radiative recombination may also occur through localized defects which produce a local continuum of states between the bands. These localized defects may include physical defects in the crystal such as pores, edge boundaries, and dislocations. When an electron moves into this defect it looses its energy via this continuum of states.

Traps represent another important transition effect. Traps are impurity-related metastable states (typically non-radiative deep levels) which can capture an electron or hole from a higher-energy state and retain it for a considerable time at the end of which the electron or hole is released back to the higher-energy state (Pankove, 1971:370). The electron can then make a transition to a lower-energy state via a radiative or non-radiative process. Thus traps in semiconductors can result in delayed luminescence and afterglow luminescence by holding potentially luminescent electrons in state for a time.

The energy transfer and excitation mechanisms of outer or valence electrons of atoms in semiconductors are thus relatively well understood. The process which allows energy to transfer to inner, well-shielded rare earth electron states and facilitates optical transitions of interest in RE atoms is far from being well understood.

The Crystal Field

The symmetry of the location in which a RE resides in the host lattice dictates the splitting of the energy levels and thus the number of luminescent transitions. The energy level terms for the RE refer to the free ion energy levels. These free ion energy levels have a $2J+1$ degeneracy associated with the symmetry of isotropic 3-dimensional space. When this free ion is placed in a host lattice, the symmetry is reduced and the

TABLE 1

Energy Level Term Splittings for Integral J
(after DiBartolo, 1968:203)

	Atomic Energy Level J Value								
Host Symmetry	0	1	2	3	4	5	6	7	8
Cubic	1	1	2	3	4	4	6	6	7
Hexagonal	1	2	3	5	6	7	9	10	11
Tetragonal	1	2	4	5	7	8	10	11	13
Lower Symmetry	1	3	5	7	9	11	13	15	17

native crystal field will lift some or all of this degeneracy thereby splitting these free ion energy levels. The number of split levels may be predicted using group theoretical methods based on the host crystal lattice symmetry and the symmetry of free space.

The splitting of these energy levels may be observed directly in PL spectra as multiple, relatively closely spaced, groups of emission lines corresponding to transitions between the crystal field split ion energy terms. A very complete tabulation of the number of perturbed energy levels arising from J value decompositions in different symmetry groups has been completed by Prather (Prather, 1961:Table 9,38-45). A summary of energy term splits for integral J's is given in Table 1. As an example, the ground state of trivalent praseodymium is $^3H_4$ (J=4) and another termination state for an important transition is $^3H_5$ (J=5). In a crystal with cubic symmetry such as GaAs in which the Pr ion occupies a lattice site, each of these is split into 4 energy levels. For cases in which only the lowest upper level state is occupied, only 4 transitions would occur to the states of these levels.

In general, lower symmetry always implies the same or increased numbers of levels allowing larger numbers of transitions. It is also important to note that this method gives no information about the energy level spacings of these crystal field split levels, only the number of levels arising is given by group theory.

Rare Earth Elements

As previously mentioned, rare earths in semiconductors are technologically important due to the insensitivity of 4f electron transitions to temperature and host semiconductor type. All rare earths share a closed set of inner electron shells through $4d^{10}$ (equivalent to Palladium or Pd) which do not participate in the transitions of interest. In the neutral atomic state, rare earths have an electronic configuration of

$$[Pd]4f^n5s^25p^66s^2. \quad (1)$$

Cerium, gadolinium, and lutetium also have a single $5d^1$ electron in this electron configuration. Note that the $5s^2$ and $5p^6$ shells are filled and are part of the xenon-like electronic basis of REs (Table 2). Table 2 also lists the spectroscopy term symbols for the ground state configurations in the standard form $^{2S+1}L_J$ in which S is the atomic spin, L is the rotational angular momentum, and J is the total angular momentum. All rare earths share a main valence state of 3 (the number of easily removed electrons). These trivalent (triply ionized) RE ions have an electron configuration of

$$[Pd]4f^{n-1}5s^25p^6. \quad (2)$$

in which the $6s^2$ shell and one 4f electron participate in the bonding. As before, the minor exceptions are cerium, gadolinium, and lutetium with trivalent form of $4f^n5s^25p^6$, where the $5d^1$ electron is lost instead of the $4f^n$.

In the crystal lattice, the unfilled inner 4f electron shell of trivalent RE elements is screened by the outer $5s^2$ and $5p^6$ shells. This screening allows only very small lattice field-induced changes to the 4f shell energy levels. Since the 4f electron shell is partially empty, intra-4f shell transitions to higher unoccupied 4f states may take place. The wavelengths of interest emanate from these intra-4f shell optical transitions. The

TABLE 2

The Rare Earth Elements

Atomic Number	Element	Symbol	Electron Configuration	Triply Ionized Configuration	Trivalent Ground State Term
58	Cerium	Ce	$[Xe]4f^{1}5d^{1}6s^{2}$	$[Xe]4f^{1}$	$^{2}F_{5/2}$
59	Praseodymium	Pr	$[Xe]4f^{3}6s^{2}$	$[Xe]4f^{2}$	$^{3}H_{4}$
60	Neodymium	Nd	$[Xe]4f^{4}6s^{2}$	$[Xe]4f^{3}$	$^{4}I_{9/2}$
61	Promethium	Pm	$[Xe]4f^{5}6s^{2}$	$[Xe]4f^{4}$	$^{5}I_{4}$
62	Samarium	Sm	$[Xe]4f^{6}6s^{2}$	$[Xe]4f^{5}$	$^{6}H_{5/2}$
63	Europium	Eu	$[Xe]4f^{7}6s^{2}$	$[Xe]4f^{6}$	$^{7}F_{0}$
64	Gadolinium	Gd	$[Xe]4f^{7}5d^{1}6s^{2}$	$[Xe]4f^{7}$	$^{8}S_{7/2}$
65	Terbium	Tb	$[Xe]4f^{9}6s^{2}$	$[Xe]4f^{8}$	$^{7}F_{6}$
66	Dysprosium	Dy	$[Xe]4f^{10}6s^{2}$	$[Xe]4f^{9}$	$^{6}H_{15/2}$
67	Holmium	Ho	$[Xe]4f^{11}6s^{2}$	$[Xe]4f^{10}$	$^{5}I_{8}$
68	Erbium	Er	$[Xe]4f^{12}6s^{2}$	$[Xe]4f^{11}$	$^{4}I_{15/2}$
69	Thulium	Tm	$[Xe]4f^{13}6s^{2}$	$[Xe]4f^{12}$	$^{3}H_{6}$
70	Ytterbium	Yb	$[Xe]4f^{14}6s^{2}$	$[Xe]4f^{13}$	$^{2}F_{7/2}$
71	Lutetium	Lu	$[Xe]4f^{14}5d^{1}6s^{2}$	$[Xe]4f^{14}$	^{1}S

Note: $[Xe] = 1s^{2}2s^{2}p^{6}3s^{2}p^{6}d^{10}4s^{2}p^{6}d^{10}5s^{2}p^{6}$

outer shell screening directly results in the very sharp host matrix-independent and temperature-independent optical transitions between 4f energy levels. It is this property of the invariance of inner triply-ionized 4f emission wavelengths which may be utilized for obtaining light emitting (and lasing) devices from REs introduced into the semiconductor material.

The energy levels of trivalent RE ions have been calculated and presented in books by Dieke (Dieke, 1968:142) and more recently by Reisfeld and Jorgensen (Reisfeld and Jorgensen, 1977:93). The energy levels for praseodymium are shown in Table 3. Usually, only very small differences in RE emission wavelengths are seen between differing hosts.

TABLE 3

Praseodymium Energy Levels (after Dieke, 68:196)

Energy Level Term Symbol	Free Ion Energy above Ground State (eV)
$^1D_2$	2.062
$^1G_4$	1.207
$^3F_4$	0.831
$^3F_3$	0.779
$^3F_2$	0.610
$^3H_6$	0.525
$^3H_5$	0.265
$^3H_4$	0

The presence of REs in substitutional sites in the host lattice introduces strain as a defect into the lattice. This is due to the different size of the REs compared with the host atoms they replace. Table 4 lists the radii of ions of RE and semiconductor constituents of interest in this study. Being trivalent, the REs typically substitute for the group III elements in semiconductors (Ga & Al). Pr^{3+} is significantly larger than either the Ga^{3+} or the Al^{3+} atom it replaces, while Er^{3+} is only slightly larger than Ga^{3+}. It is these deviations from a perfect lattice which destroy the spatial T_d symmetry of GaAs and AlGaAs at least in the local lattice area of the Pr ion.

The relation between the bandgap of the host semiconductor and the energy levels of the rare earth dopant is also critical importance. Figure 3 shows the Pr^{3+} energy levels and transitions of interest in comparison with the host bandgaps used in this study. Most transitions of interest are smaller than the bandgap in all hosts except for Si and the increased complexity of the Pr energy spectrum below 2 eV is shown.

TABLE 4

Crystal Ionic Radii (Weast, 1984:F-165)

Ion	Radius (Å)
Al^{3+}	0.51
As^{3-}	2.22
Ge^{3+}	0.81
$Si^{4+,4-}$	0.42, 2.71
Pr^{3+}	1.013
Er^{3+}	0.881

Erbium energy levels are also shown for comparison. This large number of energy levels has the potential for a very diverse emission spectrum limited only by transition rules. For example, the Pr^{3+} $^3F_3 \rightarrow {}^3H_4$ transition is spin forbidden in a free ion state, but perturbations introduced by the crystal field can facilitate this transition.

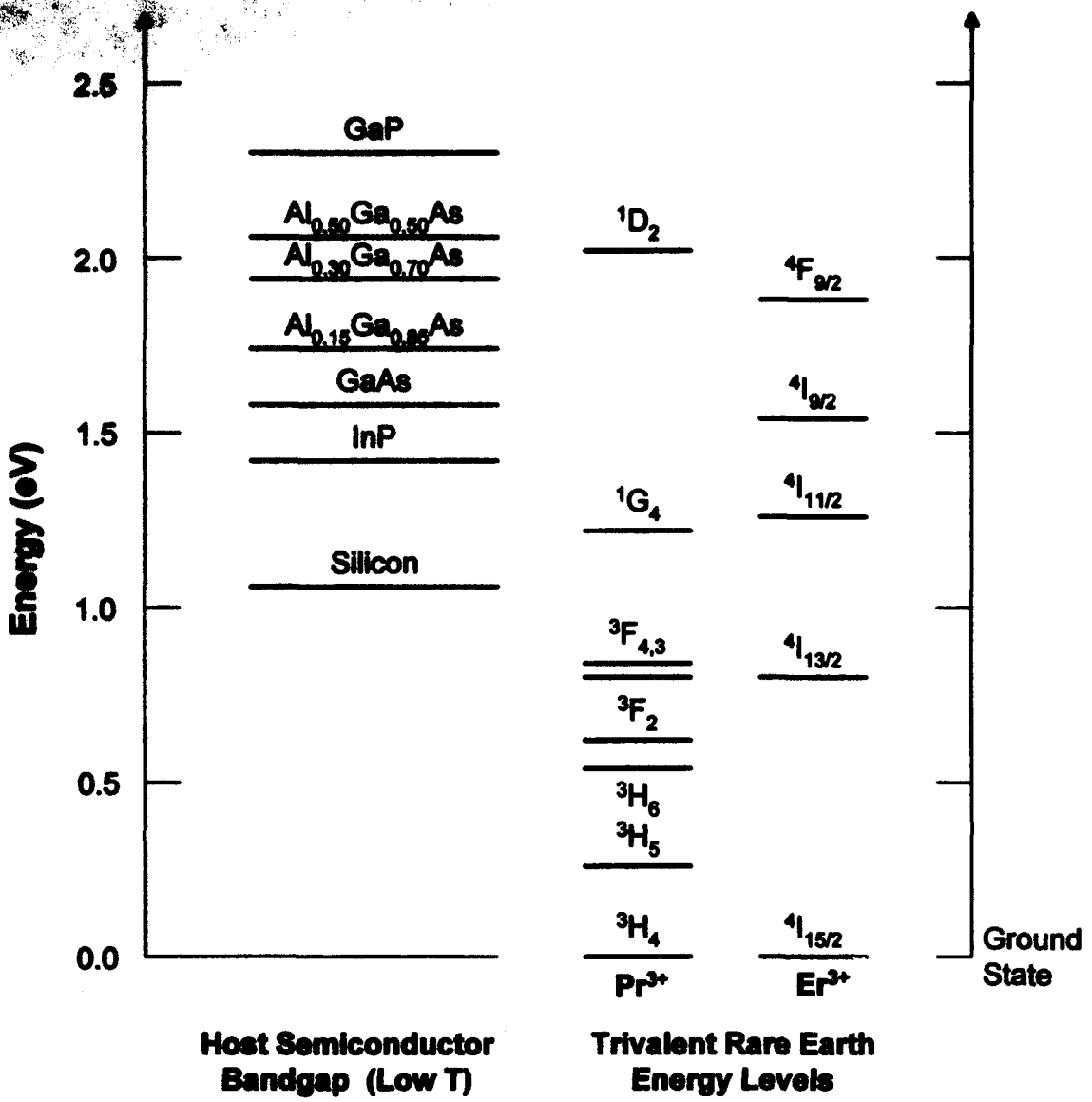

Figure 3. Host Bandgap, Trivalent Pr, and Trivalent Er Energy Levels

III. PREVIOUS WORK

Much work has been done on rare earth elements in semiconductors, primarily over the last decade. Although the vast majority of research has concentrated on Yb and Er, limited research has also been done on Nd, Pr, and a few others. A review of past work on the rare earths erbium and praseodymium and bandgap engineering is presented in this chapter.

Erbium

Erbium (Er) has been studied nearly as extensively as Yb. A summary of some important papers dealing with erbium is given in Table 5. Its importance lies in the internal transition $^4I_{13/2}$ to $^4I_{15/2}$ of Er^{3+} ($4f^{11}$) producing sharp emissions near 1.54 microns. This luminescence was first reported by Ushakov *et al.* in 1982 for GaP:Er and GaAs:Er (Ushakov *et al.*, 1982:723). In both cases a weak luminescence of the Er impurity was observed in the form of a small maximum whose profile indicated that it probably represented an envelope of a group of closely spaced unresolved lines.

The first observation of the fine structure of sharp-line intra-4f luminescence spectra of Er in semiconductors was reported by Ennen *et al.* in 1983 for Er implanted in GaP, GaAs, InP, and Si (Ennen *et al.*, 1983:943). Pomrenke, Ennen, and Haydl's 1986 paper showed that the PL of erbium in GaAs, InP, and GaP was critically dependent on post-implantation annealing temperature and times (Pomrenke *et al.*, 1986:601). An example of their annealing study on GaAs:Er is given in Figure 4. Their data showed that the variation in host semiconductor and treatment allowed identification of numerous lines in all the semiconductors suggesting the existence of several different erbium-related centers. Pomrenke, Yeo, and Hengehold later showed that the luminescence signal was also strong from the ternary material $Al_{0.4}Ga_{0.6}As$:Er; specifically, stronger than that from GaAs:Er (Pomrenke *et al.*, 1991b:415).

TABLE 5

Significant Papers on Erbium in Semiconductors

Citation	Host	RE Doping	Data	Results
Ushakov, 1982	GaAs, GaP	Implant	PL	1.54 μm PL
Ennen, 1983	GaAs, Si, GaP, InP	Implant	PL	Er sharp line luminescence observed
Ennen, 1985	Si	MBE	EL	Si:Er LED demonstrated, low efficiency
Pomrenke, 1986	GaAs, GaP, InP	Implant	PL	Optimized annealing for PL, Dif. centers
Uwai, 1987	GaAs, InP	MOCVD	PL	First MOCVD PL from Er
Bantien, 1987	GaAs	LPE	PL, Hall	LPE GaAs:Er luminescence requires annealing
Smith, 1987	GaAs	MBE	PL, Hall	Best growth temperature and concentration
Ennen, 1987	GaAs	MBE	SEL	1.54 μm PL from one Er^{3+} center type in less than cubic symmetry
Zhao, 1988	GaAs, InP	Diffusion	PL	First Er Diffusion PL
Whitney, 1988a	GaAs	MOCVD	EL	MOCVD GaAs:Er LED up to room temperature
Roland, 1988	GaAs	MBE	EL	MBE GaAs:Er LED at 77 & 300 K
Klein, 1988	Si, GaAs, InP, GaP	Various	PL	1 msec luminescent lifetime in all hosts
Nakagome, 1988	GaAs	MOCVD	PL	Narrow, high intensity line when V/III = 3
Solomon, 1989	InP	Implant	PL, SIMS	InP:Er PL & SIMS study
Favennec, 1989	GaAs, GaInAs, GaInAsP, GaAlAs	Implant	PL, SEM	1.54 μm emission not uniformly dispersed, Er-rich microparticles
Pomrenke, 1990	GaAs, InP	Implant	PL	Free carriers needed to excite Er centers
Klein, 1990	GaAs	Implant	EL	Implant GaAs:Er EL
Favennec, 1990	Si	Implant	PL	Oxygen activation of Er luminescence
Ishiki, 1991	InP	Implant	EL	1.54 μm EL from impact excitation
Michel, 1991	Si	Implant	PL	Effects of Si:Er coimplants on PL
Benton, 1991	Si	Implant	DLTS..	Er-related defect levels in Si
Kozanecki, 1991	GaAs	Implant	RBS	Er location displaced toward <110>
Klein, 1991	GaAs	Implant	EPR, PL	Most of Er is in Er^{2+} state
Benyattou, 1991	AlGaAs	MBE	PL	Auger losses during PL excitation
Poole, 1992	GaAs	MBE	TEM	Above $7\times10^{17}/cm^3$ ErAs microparticles form
Klein, 1992	GaAs	Implant	PL	Er^{3+} as nonequilibrium state
Colon, 1992	GaAs	Implant	PL,SEL, DLTS	Er implantation produces 2 hole traps involved in excitation of 4f luminescence
Elsaesser, 1993	GaAs	Implant, MBE	DLTS, Hall	Er-related hole traps identified

An increase in the PL of Czochralski-grown Si crystals doped with erbium and oxygen was presented in a paper by Favennec (Favennec *et al.*, 1990:L524). They found that oxygen implantation enhanced the Er PL emission by an order of magnitude. Their PL data showed that this Er luminescence was correlated with the oxygen density in the sample suggesting the formation of Er-O radiative complexes. Coimplantation of

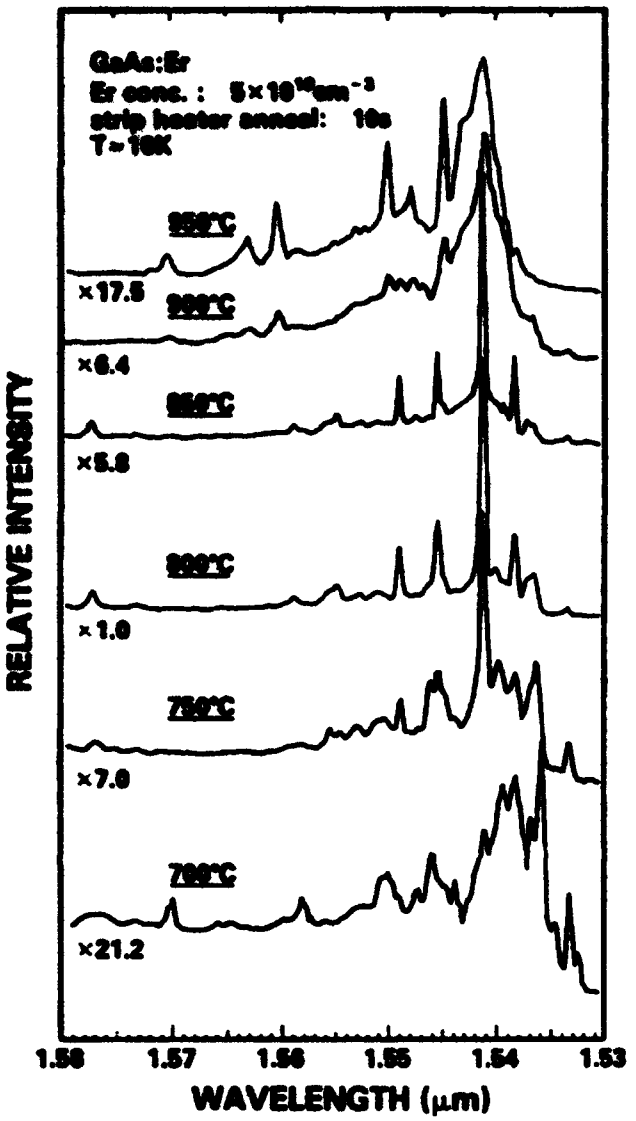

Figure 4. PL Dependence of GaAs:Er on Anneal-Temperature (Pomrenke *et al.*, 1986:604)

impurities in Er-implanted Si was also studied by Michel *et al.* (Michel *et al.*, 1991:2672). This team found that implantation of erbium followed by an additional implant yielded species-dependent changes in the PL intensity. The presence of light elements such as O, C, N, and F enhanced the Er luminescence, while heavier elements like Al, S, Cl, and P have little effect on the luminescence.

Characteristic Er-associated optical transitions have also been observed for Er incorporated in MOCVD-grown GaAs and InP (Uwai *et al.*, 1987:87), LPE-grown GaAs (Bantien *et al.*, 1987:2803), and GaAs and InP by diffusion (Zhao *et al.*, 1988:277). Nakagome *et al.* have observed a drastic change in the 1.5 micron Er-related PL spectra for MOCVD-grown GaAs:Er when growth temperature is reduced to 550 °C and the V/III ratio is increased to 3 (Nakagome *et al.*, 1988:1726). Under these conditions, an optically efficient Er-emitting center with an extremely narrow linewidth (less than 0.03 nm) and high peak intensity is preferentially photoexcited.

Electroluminescence has also been demonstrated from semiconductors doped with erbium by several methods. Ennen *et al.* reported an MBE-grown Si:Er LED (Ennen *et al.*, 1985:381). The efficiency of about 5×10^{-4} was far too low for device application. A GaAs:Er MOCVD-grown LED was demonstrated by Whitney *et al.* in 1988 (Whitney *et al.*, 1988a:740), an LPE-grown version was reported by Roland *et al.* in the same year (Roland *et al.*, 1988:956), and electroluminescence at 1.54 microns was obtained from Er-implanted GaAs by Klein, Moore, and Dietrich in 1990 (Klein *et al.*, 1990:1299). In addition, Isshiki *et al.* observed EL at 1.54 microns from direct electron impact excitation of InP:Er (Isshiki *et al.*, 1991:L225). This group found a fairly strong EL signal at room temperature which decreased to about half the intensity observed at 77K.

Parallel investigations concentrated on determining the exact nature of Er in semiconductors and the energy transfer mechanism for excitation of the 4f levels. In 1987, Ennen *et al.* found that only one type of Er^{3+} center was responsible for the 1.54 micron band in MBE-grown GaAs (Ennen *et al.*, 1987:4877). Their study showed erbium-doped MBE-grown GaAs layers formed a number of erbium complexes depending on the growth temperature. For the previously reported optimum substrate growth temperature of 580 °C (Smith *et al.*, 1987:49), only one type of luminescent

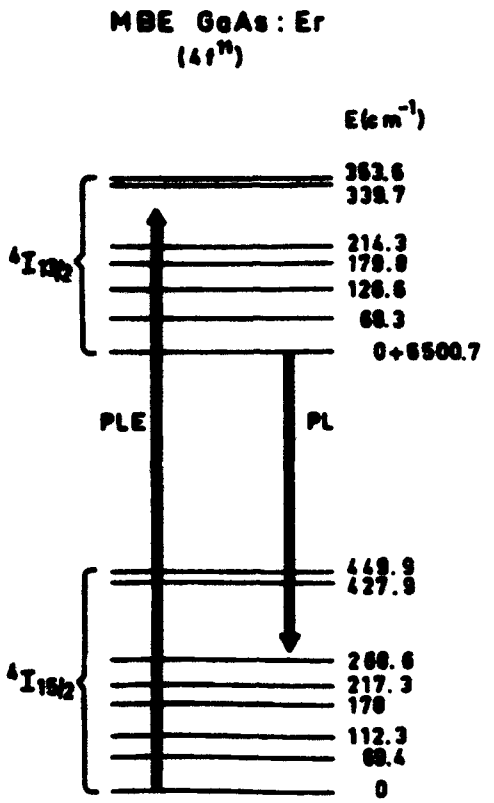

Figure 5. Energy Level Scheme of the Non-Cubic Er Complex in MBE-grown GaAs (Ennen *et al.*, 1987:4879)

erbium center was observed with 8 emission lines recorded from 6 K PL. The multiplicity of zero-phonon lines indicated that this Er^{3+} center occupies a position of lower than cubic symmetry. From these data, the researchers constructed an energy level scheme for the non-cubic Er^{3+} complex in MBE-grown GaAs (Figure 5). Kozanecki *et al.* further refined this by reporting that erbium-implanted GaAs was displaced from the substitutional position to the <110> channel (Kozanecki *et al.*, 1991:763). In agreement with Pomrenke *et al.* (Pomrenke *et al.*, 1986:601), they also found that the optical activity of erbium disappeared as higher annealing temperatures moved the erbium toward a substitutional location.

Klein and Pomrenke reported on the lifetime of the Er^{3+} excited state in a variety of materials in a 1988 article (Klein *et al.*, 1988:1503). Their study showed the

lifetime of the $^4I_{13/2}$ excited state of Er^{3+} is about 1 millisecond for all the hosts including MBE-grown and implanted Si:Er, MBE-grown and implanted GaAs:Er, MOCVD-grown and implanted InP:Er, and implanted GaP:Er. This constancy of the lifetime across several hosts strongly suggests that Er decay is largely radiative, that is, there appear to be no strongly competing non-radiative decay mechanisms to reduce this lifetime. They also report that these PL decay times are about 100 times longer than those from comparable InP:Yb samples. Thus Er-doped materials appear to offer more potential in device applications than their Yb counterparts. Benyattou *et al.* reported nearly the same lifetime of 1.2 milliseconds for Er in $Ga_{0.55}Al_{0.45}As$ (Benyattou *et al.*, 1991:2132).

Similar to observations in InP:Yb (Korber and Hangleiter, 1988:114), Pomrenke, Hengehold, and Yeo established that free carriers are required to excite the rare earth centers for GaAs:Er and InP:Er along with InP:Yb, GaAs:Yb, GaAs:Tm, and GaAs:Pr (Pomrenke *et al.*, 1989:339). These free carriers may be manifest in excitation via direct capture of excitons or hot carrier impact excitation. In conclusion, these workers propose GaAs:Er as the best candidate for devices.

> With Er centers in GaAs being excited over the widest range of states, combined with the observed room temperature luminescence, long lifetimes, and the technological importance of the 1.54 microns wavelength, allows one to conclude that the GaAs:Er system shows the greatest promise for electro-optic applications. (Pomrenke *et al.*, 1989:344)

Favennec *et al.* reported in 1989 that the 1.54 micron Er-related emissions are not uniformly spaced over the surface of a sample (Favennec *et al.*, 1989:333). These results were obtained from CL-SEM experiments in Er-implanted GaAs, GaInAs, GaInAsP, and GaAlAs and imply that optically active erbium atoms could be clustered

in the implanted layer as microparticles of Er-rich compounds. Poole, Singer, and Peaker confirmed this in MBE-grown GaAs:Er in which Er concentrations greater than $7\times10^{17}/cm^3$ form ErAs microparticles (Poole *et al.*, 1992:121).

A significant paper by Klein, Moore, and Dietrich in 1991 reported that Er^{2+} was a major player in erbium luminescence (Klein *et al.*, 1991:502). They measured the dependence upon anneal temperature of the band-edge and Er^{3+} PL and EPR in Er-implanted GaAs and concluded that:

> (1) The Er^{3+} PL spectrum consists of a superposition of spectra from several distinct erbium sites,
> (2) almost all the erbium in the sample was in the Er^{2+} state, and
> (3) the important Er^{3+} PL is excited from Er^{2+} occupied centers.

They also proposed that these Er^{2+} sites involve complexes of interstitial Er with defects or impurities and the small number of Er^{3+} centers (<0.1% of erbium in the sample) occupy tetrahedral interstitial sites. In a 1992 paper, these researchers proposed that Er^{3+} might, in fact, be a non-equilibrium state for above gap excitation (Klein *et al.*, 1992:665).

Benyattou and workers in France suggested a model for the erbium PL excitation process in MBE-grown AlGaAs:Er (Benyattou *et al.*, 1991:2132). Two beam time-resolved PL measurements showed that there are significant losses related to free carriers occurring in the PL excitation process. Their model proposed that bound excitons recombine and transfer energy to the Er via an Auger recombination process or direct energy transfer to the erbium ion.

Colon *et al.* proposed the first excitation mechanism for GaAs:Er in 1992 (Colon *et al.*, 1992:671). Using DLTS measurements, this group found that erbium implantation introduces hole traps at 35 meV and 360 meV above the valence band, while selective excitation showed that the 4f emissions can be strongly excited with

photon energies less that the bandgap. Colon proposed that the Er-related hole traps explain the above- and below-bandgap excitation energy and participate in the excitation process. Two different excitation mechanisms were put forth, depending on the excitation energy:

1. *Excitation energy greater than bandgap* creates electron-hole pairs with free holes trapped in the Er-related hole traps. This trap then captures a free electron forming a bound exciton. Subsequent recombination of this pair transfers energy to the 4f shell via an Auger process.

2. *Excitation energy less than bandgap* provides sufficient energy to excite electrons at the traps into the CB leaving a hole behind. An electron recombines with this bound hole contributing the recombination energy to the 4f shell.

Summarizing erbium's potential importance, Taniguchi's statement in a 1991 paper is telling.

> The characteristic sharp-line 4f luminescence has been observed from various RE and III-V compounds. However, it was found that the RE-related luminescence intensity drops drastically as the sample temperature increases, and that only GaAs:Er and InP:Er can still emit luminescence up to room temperature. (Taniguchi *et al.*, 1991:2930)

(Note: Some MOCVD-grown GaP:Nd samples exhibited room temperature luminescence as reported by Takahei and Nakagome in 1989) (Takahei and Nakagome, 1989:913). Pomrenke also echoes the importance of Er in a paper on Er, Tm, and Pr in GaAs and AlGaAs where only Er showed emissions at room temperature (Pomrenke *et al.*, 1991b:415).

Praseodymium

Praseodymium (Pr) papers are listed in Table 6. Luminescence was first reported in 1981 by Kasatkin *et al.* who reported four groups of closely spaced Pr-

TABLE 6

Significant Papers on Praseodymium in Semiconductors

Citation	Host	RE Doping	Data	Results
Kasatkin, 1981	GaP	-	PL	First reported PL
Kasatkin, 1985	GaP	-	PL	PL decay during storage
Gippius, 1986	GaP, ZnSe	Implant	PL,CL	Pr and Pr:Li PL reported
Rzakuliev, 1988	GaAs,GaP	Implant	PL	Pr,Nd,Yb each form different complexes
Solomon, 1989	InP	Implant	PL,SIMS	InP:Pr PL & SIMS study
Pomrenke, 1989	GaAs	Implant	PL, SE	Free carriers as main excitation mechanism
Pomrenke, 1991a	InP, GaAs	Implant	PL	Pr PL in InP & GaAs reported
Pomrenke, 1991b	GaAs	Implant	PL(T)	Different emission lines temperature quenching
Kourtoutas, 1991	InGaAs	LPE	Hall	Transport properties & scattering mechanisms study
Lai, 1992	InGaP	LPE	Hall, PL	Pr gettering in LPE InGaP
Erickson, 1993	GaAs	Implant	PL(T)	Wide PL spectra, fit to D_4 crystal model

based emissions from GaP near 1.3, 1.7, 2.0 and 2.3 eV (Kasatkin *et al.*, 1981:353). In a unique follow-up paper 4 years later, Kasatkin reported that the Pr intracenter luminescence had disappeared after prolonged storage (Kasatkin, 1985:1174).

Gippius *et al.* found that coimplantation of lithium in Pr-doped GaP changed the spectrum by shifting emissions to near 1.1 microns and introducing lines near 0.9 microns (Gippius *et al.*, 1986:1196). They attributed this effect to the formation of Pr-Li complexes, and proposed that Li plays a certain role in the energy transfer from electron-hole pair recombination to the Pr-related centers.

Pomrenke, Hengehold, and Yeo also reported complex behavior of GaAs:Pr with emission lines near 1.1, 1.3 and 1.6 microns (Pomrenke *et al.*, 1989:343). By investigating the selective excitation spectra for the strongest lines, they found no significant excitation of the three Pr^{3+} emissions by DAP or lower lying states. Their study showed that the main excitation mechanism for Pr^{3+} is also through free carriers, but states at or below the donor-acceptor states are not excluded from the excitation process.

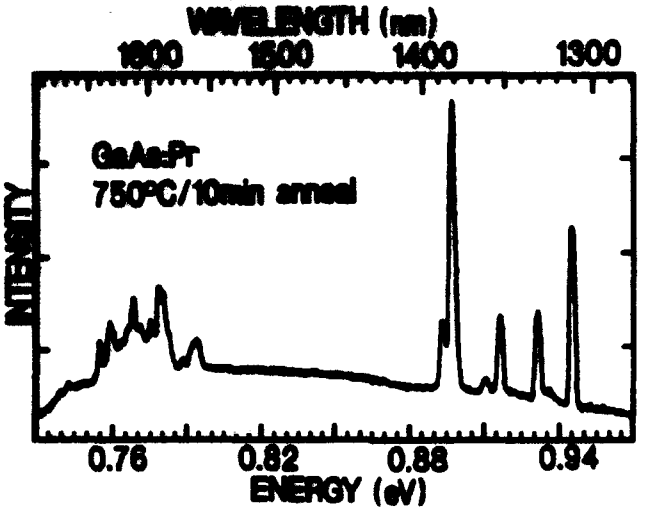

Figure 6. Photoluminescence of GaAs:Pr (Pomrenke *et al.*, 1991a:162)

In a latter paper, Pomrenke, Hengehold, and Yeo observed characteristic 4f emissions of Pr^{3+} ($4f^2$) from GaAs (Figure 6) and InP. The 3 sets of sharp GaAs:Pr emissions reported at 1.05, 1.35, and 1.6 microns were due to transitions between the crystal-field-split spin-orbit levels $^1G_4 \rightarrow {}^3H_4$, $^1G_4 \rightarrow {}^3H_5$, and $^3F_3 \rightarrow {}^3H_4$, respectively (Pomrenke *et al.*, 1991a:161). At optimum anneal temperatures, they found no evidence of near-band-edge emissions (DA transitions). The existence of these would imply the presence of competing processes which favor Pr excitation over FB or DAP recombinations. They also reported different temperature quenching behavior of these lines. The 1.35 micron emissions disappeared around 107 K, but the 1.6 micron lines continued until 174 K. The low intensity of the 1.05 micron line precluded temperature dependent studies. They concluded that Pr may occupy substitutional and/or interstitial sites.

Photoluminescence studies of Pr have also been reported for InP and InGaP. In the only other ternary host tested for Pr PL, Lai and Chang observed no InGaP:Pr

intra-4f transitions in the 600-800 nm range (2.07-1.55 eV) (Lai and Chang, 1992:1314). It has also been found that Pr-implanted InP emissions differ from that of GaAs:Pr. Reported emissions from InP:Pr were between 1.34 and 1.44 microns and lacked the 1.1 and 1.6 micron signals found previously in GaAs:Pr (Solomon *et al.*, 1989:574).

In a most recent paper, Erickson *et al.* have collected a very wide spectra of Pr in GaAs (0.49-1.49 eV). The main thrust of the paper is the theoretical calculation of the predicted emissions using a D_4 symmetry model which has less intrinsic symmetry than T_d.

Praseodymium has been studied mainly in GaAs, GaP, and InP. Luminescence has never been studied in silicon or ternary compounds while only PL demonstrations have been reported from GaAs:Pr, InP:Pr and, GaP:Pr. Thus praseodymium requires much more research.

Bandgap Engineering

An alternate method of producing luminescence from semiconductors at desired wavelengths is bandgap engineering. In this method, compounds are fabricated to obtain specific bandgaps which then allow strong luminescence at this bandgap energy via electrical excitation. This is accomplished by using ternary and quaternary compounds. Ternary III-V solids have 2 different group III atoms at group III sites or 2 different group V atoms at group V sites. The notation used for this is $A_xB_{1-x}C$ or AC_yD_{1-y} where A and B represent group III elements while C and D are group V elements and x and y are the mole fractions. Quaternary compounds involve 4 different elements, typically a pair of group III's and a pair of group V's with notation $A_xB_{1-x}C_yD_{1-y}$. The property of primary interest in these compounds is the variation of the energy gap with the mixture ratio. That is, the energy gap of the alloy will assume

a value intermediate between the gaps of the two 'pure' semiconductors of which it is composed.

This bandgap engineering has been studied most intensively in $Al_xGa_{1-x}As$ because of its close lattice match to GaAs. This greatly facilitates the fabrication of heterojunctions (junctions between two dissimilar semiconductors). Heterojunctions are important because the difference in energy gaps allow high injection efficiency of minority carriers into the lower-gap semiconductor (Pankove, 1971:197). Semiconductor lasers based on heterostructure designs can operate on much less current than similar homojunction lasers (Sze, 1985:268).

Rare-earth luminescence from ternary compounds have also been studied (Pomrenke *et al.*, 1991a:415; Favennec *et al.*, 1989:330) and continue to be of interest because of the advantageous laser effects. For example Benyattou *et al.* found Er-related emissions from $Ga_{0.55}Al_{0.45}As$ at 0.98, 1.54, and 1.57 microns (Benyattou *et al.*, 1992:350). They conjectured that the 1.57 micron emissions emanate from Er-Al complexes since they did not occur in GaAs. Interestingly, Tsang and Logan achieved semiconductor lasing at 1.5 microns using GaInAsP (Tsang and Logan, 1984:1025) and at 1.55 microns with erbium-doped GaInAsP (Tsang and Logan, 1986:1686). However, doubts have surfaced as to whether the 1.55 micron emissions were actually erbium-based transitions (van der Ziel *et al.*, 1987:1313; Wu *et al.*, 1992:456).

Bandgap engineering techniques are attractive in their versatility, however this method will be afflicted by both temperature dependent bandgaps and relatively wide emission linewidths due to processes contributing to band-tailing. Thus work on RE emissions from semiconductors is still important because of their temperature independence and narrow linewidths.

IV. EXPERIMENTAL SAMPLES

One of the major issues to be dealt with when attempting semiconductor research is procuring, fabricating, or growing the samples. Since the sample growth technique and post-growth processing conditions directly affect the electrical and optical properties of the sample, these are important issues. In this chapter, the samples used in this research are detailed and the semiconductor host growth and rare earth implant methods are explained.

Host Semiconductors

Praseodymium was incorporated into 3 main host semiconductor materials including gallium arsenide (GaAs), several variants of aluminum gallium arsenide (AlGaAs), and silicon (Si). These materials were chosen based on their important technological applications. Bulk silicon forms a diamond crystal structure with covalent bonding while both GaAs and AlGaAs have mixed atomic bonding, being partially ionic and partially covalent, in a zincblende crystal structure.

GaAs is the main compound semiconductor serving as the basis of many microwave and photonic devices. It has been heavily studied especially as the most widely used III-V compound in lasers and LEDs. AlGaAs is also a major compound used in photonic devices due to its extremely close lattice match to GaAs. This allows growth of simple heterostructure or layered devices with minimum interface defects. AlGaAs is also used for its "adjustable" bandgap which may be varied from 1.42 to 2.17 eV (300 K) by changing the Al/Ga ratio. This allows creation of material with a bandgap tailored to suit the electronic device. The bandgap may be fabricated to aid or control the current injection across the junction of a semiconductor laser and, indeed, AlGaAs has found wide applications in heterostructure lasers, LEDs, photodetectors and solar cells (Sze, 1985:265-269; Casey and Panish, 1978:27-28). Finally, silicon is

currently the preeminent material for semiconductor device fabrication. These three materials represent technologically the most important semiconductors in use today and will serve as the hosts for praseodymium research conducted in this study.

Liquid Encapsulated Czochralski Growth

There are many so-called classical methods of crystal growth which depend on a natural mechanism such as growth from molten solution. These methods are extensively reviewed elsewhere (Boer, 1992; Sze, 1985). In the liquid encapsulated Czochralski method (LEC), an apparatus called a puller which consists of a furnace containing a crucible with a molten solution of the compound to be grown. A seed of the compound is dipped into the solution and slowly withdrawn while rotating to create the crystal. An inert gas is flowed over the melt and the system is typically controlled to optimize temperature, rotation rate, gas flow, and pull speed. Progressive freezing at the liquid-solid interface results in a single, large crystal (Sze, 1985; 304-306). For LEC-growth of GaAs, an inert cap of liquid encapsulant of molten boron trioxide is floated on top of the molten GaAs in order to prevent decomposition of the GaAs.

The LEC-grown GaAs wafers in this study were purchased from Epitronics Corporation as grown by Hitachi. As reported by the vendor, the wafer thickness varies between 627 and 636 microns, the mobility is from 7100-6800 $cm^2V^{-1}sec^{-1}$, and the resistivity is $2.3\text{-}4.5\times10^7$ ohm/cm. Appendix A gives specific characteristics of all wafers used in this study.

Metalorganic Chemical Vapor Deposition Growth

Metalorganic chemical vapor deposition (MOCVD) crystal growth is achieved via high temperature chemical reactions of a vapor of desired compounds onto a substrate surface. The reactions are carried out thermally with the gases flowing over a reactor cell containing the substrate. The rate of growth is determined by

decomposition of the feedstock gas at or near the surface (feedstock depletion is due to substrate surface adhesion) and the necessity of removing the reaction by-products (Boer, 1992:185). MOCVD tends to produce excellent crystals because it operates close to thermodynamic equilibrium. Control of layer thickness is not as precise as other epitaxial methods such as molecular beam epitaxy. MOCVD layer thickness is controlled simply by calibration and timing of the supply of feedstock gases.

The MOCVD-grown GaAs and AlGaAs wafers used in this study were grown by Epitronics Corporation on LEC-grown GaAs substrates with the same characteristics as reported above. The AlGaAs layers were generally 5000 Å thick, with doped carrier concentrations of 1×10^{17}/cc and undoped concentrations of $<5.0\times10^{16}$/cc as reported by the vendor. Thin GaAs cap layers (50-200 Å) were grown over all AlGaAs wafers to prevent surface oxidation. Appendix A gives specific characteristics of all wafers used in this study.

Ion Implantation

Ion implantation has become a mainstay method of introducing impurities into semiconductors since the 1970s and consists of shooting energetic, charged dopant particles into a substrate via a controlled ion beam (Figure 7). The advantages of ion implantation are precise control over the amount of doping, better impurity profile reproducibility, and lower temperature processing requirements compared to diffusion techniques (Sze, 1985:382). Another pragmatic advantage is that several different substrates of entirely different host semiconductors can be implanted simultaneously.

The praseodymium and other species used in this study were implanted by Universal Energy Systems (UES), Dayton, Ohio under contract with AFIT. All praseodymium was implanted at 390 keV. A wide variety of host lattice types were implanted at 3 different doses as shown in Table 7. In addition, small amounts of

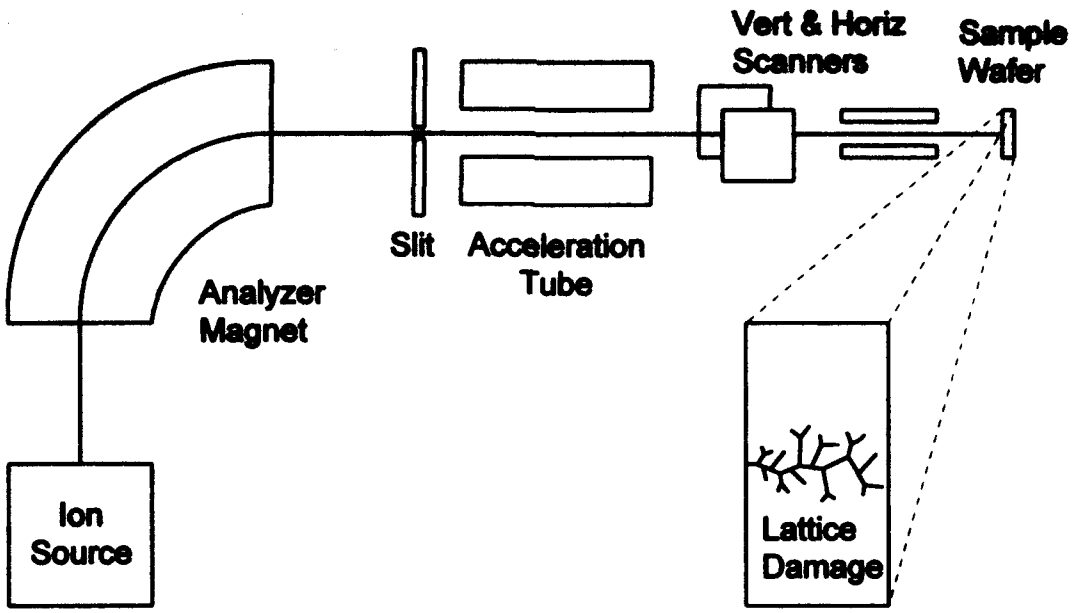

Figure 7. Ion Implantation System Showing Lattice Damage (after Sze, 1985:405)

$Al_xGa_{1-x}As$ with x=0.10, 0.14, and 0.20 were implanted to *augment and confirm* results found in the main implant hosts. Appendix B shows a complete table of all samples created in this effort.

Using the Profile Code, a computer program designed to calculate ion implanted depths (Implant Sciences, Danvars, MA), the Pr depth profile and peak density were calculated for each of the main host lattices. For each of these calculations, a Gaussian profile is used to approximate the implant profile density distribution function *n(x)* (Sze, 1985:406-407)

$$n(x) = \frac{S}{\sqrt{2\pi}\Delta R_P} e^{\left[-\frac{(x-R_P)^2}{2\Delta R_P{}^2}\right]}, \tag{3}$$

where projected range R_P corresponds to the peak of the Gaussian ion concentration

TABLE 7

Praseodymium Implant List

Host Composition	Host Types	Implant Doses (/cm^2)
Silicon	p,n	5×10^{12},1×10^{13},5×10^{13}
GaAs	Si,n,p	5×10^{12},1×10^{13},5×10^{13}
$Al_{0.15}Ga_{0.85}As$	Si,n,p	5×10^{12},1×10^{13},5×10^{13}
$Al_{0.30}Ga_{0.70}As$	Si,n,p	5×10^{12},1×10^{13},5×10^{13}
$Al_{0.50}Ga_{0.50}As$	Si,n,p	5×10^{12},1×10^{13},5×10^{13}

profile, the projected straggle ΔR_p is the distance from the peak where the ion concentration is reduced by 40% from the value at R_p, and S is the ion dose per unit area. Table 8 shows the results of these calculations for praseodymium implanted at 390 keV. These figures show very little variation of the implant profile across all the GaAs and AlGaAs samples. Note that the implant depths are far less than the 5000 Å minimum host layer, so that none of the emissions may be attributed to Pr located in the substrate.

The presence of RE ions as impurities in the lattice does not significantly affect the native crystal field. This can be seen by calculating the implant density as a function of depth in the host. The implant density $n(x)$ varies linearly with the dose S, so only one dose needs to be examined for a given implantation energy. The density profile was calculated with the Profile Code for the implant dose of 5×10^{13}/cm^2. The peak density was found to vary between 6.25×10^{18}/cc in GaAs and 6.63×10^{18}/cc in $Al_{0.50}Ga_{0.50}As$. The concentration of the host atoms is much greater; 4.42×10^{22}/cc for GaAs and 5.0×10^{22}/cc for silicon. Thus the peak Pr concentration is about 1/7000 of the host concentration making the effect of Pr on the crystal lattice negligible.

TABLE 8

Praseodymium Implant Characteristics (390 keV)

Host	Range, R_p (Å)	Straggling, ΔR_p (Å)
Silicon	1463	304
GaAs	922	319
$Al_{0.15}Ga_{0.85}As$	947	323
$Al_{0.30}Ga_{0.70}As$	982	330
$Al_{0.50}Ga_{0.50}As$	1033	340

Annealing

When the energetic ions enter the substrate, they loose their kinetic energy via a series of collisions with host lattice atoms. Some of these collisions impart sufficient energy to displace host atoms from lattice sites resulting in lattice disorder (amorphization) or damage (Figure 7). The damaged, disordered regions that result from ion implantation can severely degrade important semiconductor parameters such as carrier mobility and lifetime. The disordered parts of the lattice can be reordered by heating or annealing the sample. Annealing or heating the damaged semiconductor to high temperatures for an appropriate length of time can restore the lattice integrity. Annealing restores the crystal structure by providing the atoms enough thermal energy to move to their natural crystal lattice positions. During the annealing process, the implanted atoms may diffuse and broaden the density profile. Rapid Thermal Annealing (RTA) processes very quickly heat the sample for a limited duration compared to furnace annealing (seconds versus minutes). The RTA methods also fully restore the crystal, but with minimal redistribution of the implants (Sze, 1985:415).

In this effort, RTA was performed to anneal all samples. An A. G. Associates Heatpulse 210 machine was used with forming gas (3% H, 97% Ar) flowing during

annealing. Flowing nitrogen gas was used for pre- and post-anneal purging. Samples were annealed face up and covered with a capping wafer of GaAs to minimize As boil off and potential chemical contamination. The ramp up of the sample temperature from ambient to desired annealing point ranged from 30 to 38 seconds, while cool down to 300 °C generally took about 4 minutes. The variance of the annealing temperature as reported by the RTA system was always between -5 to +7 °C of the target temperature.

V. CHARACTERIZATION TECHNIQUES

Several experimental techniques have been developed to analyze the characteristics of semiconductors. Each has particular strengths and applications, and gives different information. It is advantageous to employ more than one technique on a given problem since, usually, no single method will yield all the vital evidence. The techniques used in this research are described in this chapter.

Photoluminescence

Photoluminescence spectroscopy is the most common technique for investigating the electronic transitions in semiconductors. In this method, electrons are excited from their ground state to higher energy (non-equilibrium) states by photon absorption. The radiated light spectrum resulting from recombination of these excited electrons with holes can reveal much information about the electronic processes occurring in the semiconductor.

PL measurements are practiced at low sample temperatures for two principal reasons. The first strong advantage of low temperature measurements is to minimize broadening of otherwise sharp spectral features by lattice vibrations (phonon absorption). The vibration of neighboring ions creates a changing crystal field at the place of rare earth ions which is not the same for all ions. This broadens the resulting spectral lines (Dieke, 1968:32). Liquid helium cooling of the sample to 4 K is effective for minimizing this line broadening. Low temperatures are also desirable because most substances have a fairly closely spaced group of levels from which absorption can take place. The occupation of levels greatly decreases with increasing energy according to Boltzmann's exponential law. By keeping electrons mainly in the ground state via very low temperatures, the spectral analysis is simplified by

eliminating the complication of overlapping lines from multiple thermally populated lower levels (Dieke, 1968:32).

Application of PL. In PL, excitation with photons of energy greater than the bandgap produces a non-equilibrium concentration of electrons and holes. At low temperatures, these mainly form excitons which can decay directly or after capture by impurities or defects (Lightowlers, 1990:1161). The fate of the electron-hole pairs created by the laser photons depends on the nature of the semiconductor. In a high purity material (relatively small impurity concentrations), these electrons and holes pair up to form free excitons which subsequently decay producing free exciton luminescence. Materials containing significant donor or acceptor impurity concentrations ($>10^{15}$ cm^{-3}) have virtually all of these free excitons captured by impurities giving rise to impurity-specific bound exciton luminescence (Stradling and Klipstein, 1990:143). Because of the competition between these various capture mechanisms and both radiative and non-radiative decay mechanisms, PL is not generally a quantitative technique in that absolute line intensity is rarely used. The strength of PL is in unambiguous identification of transition energies and the consequent determination of relative energy levels.

The sample temperature and excitation energy and power may also be varied in PL experiments in order to obtain more information about the energy levels in luminescent centers.

PL Experimental Apparatus. Figure 8 shows the experimental arrangement used for PL spectroscopy in this effort (the tunable Ti:Sapphire laser pumped by the argon laser is required for SEL). The specific apparatus is listed in Table 9.

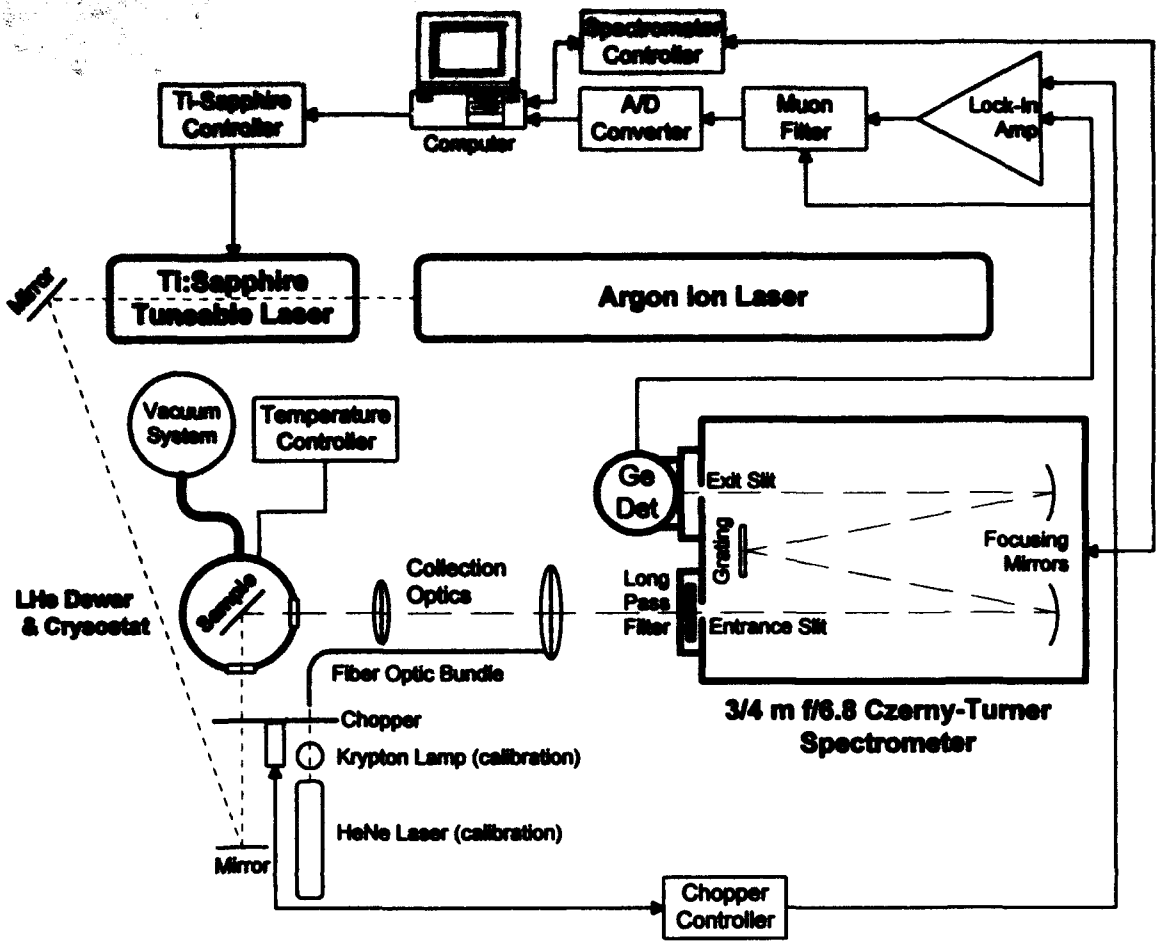

Figure 8. PL and SEL Experimental Arrangements

The cryostat serves to maintain the sample at very low temperatures using liquid helium and is surrounded by a liquid nitrogen filled insulation jacket. The laser excites the cryostat-mounted sample with photons of energy greater than the host bandgap in order to excite VB electrons up to available states in the CB. The low temperature energy gap of some materials of interest are 1.16 eV for silicon, and 1.52 eV for GaAs, so a convenient excitation source is the argon ion laser operating at 514.5 or 488.0 nm (2.4 eV).

TABLE 9

PL and SEL Experimental Apparatus List

System	Item	Make/Model	Description/Function
Excitation	Argon Ion Laser	Spectra Physics 171 or 2085	20W+,4880 & 5145 Å output
	Ti:Sapphire Laser	Spectra Physics 3900	Tunable from 700-1100 nm
Cryogenics	Cryostat/Sample Mount	Janis Super VariTemp 10DT	LN & LHe cooled to 1.4K
	Temperature Controller	Lakeshore 805	Monitor/Control sample Temp
	Vacuum Pump (Sample Chamber)	Welch Scientific 1397	Evacuation of sample chamber
	Vacuum Pump (Cryostat Insulation Jacket)	Alcatel CFV100 Turbo Pump	Thermal isolation of LN and LHe reservoirs
Optics	Collection Lenses	Newport KBX154,d=50.8,f=100mm Newport KBX193,d=76.2,f=300mm	f-matched to sample chamber f-matched to spectrometer
	Long Pass Filter	Oriel 830, 780, or 1000 nm LP	Filter laser light
	Spectrometer	Spex 1702 or 750M	3/4 m Czerny-Turner, f/6.8
Detection	Ge Detector	Applied Detector Corp 403L	LN cooled, 0.8-1.7 micron
	Optical Chopper	SciTec, or Stanford Research SR540	Provide Lockin with signal of known frequency
	Muon Filter	North Coast 829B	Filter gamma ray spikes
	Lockin Amplifier	SciTec 500MC, or Stanford Research SR530, or SR850	Extract weak signals from strong background
Data Acquisition	A/D Interface Board	MetraByte DASH16F	Digitize analog Lockin Signal
	Computer	Zenith Z-248, or Spex 486	Operate spectrometer
	Acquisition Software	LabTech Notebook v.5.0.3, or Spex DM3000S	Collect and store data as ASCII

The emissions from the sample are then collected and analyzed by a spectrometer. Collection optics efficiently gather and direct the emissions to the grating spectrometer. Filters are mounted at the spectrometer input to remove unwanted laser and emission light. The detector mounted at the spectrometer output measures the luminescence intensity from the sample, and the emission intensity versus wavelength is recorded on a computer. A sensitive detector for near-infrared emissions is the liquid nitrogen-cooled germanium detector. A chopper mounted between the final laser beam steering mirror and the sample chamber repetitively chops the emission light allowing the weak sample signal to be extracted from relatively bright background using a "lock-in" amplifier.

Characterization of the Laser Beam. To measure the laser beam spot size to determine the power density on the sample, the method described by Yoshida and Asakura was used (Yoshida and Asakura, 1976:273). The spot size diameter near the sample was determined to be 2.79±0.16 mm for the Spectra Physics model 171 argon laser and 2.87±0.14 mm for the Spectra Physics model 2085 argon laser. The width of the Spectra Physics model 3900 Ti:Sapphire beam was measured to be 1.92±0.02 mm. These values correlate very well with the manufacturer's specifications.

The average laser power density on the sample is then found using this spot size and accounting for the beam losses and the sample orientation. This average power density can be described as

$$p_{av} = \frac{P_0 T_{optics} f_{spot} \cos(\theta)}{\pi \varpi^2}, \tag{4}$$

where P_0 is the power output from the laser, T_{optics} is the fraction of laser power reaching the sample, f_{spot} is the fraction of the beam power in the spot, θ is the angle of the sample to the beam, ω is the spot size radius. The fraction of the Gaussian beam in the spot is $(1-e^{-2})^{-1}$ or about 86.5%. The samples are at an angle of about 37° to the laser beam in order to prevent direct reflection of the laser into the spectrometer. It was determined that losses from the steering mirrors and sample chamber windows allow about 64% of the emitted laser power to reach the sample. Then for a 100 mW beam from the laser, an average laser power density over the spot on the sample of 723 mW/cm^2 is obtained which can be immediately scaled to higher powers since this function is linear with P_0.

Laser Penetration Depth. One of the most important influences on the strength of the RE PL emissions is the laser excitation depth. If the laser does not penetrate to a

TABLE 10

Absorption Coefficients for Argon Laser Light

Host Material	Absorption Coefficient α (/cm)	Penetration Depth (1/e Point) (Å)
Si	18480	5411
GaAs	90000 (21 K)	1111
$Al_{0.149}Ga_{0.851}As$	91670	1091
$Al_{0.315}Ga_{0.685}As$	77300	1294
$Al_{0.491}Ga_{0.509}As$	62120	1610

depth of significant Pr density, little, if any, luminescence can be expected. The energy flux of the laser is damped as $e^{-\alpha x}$ where α is the optical absorption coefficient which depends on both the laser wavelength and the material, and x is the depth into the material (Boer, 1990: 263). Thus the 1/e point for intensity reduction is simply the inverse of the absorption coefficient. The light from an argon laser is primarily at 4880 and 5145 Å which corresponds to about 2.5 eV. The absorption coefficients have been published for the host materials used in this research for light in this energy range. The room temperature absorption coefficients and corresponding 1/e points are listed in Table 10 (Aspnes and Studna, 1983; Aspnes *et al.*, 1986; Sturge, 1962). The values shown are those nearest the exact Al fractions, but the $Al_{0.149}Ga_{0.851}As$ value is interpolated.

Comparing the penetration depth of the laser to the praseodymium implant depth distribution (Table 8), the laser penetration is within the straggling range of each host except Si and $Al_{0.50}Ga_{0.50}As$. The Si represents an especially poor match between the laser excitation and the Pr distribution, so the Pr PL signal may be weak in this combination.

System Calibration. The calibration of the system is a critical step in this experimental process. Calibration consists of steps taken to assure the accuracy of the wavelengths reported in the data. Since the mechanical portion of the spectrometer is subject to wear and misalignment over time, an independent method of establishing the position of wavelength in a spectrum is required. This independent calibration is provided by the well-known lines of a krypton lamp and a helium-neon laser (Calibration items in Figure 8). The wavelengths corresponding to these lines are known to a high degree of precision, and they serve to allow wavelengths to be assigned to the data accurately using linear regression techniques since the data collected is linear in wavelength. In PL experiments, these calibration lines were added to RE PL spectra either concurrently or during daily calibration runs. It was found that the spectrometer showed virtually no change in calibration over the period of data collection for this effort.

System Response. Ideally, the output signal from the PL system would be linear with the input luminescence across the entire wavelength range. This is not the case with each part of the collection and detection systems contributing responses which vary with the input wavelength. Specific effects include the transmission of the collection optics and filter, the efficiency of the spectrometer grating and mirrors, the efficiency of the detector, and even the transmission of the air in the lab. By inputting a signal of known intensity at each wavelength, the system response can be calculated and compensated for. Using a blackbody source at a known temperature, the PL system response was investigated. The response factor for the system is then calculated as the ratio of the blackbody power input to the signal report by the experimental system. Figure 9 shows this system response factor calculated for the PL apparatus with a 1000 nm long pass filter, 1.25 micron grating, and Ge detector using a 950 °C

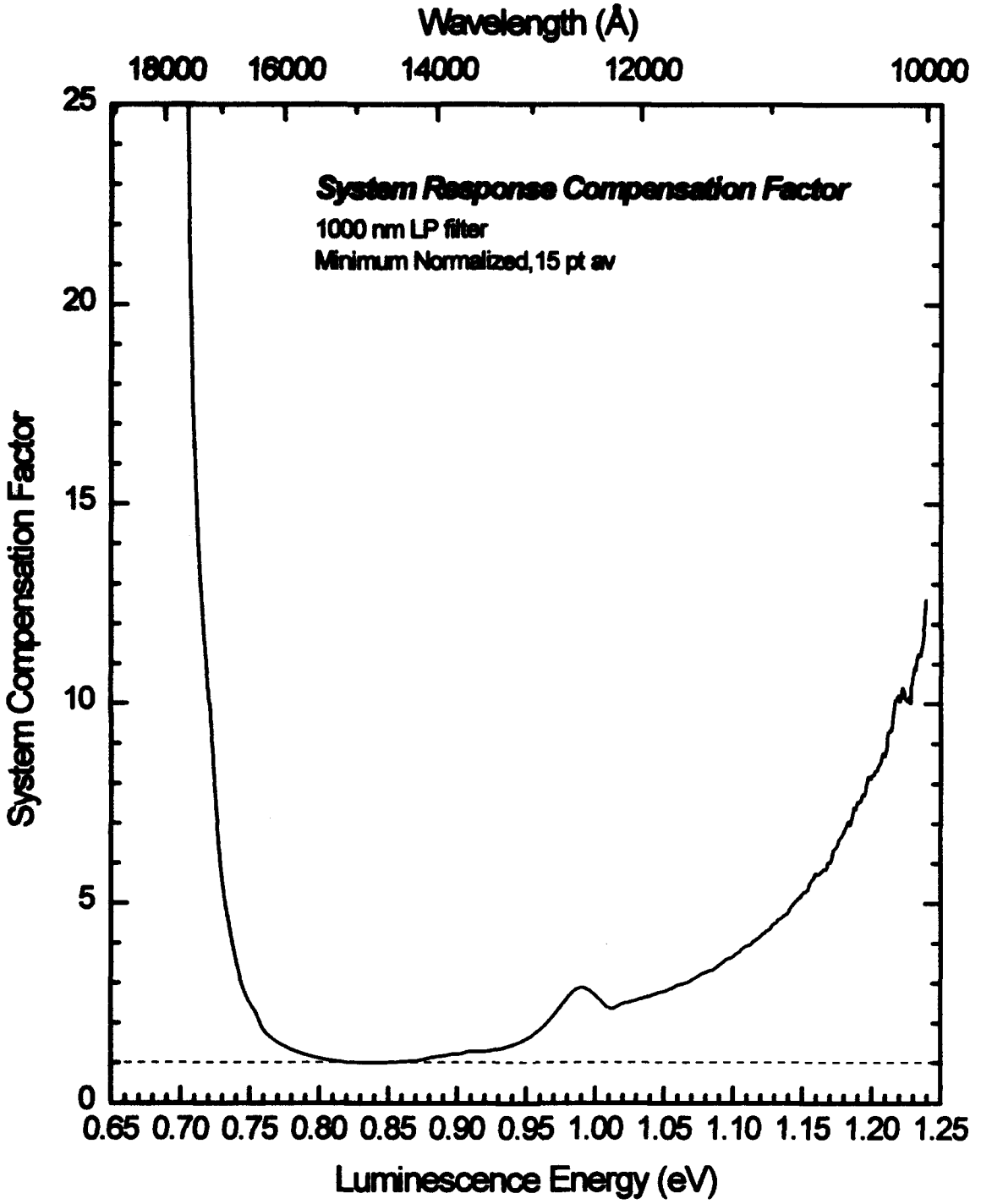

Figure 9. Normalized System Compensation Factor for the PL Apparatus using a 1000 nm LP Filter and Ge Detector

blackbody. Background fluctuations have been smoothed using a 15 point smoothing algorithm. To apply this, all of the intensity values of a PL spectrum would have to be multiplied point by point (discretely) by this system compensation factor. In most cases in this work, the absolute intensity of spectral lines is not important, and they have not be compensated. The Pr emission lines of interest occur in the 0.75 through 0.80 eV and the 0.85 through 0.90 eV regions and have nearly the same response factor, so compensation would accomplish little.

Error Analysis. There are three major sources which contribute to energy and/or intensity uncertainty in the PL experiment. These are 1) linewidths introduced by the system, 2) finite data resolution, and 3) background variations. Each of these effects influence the data in different ways.

A spectrometer will produce an output line having a finite width even if the incoming light is perfectly monochromatic. This instrument linewidth is a measure of how much the instrument smears or broadens the lines and is due to the finite optics employed by the spectrometer. Specifically, this is mainly due to diffraction effects including the resolving power of the grating and the width of the slit being used. The grating linewidth $\Delta\lambda_g$ is defined as

$$\Delta\lambda_g = \frac{\lambda}{mN}, \tag{5}$$

where λ is the wavelength of the light, m is the order of operation of the grating (typically 1), and N is the number of grating lines. The linewidth due to the finite slit of the spectrometer is

$$\Delta\lambda_s = \frac{a\cos\theta_m}{mf}, \tag{6}$$

where a is the slit width, θ_m is the diffraction angle off the grating, m is the grating order and f is the instrument focal length. Thus, the overall linewidth of the instrument is $\Delta\lambda = \Delta\lambda_g + \Delta\lambda_s$. Typically, the slit width contribution to the overall linewidth is dominant. The linewidth for a typical PL spectra in this study using the 3/4 m spectrometer with 400 micron slit results in an 8 Å or less linewidth for the Pr emissions of interest. This equates to a maximum linewidth of 0.59 meV for the Pr emissions found at 13000 Å. Thus the very narrow RE emissions will appear to be at least 0.59 meV wide and 2 lines separated by less than this energy will be very difficult to distinguish.

Finite data resolution results from the periodic sampling of the luminescent intensity by the data acquisition software. This periodic data sampling limits both the accuracy that can be ascribed to a wavelength information and also the maximum intensity of a peak. For example, using a 2 Hz sampling rate with the spectrometer scanning at 400 Å/min gives a data resolution of 3.33 Å per data point. This serves as the uncertainty assigned to wavelength positions throughout this study. In addition, the finite data resolution limits the accuracy which can be ascribed to any peak's intensity since the intensity sampling is unlikely to occur exactly at the peak. In fact, the worst case data sampling event occurs when the sampling occurs exactly equally on either side of the actual peak. This worst case can be quantified and used as the upper limit for uncertainty of all peak intensities. In order to model this case, the shape of the intensity peaks must be determined. There are two main optical mechanisms in the spectrometer which contribute to this: 1) the far-field diffraction effects of the slit and the grating, and 2) the one-to-one slit imaging designed into the spectrometer. The far field diffraction effects would cause a peak shape of sinc^2 (Hecht and Zajac, 1979:343-347,358-361), while the imaging of the slits produces a convolution of slit images and

would produce a triangle-shaped peak (Brügel, 1962:123). In both cases, the width of the modeled peak is determined by the theoretical FWHM of the slits since all RE emissions reported have instrument-limited linewidths (which was confirmed by examining high resolution spectra of the peaks). For a typical PL experimental run using 400 micron slits with a scan rate of 400 Å/min (a data resolution of 3.333 Å/point), the worst case of peak intensity uncertainty is 8.9% for the $sinc^2$ model and 18.9% for the triangle model. This analysis serves as assurance that reported intensities in this study are accurate.

Finally, the actual intensity of luminescence also varies with the background fluctuations which are inherent in any measurements using an electrical or optical system. These fluctuations can be quantified by fitting a linear regression line to a portion of spectra consisting only of background signal. An intensity measurement may then be assigned an uncertainty equal to one standard error of this regression line.

Selective Excitation Luminescence

Selective excitation luminescence (SEL) differs from the PL technique in that the energy used to excite the crystal is varied. The key difference is that in PL a single excitation energy is used and a range of the output spectrum is scanned, while in SEL a single wavelength output (like a rare earth emission line) is monitored while exciting the sample over a range of energy values. Instead of greater-than-bandgap excitation for simple PL, a tunable laser is used with which energy states in the sample are selectively populated as the excitation energy is varied. The measured intensity of a particular output line peaks whenever the excitation energy of the tunable laser coincides with an energy transition intrinsic to the excitation of that particular emission. The intensity may also fall, indicating that the laser has selectively activated a competing transition mechanism. This method can then be used to determine

processes which are related to or compete with the excitation process by enhancing certain transitions selectively.

Electroluminescence

In electroluminescence (EL), the excitation is provided by supplying potential and/or kinetic energy to free carriers in the sample (Pankove, 1977:9). These free carriers then recombine producing light. For example, a p-n junction forward-biased sufficiently to allow propagation of electrons throughout the CB beyond the junction will assume current injection mode (Figure 10) and those electrons will recombine with holes on the p-side of the junction to produce light. The flow of CB electrons across the junction (injection current I) and the corresponding photon emissions increase rapidly with the bias voltage V according to the diode equation (Pankove, 1977:180)

$$I = I_0\left(e^{qV/kT} - 1\right), \tag{7}$$

where I_O is a current constant which is proportional to

$$e^{\left[-(E_g-\xi)/kT\right]}, \tag{8}$$

where E_g is the bandgap, k is the Boltzmann constant, and T is the sample temperature. The energy term ξ is the smaller of ξ_n or ξ_p for which $E_g+\xi_p$ is the barrier which electrons must overcome for injection into the p-type junction region and $E_g+\xi_n$ is the barrier for hole injection into the n-side (Figure 10). In this injection mode, direct and indirect band-to-band recombinations become possible, along with the most of other radiative and non-radiative transitions already mentioned. Alternate decay modes, such as trapped-charge luminescence or Auger recombinations, compete with the desired radiative transition and need to be minimized if possible.

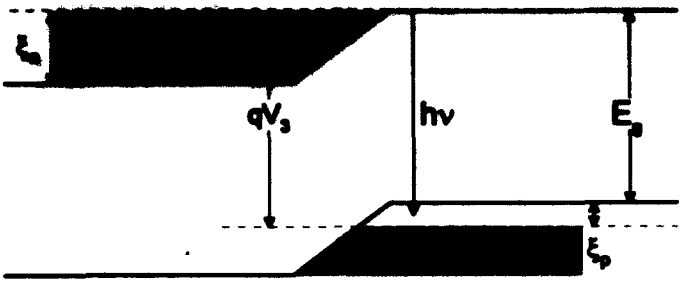

Figure 10. Electron Injection in a p-n Junction (after Pankove, 1971:181)

As the injection diode is electrically pumped, many free carriers and excitons are created. Hopefully, some of the recombination energy will be transferred to the RE 4f energy levels with accompanying decay to produce technologically desired wavelengths. Since excitation of rare earths in practical devices will probably be exclusively through electrical pumping (electroluminescence via carrier injection), demonstration of efficient electroluminescence is an important step in research leading to fabrication of devices.

VI. RESULTS AND DISCUSSION

The results can be grouped according to the objectives for this research effort. The first studies, which include examination of the Pr PL control sample runs, annealing dependence, dose dependence, and doping dependence, are directed primarily toward optimization of the Pr emissions. The next series of studies including host material dependence, laser excitation power dependence, temperature dependence, and excitation energy dependence aim at the heart of this effort; that being to understand the excitation mechanism of Pr in semiconductors. The codoping and dual-doping efforts are attempts to enhance the Pr luminescence through the use of additional elements in the lattice. The last research study consists of fabrication of a Pr-based electroluminescent diode.

Pr Luminescence Study of Control Samples

Verification that the emissions attributed to Pr are valid requires comparison of samples with and without Pr. In this case, both implanted and unimplanted control samples were identically prepared and annealed for each of the semi-insulating (SI) hosts. All $Al_xGa_{1-x}As$ hosts were MOCVD-grown on GaAs substrates, while the SI-GaAs is LEC-grown. The LEC-grown GaAs was used because greater amounts of material were available and tests showed that Pr emissions from LEC-grown and MOCVD-grown GaAs were virtually identical. Figure 11 shows the low temperature photoluminescence of each pair of samples for the SI-GaAs and SI-$Al_xGa_{1-x}As$ with $x=0.15$, 0.30, and 0.50 hosts. Anneal temperatures are representative of significant Pr emissions, although they are not optimal; this will be shown in the next section. Although the emission intensities vary, in all cases the sharp line emissions in the two ranges from 0.755-0.783 eV and 0.893-0.945 eV are evident only in the Pr implanted

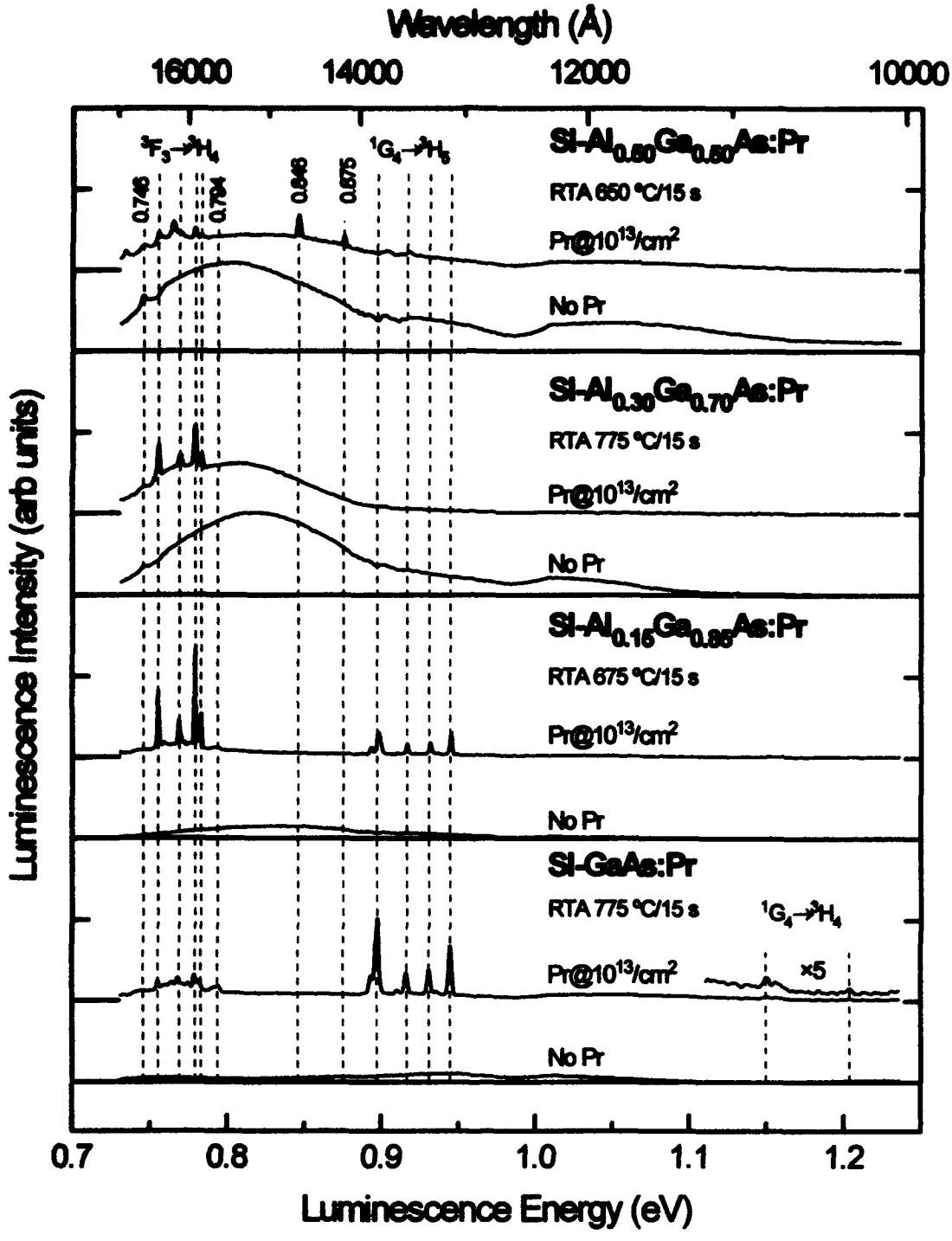

Figure 11. Photoluminescence spectra taken at 3 K for SI-GaAs, SI-$Al_{0.15}Ga_{0.85}As$, SI-$Al_{0.30}Ga_{0.70}As$, and SI-$Al_{0.50}Ga_{0.50}As$ with and without Pr implanted at 390 keV with a dose of $10^{13}/cm^2$ and annealed at various temperatures

hosts and are thus attributed to Pr emissions. In addition, weak, sharp line emissions are seen 1.150 and 1.204 eV in SI-GaAs:Pr only. All the emissions from the SI-GaAs:Pr are the same as reported by Pomrenke *et al.* and the common energy positions and emission structures of each group provide evidence that the same transitions are responsible for the emissions in each host (Pomrenke *et al.*, 1991b:418-419). No phonon absorption-based replicas of the Pr emissions can be identified, implying that these Pr-related transitions are not coupled to phonons in the host lattice. Phonon lines are not expected, since the shielding of the Pr 4f electrons should prevent any direct coupling to the lattice and this lends more evidence to the intra-4f level transition origin of these emissions. These emissions are thus assigned to Pr^{3+} 4f transitions following assignments first determined by Pomrenke *et al.* (Pomrenke *et al.*, 1991b:418-419): the 0.75 eV group results from $^3F_3 \rightarrow ^3H_4$ transitions, the 0.9 eV group results from $^1G_4 \rightarrow ^3H_5$ transitions, and the 1.150 and 1.204 eV emissions result from $^1G_4 \rightarrow ^3H_4$ transitions. Assuming no forbidden transitions, the highest energy peak in an emission group results from a transition between the lowest state of the thermalized upper energy level and the lowest crystal field split state of the termination level. Using this as a guide, the lowest energy peak in these emission groups are offset from the Pr^{3+} free ion energy level transitions (Table 3) by -4 meV for $^3F_3 \rightarrow ^3H_4$, -4 meV for $^1G_4 \rightarrow ^3H_5$, and +3 meV for $^1G_4 \rightarrow ^3H_4$. This offset is due to the crystal field splitting of the free ion levels into states with both higher and lower energies.

In order to determine the actual linewidth of these emissions, the full-width-at-half-maximum (FWHM) was measured for several lines of the Pr emissions. All lines in the Pr $^3F_3 \rightarrow ^3H_4$ emission group were examined in the SI-$Al_{0.15}Ga_{0.85}As$ host for spectrometer slit widths ranging from 600 to 100 microns. All peaks showed a smoothly decreasing FWHM, but below 100 microns the peaks were too weak to measure. The strongest and narrowest is the 0.779 eV (15914 Å) peak which exhibited

a FWHM of 6.0±0.5 Å for a 100 micron slit. This corresponds to an upper bound of 0.294 meV for the most narrow Pr emission linewidths.

The broad emissions visible in both implanted and unimplanted samples centered near 0.82 eV are due to unidentified impurity- or defect-related deep levels in the host semiconductor. The very weak structure noticeable near 0.9 eV in these broad emissions is an artifact of the system response in that energy range. An emission line at 0.746 eV was detected in all implanted and unimplanted samples, which must then be host semiconductor-related. A small unknown emission line at 0.794 eV is seen only in Pr-implanted SI-GaAs and SI-$Al_{0.15}Ga_{0.85}As$ and it is not related to the Pr^{3+} emissions. This conclusion was made based on the dissimilar behavior of this emission line to Pr emissions. For example, the 0.794 eV peak decreases with increasing anneal temperature (Figure 12), but increases with increasing dose (Figures 14 and 15) in contrast to the behavior of Pr emissions. The emission lines at 0.846 and 0.875 eV are detectable in the SI-$Al_{0.50}Ga_{0.50}As$ hosts only for RTA temperatures less than 700 °C and most likely emanate from unannealed ion implantation damage.

No direct evidence of the $^3F_4 \rightarrow {}^3H_4$ transition was found implying that either selection rules preclude this or, more likely, that the closeness of $^3F_3$ and $^3F_4$ allows a strong path of non-radiative (thermalized) transitions from $^3F_4$ to $^3F_3$. Erickson *et al.* noted that for levels with an energy difference of less than 4 phonons, the ion relaxes via non-radiative phonon processes, while larger energy difference transitions produce a photon (Erickson *et al.*, 1993:2348). The $^3F_4 \rightarrow {}^3F_3$ spacing is less than 2 GaAs phonon energies and is thus consistent with this.

The strong emission groups have been identified with transitions to a lower state of J = 4 and 5, respectively. As shown in Table 1, both of these J states have crystal field splittings of 4 in cubic symmetry. However, the main emission groups have at least 4 strong and several weaker sharp emission lines. This number of emission lines

then implies that the emissive Pr atoms occupy less than cubic symmetry, but no specific site symmetry may be assigned since the exact number of energy level splittings cannot be directly inferred simply from the number of emission lines.

No Pr-related emissions were detected from Pr implants in n- or p-type silicon over a tested anneal range of 450-900 °C and doses of 1×10^{13} and $5\times10^{13}/cm^2$. Only emissions from the band-edge and near band-edge levels were found. This is attributed to the comparatively narrow silicon bandgap (1.17 eV at 0 K) which is slightly lower than the $^1G_4$ energy level in Pr and more than 0.3 eV from the next lower level ($^3F_4$) causing an energy mismatch of the exciton bound to Pr^{3+} and any energy levels in Pr^{3+}.

Effect of Annealing Conditions on Pr Luminescence

Establishment of the RTA conditions which are most conducive to Pr photoluminescence is a vital first step. This step serves the primary purpose of creating a sample set with the maximum possible PL for each host. All annealing was conducted using the RTA method at various temperatures for 15 second durations. Hosts used were SI-GaAs and SI-$Al_xGa_{1-x}As$ with x=0.15, 0.30, and 0.50 implanted with Pr at 390 keV with $10^{13}/cm^2$ doses.

Figure 12 shows the PL spectra obtained at 3 K from SI-GaAs:Pr. The zero luminescence level of each spectrum is indicated by a short horizontal line on the left axis. The emission spectra consist of two main emission groups: one based near 0.78 eV and the other near 0.94 eV. The former group consists of a series of small peaks punctuated by 3 main peaks at 0.756, 0.769, and 0.779 eV, and are attributed to intra-4f transitions between crystal-field-split states of the excited level $^3F_3$ and the ground state $^3H_4$ of Pr^{3+}. The latter group consists of at least 5 relatively strong peaks at 0.893, 0.898, 0.917, 0.931, and 0.945 eV, and these are attributed to the transitions

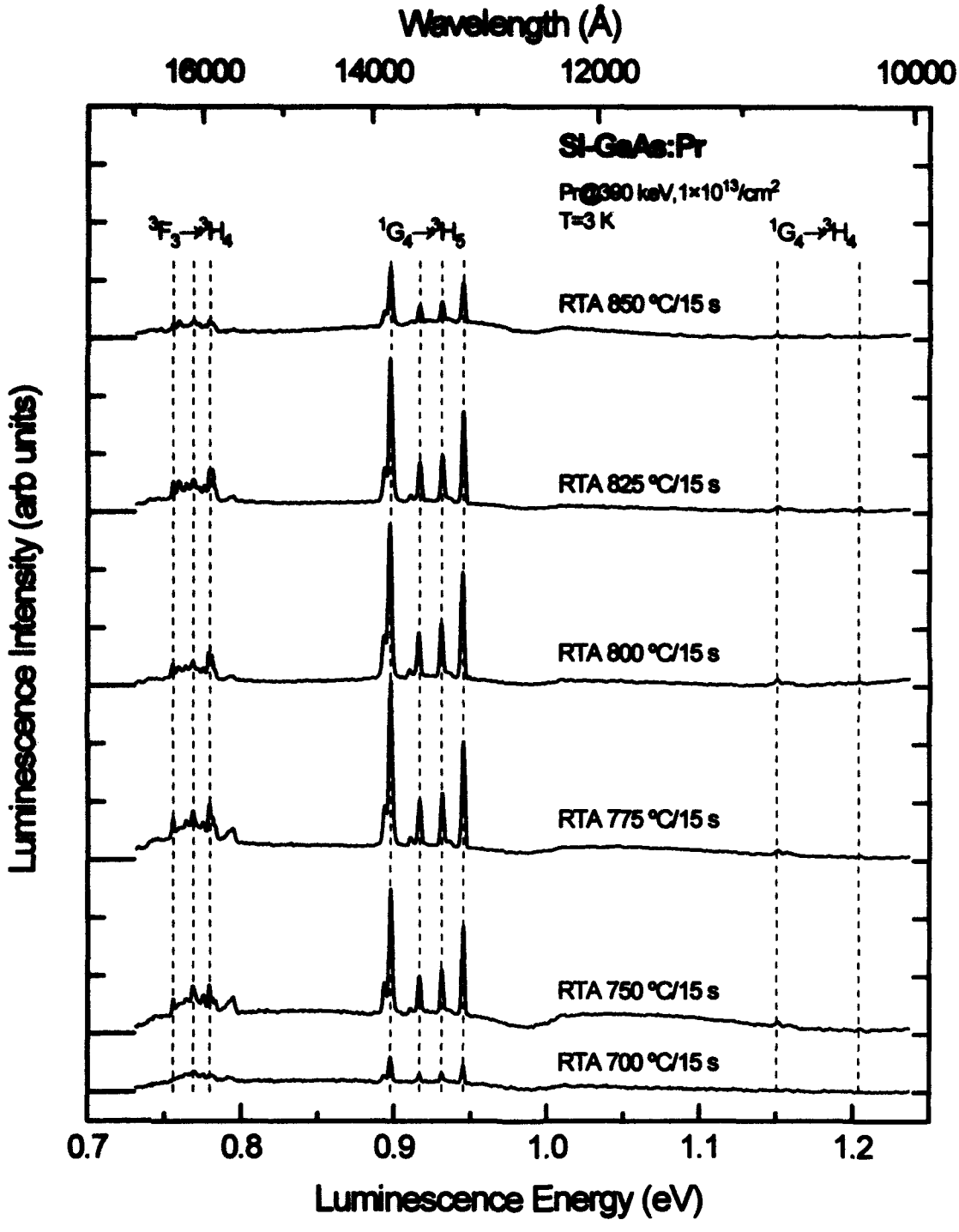

Figure 12. Photoluminescence spectra taken at 3 K for SI-GaAs implanted with Pr at 390 keV with a dose of $10^{13}/cm^2$ and annealed at various temperatures

between the crystal field split states of the excited states $^1G_4$ and $^3H_5$ of Pr^{3+}. Also, very weak transitions between $^1G_4$ and $^3H_4$ are observed at 1.150 and 1.204 eV. This annealing study showed that the annealing temperature of 700 °C is certainly too low to activate the Pr emissions due to unannealed implantation damage. The luminescence intensity increased strongly at 750 °C and increased further up to the maximum intensity at an RTA temperature of 775 ±25 °C. Above 800 °C, the peak intensities in both emission groups fall off with the intensity becoming much smaller at 850 °C. Probably, at higher annealing temperatures, the GaAs sample may start to dissociate.

For the SI-$Al_{0.15}Ga_{0.85}As$ host as shown in Figure 13, the Pr emission groups are seen in the same energy bands as those observed for GaAs:Pr. Furthermore, the emission peaks which makeup the 0.945 eV group have virtually identical intensity to those of SI-GaAs. However, very strong peaks were observed in the 0.78 eV group consisting of much sharper and stronger emissions than those for GaAs:Pr. As for the GaAs:Pr samples, the Pr related emissions of $Al_{0.15}Ga_{0.85}As$:Pr are very weak below 700 °C, but strongly increase above 725 °C. The luminescent intensity increases with annealing temperature up through 750 °C, exhibiting the strongest PL emissions at 750 °C for the 0.75 eV emission group and 775 °C for the 0.9 eV emission group. Both emission groups show significant decreases in intensity at the higher 800 °C annealing temperature.

Annealing studies for SI-$Al_{0.30}Ga_{0.70}As$ and SI-$Al_{0.50}Ga_{0.50}As$ were made for various RTA temperatures from 650 °C through 750 °C The PL results of these samples taken at 3 K show significant defect emissions in addition to the Pr emissions. Just like SI-$Al_{0.15}Ga_{0.85}As$:Pr, the intensity of the emission groups grow as the temperature is increased up to the optimal point, above which the emissions decrease. For SI-$Al_{0.30}Ga_{0.70}As$, the peak PL emissions are evident for 725±25 °C. For SI-$Al_{0.50}Ga_{0.50}As$, the peaks of each group are distinct and varied little in intensity

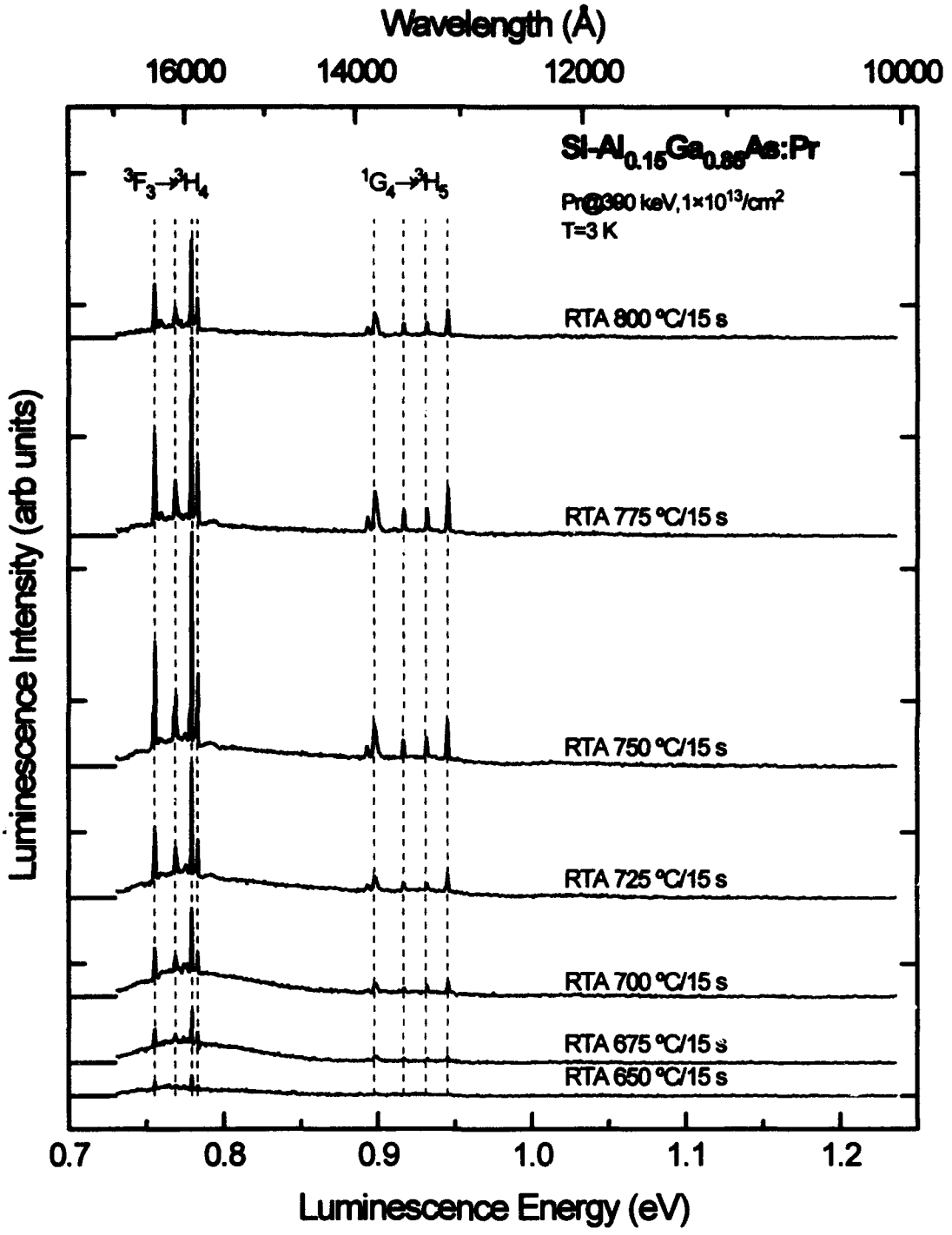

Figure 13. Photoluminescence spectra taken at 3 K for SI-$Al_{0.15}Ga_{0.85}As$ implanted with Pr at 390 keV with a dose of $10^{13}/cm^2$ and annealed at various temperatures

TABLE 11

Optimal RTA Temperatures for PL from Pr in SI-$Al_xGa_{1-x}As$ Annealed for 15 seconds

HOST:RE	OPTIMAL TEMP
SI-GaAs:Pr	775 ±25 °C
SI-$Al_{0.15}Ga_{0.85}As$:Pr	750 ±25 °C
SI-$Al_{0.30}Ga_{0.70}As$:Pr	725 ±25 °C
SI-$Al_{0.50}Ga_{0.50}As$:Pr	725 ±25 °C (?)

over the broad RTA range of 675 through 750 °C, but 725 °C was judged to produce slightly stronger and sharper Pr PL lines.

Table 11 summarizes the results for the best RTA temperature for a 15 second duration. The decreasing RTA temperature with increasing Al mole fraction may be attributed to the greater density of Al atoms in the lattice which are lighter and presumably more mobile than the Ga atoms. The emission intensity in each of the hosts is relatively stable over an RTA temperature range of 75 °C. This suggests that the Pr^{3+} luminescence center is thermally very stable as would be expected for substitutional Pr on a Ga site. However, this observation differs markedly from the annealing behavior of Er in GaAs, which exhibits strong dependence of the 1.55 micron emissions upon the annealing temperature, and was attributed to different Er luminescent centers activating at different RTA temperatures (Colon, 1992a:68). The Pr emission peaks are seen to rise and fall together as the RTA temperature is changed. This concurrent change of both emission groups points to the idea of a common Pr luminescent center at the substitutional site.

Pr Luminescence Dependence on Dose

Changing the RE dose may either increase or decrease the RE luminescence. Higher doses do introduce more potentially luminescent centers, however, accompanying the greater RE density is the problem of solubility limits. Above the solubility limit, impurities form precipitates which cause major lattice defects due to the volume mismatch. Exceeding this solubility limit has been shown to extinguish RE PL. For example, Favennec and coworkers saw a decrease in GaAs:Er PL for very high Er doses and attributed this to absorption from unannealed implant damage (Favennec *et al.*, 1989:333). The Er solubility limit was quantified to be about 7×10^{17}/cc, where, above this limit, Er forms near spherical microparticles of ErAs which are not luminescent (Poole *et al.*, 1992:121). However, Langer *et al.* reported that Er-related PL in MOCVD-grown GaAs:Er was a maximum at an Er concentration of 1.2×10^{19}/cc (Langer *et al.*, 1993:15). Higher implantation doses may also decrease the luminescence because of increased lattice damage. The defects in an amorphous lattice can trap free carriers where they will non-radiatively recombine through a continuum of states (Pankove, 1971:165), thus robbing the RE of luminescence fuel in the form of free carriers and excitons.

The purpose of this study is to determine the optimal implantation dosage for PL in each host material and to estimate the solubility limit of Pr impurity concentration in the host lattice. The doses used were 5×10^{12}, 1×10^{13}, and 5×10^{13}/cm^2 in each of the optimally annealed SI-hosts used in the RTA study. Figures 14, 15, 16, and 17 show the low temperature PL spectra of Pr at these doses in hosts of SI-GaAs, SI-$Al_{0.15}Ga_{0.85}As$, SI-$Al_{0.30}Ga_{070}As$, and SI-$Al_{0.50}Ga_{050}As$, respectively. The SI-GaAs case shown in Figure 14 is interesting because the optimal dose is different for the two emission groups. The strongest $^1G_4\rightarrow{}^3H_5$ emissions were observed from the sample with a dose of 1×10^{13}/cm^2, while the $^3F_3\rightarrow{}^3H_4$ group

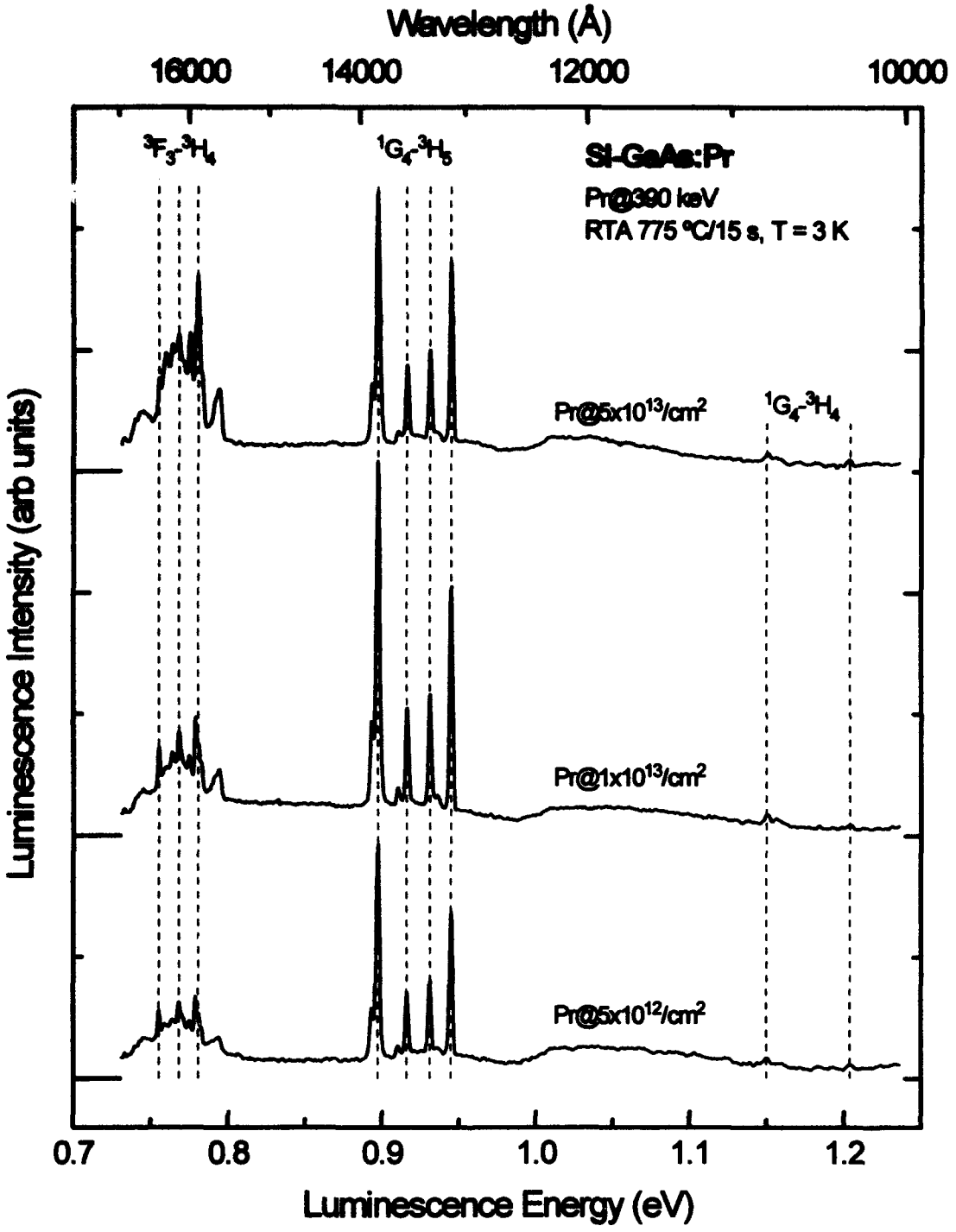

Figure 14. Photoluminescence spectra taken at 3 K for SI-GaAs implanted with Pr at 390 keV with a dose of 5×10^{12}, 1×10^{13}, or 5×10^{13}/cm^2 and annealed at 775 °C

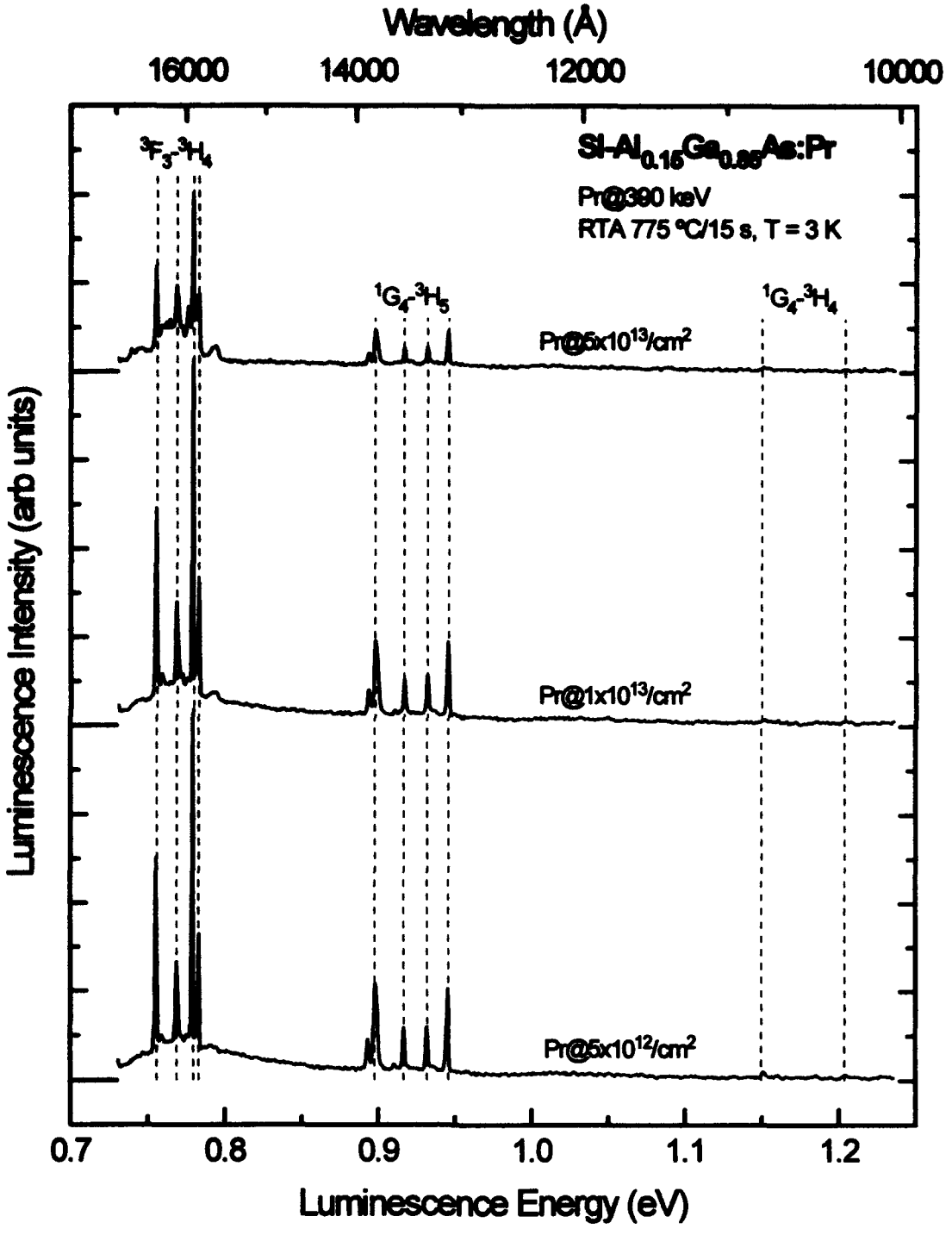

Figure 15. Photoluminescence spectra taken at 3 K for SI-$Al_{0.15}Ga_{0.85}As$ implanted with Pr at 390 keV with a dose of 5×10^{12}, 1×10^{13}, or 5×10^{13}/cm^2 and annealed at 775 °C

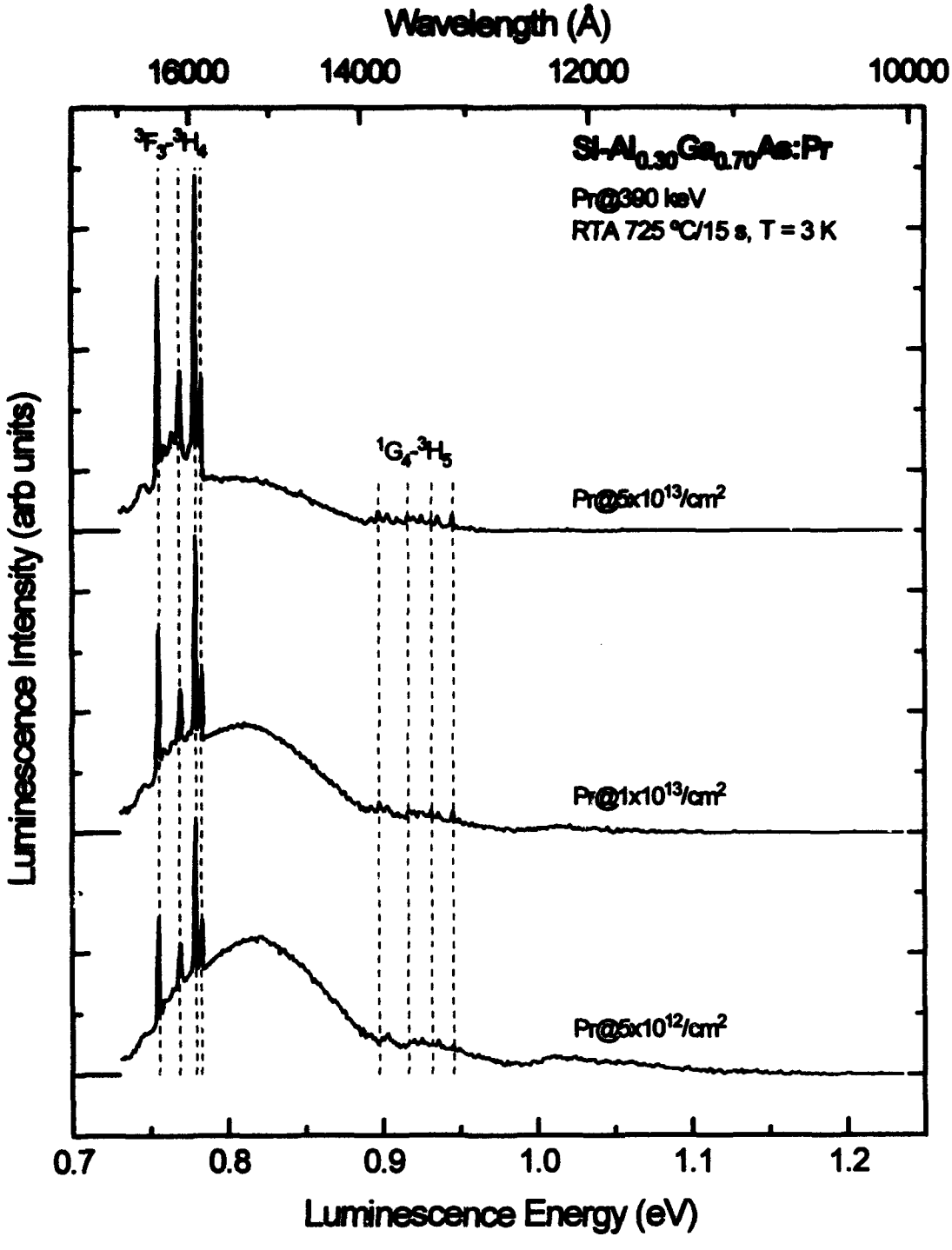

Figure 16. Photoluminescence spectra taken at 3 K for SI-$Al_{0.30}Ga_{0.70}As$ implanted with Pr at 390 keV with a dose of 5×10^{12}, 1×10^{13}, or $5\times10^{13}/cm^2$ and annealed at 725 °C

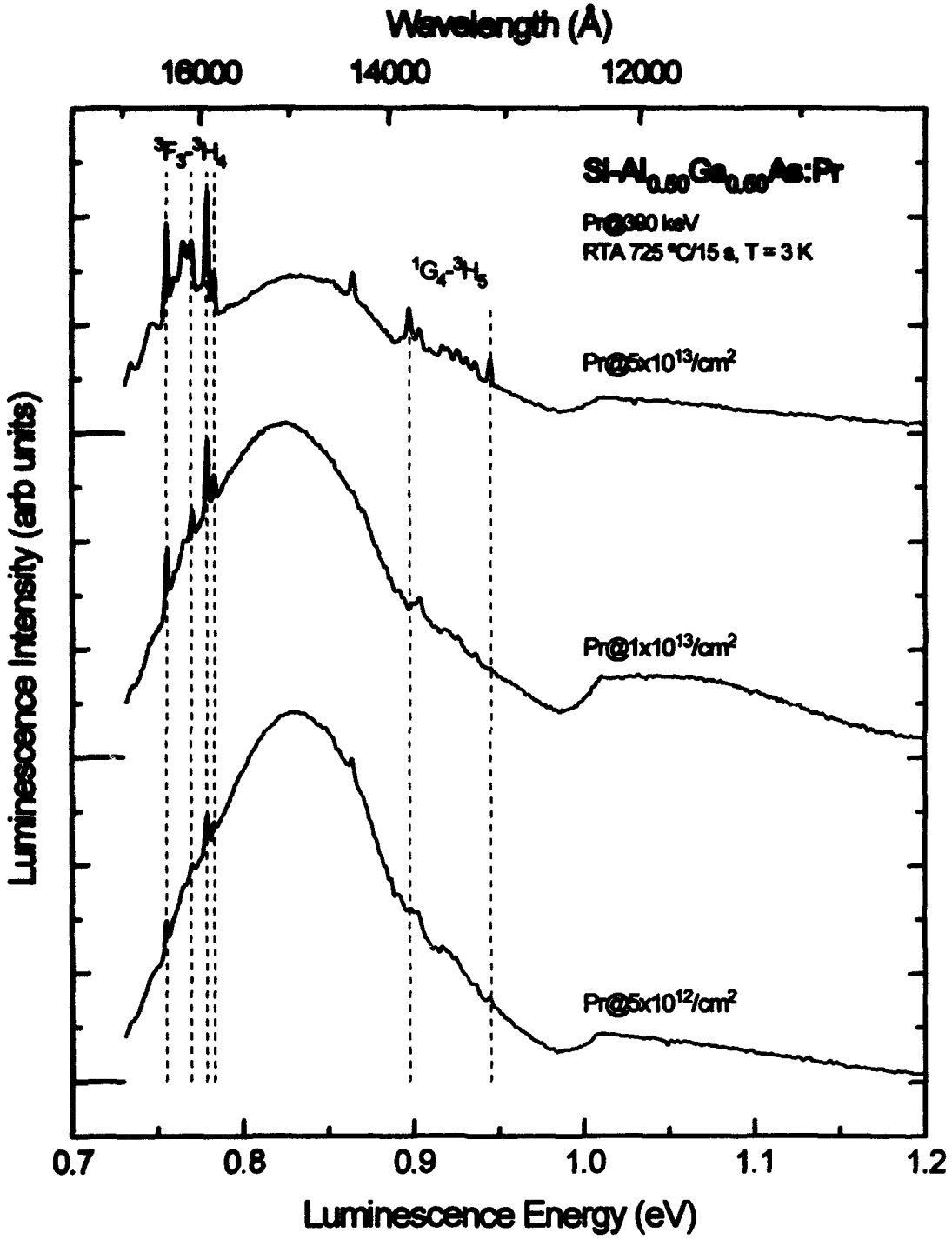

Figure 17. Photoluminescence spectra taken at 3 K for SI-$Al_{0.50}Ga_{0.50}As$ implanted with Pr at 390 keV with a dose of 5×10^{12}, 1×10^{13}, or $5\times10^{13}/cm^2$ and annealed at 725 °C

TABLE 12

Optimal Pr Dose for PL from Pr in SI-$Al_xGa_{1-x}As$

Host:Pr	Best PL Dose (cm^{-2})
SI-GaAs:Pr	1×10^{13} ($^3F_3\rightarrow{}^3H_4$) 5×10^{13} ($^1G_4\rightarrow{}^3H_5$)
SI-$Al_{0.15}Ga_{0.85}As$:Pr	$0.5,1\times10^{13}$
SI-$Al_{0.30}Ga_{0.70}As$:Pr	5×10^{13}
SI-$Al_{0.50}Ga_{0.50}As$:Pr	5×10^{13}

intensity increased with dose. The middle dose was chosen for use in subsequent experiments, since this results in the strongest and sharpest peaks in the $^1G_4\rightarrow{}^3H_5$ emission group. For the SI-$Al_{0.15}Ga_{0.85}As$ host, the PL intensities of Pr emissions were about the same for the two lower doses (Figure 15), however, the lowest dose gave a slightly higher PL in both groups, and was chosen as the best dose. The SI-$Al_{0.30}Ga_{0.70}As$ host shown in Figure 16 along with the SI-$Al_{0.50}Ga_{0.50}As$ host shown in Figure 17 displayed $^3F_3\rightarrow{}^3H_4$ emissions which increased with dose. Both spectra also show a broad defect-related emission centered around 0.82 eV, which decreases with increasing Pr dose. This can be explained if Pr and the defect center compete for the same energy source presumed to be free excitons or carriers. Thus, the increased Pr luminescence robs the defect centers of their pumping source. Alternatively, as the Pr concentration increases, the recombination energy of the defect-related center may transfer its energy more effectively to Pr^{3+} ions nonradiatively.

Table 12 summarizes the optimum Pr dose determined for each of the tested hosts based on the strongest PL peaks, although a limited number of dose variants was used. Since the implant profile is a Gaussian, the homogeneous concentration

solubility limit can not be determined. However, for reference, the peak concentration in Gaussian implant profile was computed using Eq (3) and Table 8. They are calculated to be 3×10^{18}/cc for the 0.5×10^{13}/cm^2 dose, 6×10^{18}/cc for the 1×10^{13}/cm^2 dose, and 3×10^{19}/cc for the 5×10^{13}/cm^2 dose.

Pr Luminescence Dependence on the Host Conductivity Type

The purpose of this study is to examine the effect of host carrier-type dopants on Pr photoluminescence. Semiconductors are routinely doped with impurities to alter the type and concentration of mobile carriers in order to control their electrical characteristics. In addition, RE luminescence has been shown to depend on free carriers (as excitons). Dopant elements are chosen to have valence characteristics different from those of the host in order to add free carriers (either electrons or holes). These free carriers can absorb recombination energy of free excitons via an Auger process, thus robbing the RE's pumping energy.

For this study, MOCVD-grown GaAs and $Al_xGa_{1-x}As$ hosts of x=0.15, 0.30, and 0.50 were available in SI-, n-, and p-type versions and were identically implanted with Pr. Samples were then annealed at the optimal temperatures determined for each host. Low temperature PL spectra from each variant were then examined to determine the effect of carrier-type doping of hosts. The impurities were Si for the n-types and Zn for the p-types which were doped during the MOCVD growth process. The vendor Epitronics reports that carrier concentrations in both were 1.0×10^{17}/cc.

Figure 18 shows that the Pr PL is much stronger for the SI-type $Al_{0.15}Ga_{0.85}As$ host than either the n- or p-type variants. Both emission groups suffer strong reductions in intensity with the addition of either n- or p-type dopants. Similar results were also observed for Pr PL in the $Al_{0.30}Ga_{0.70}As$ host. This probably represents an effect similar to that found in the dose dependence (Figure 16), where the Pr competes

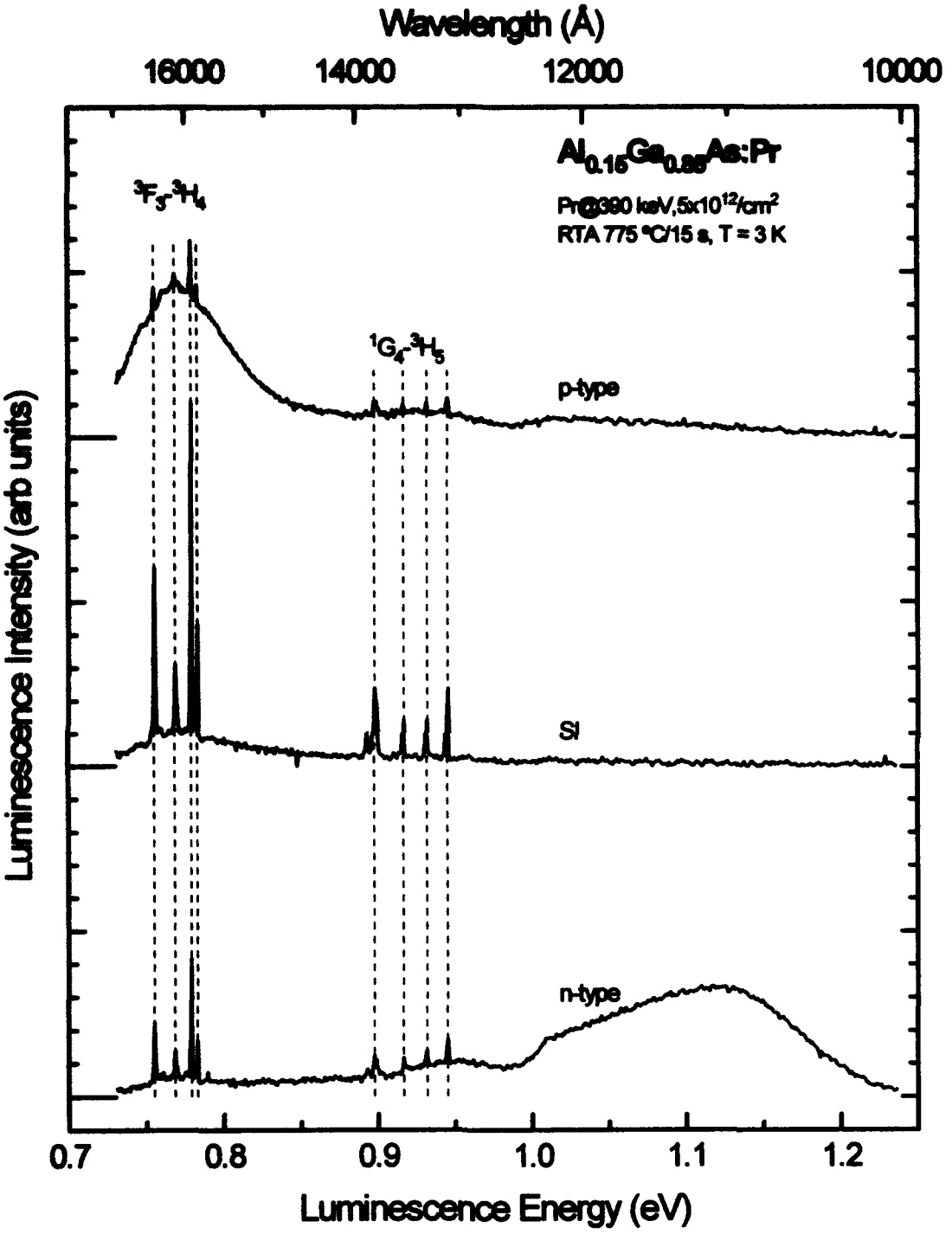

Figure 18. Photoluminescence spectra taken at 3 K for n-, SI-, and p-$Al_{0.15}Ga_{0.85}As$ implanted with Pr at 390 keV with a dose of 5×10^{12} and annealed at 775 °C

with other impurity or defect-related centers for the pumping energy of excitons/carriers or deactivation of Pr PL via non-emissive complexes formed with the extra impurities. Figure 18 supports the former theory, since strong defect emissions are evident in the doped hosts at 0.77 and 1.15 eV. This effect, in which donors and acceptors act as "shunt" recombination centers, has been noted by others studying REs (Lozykowski, 1993:17761). If this effect is dominant in moderate- to heavily-doped electroluminescent devices, Pr luminescence may be weak or non-existant due to this apparent inability to compete successfully against other impurities for the supply of free carriers or excitons.

A different PL result was found for the conductivity-type dependance of GaAs and $Al_{0.50}Ga_{0.50}As$ host as shown in Figures 19 and 20 respectively. These hosts showed increased Pr PL for both n-type and p-type doping than PL for undoped materials. The exception was the n-type GaAs which displayed a very strong, broad defect spanning 0.75 through 1.15 eV (Figure 19). The Pr lines were apparently completely quenched by the effects of this defect-related peak. The apparent n-type host peak at 1.0 eV is an artifact of the experimental system response and water absorption lines can be seen between 0.8 and 0.9 eV. Otherwise in these two hosts, the two main Pr emissions groups showed an increase in intensity of several times compared to the SI-type host.

Pr Luminescence Dependence on Host Semiconductor

Investigating the effects of changing the host semiconductor can reveal dependence of the Pr PL on controllable factors. In this study, the Al mole fraction x in SI-$Al_xGa_{1-x}As$ hosts was varied from 0 to 0.50. There are 3 major effects of the Al on the host which may affect Pr luminescence. These are 1) the increase in the bandgap with increasing aluminum fraction, 2) the alteration of the crystal field and

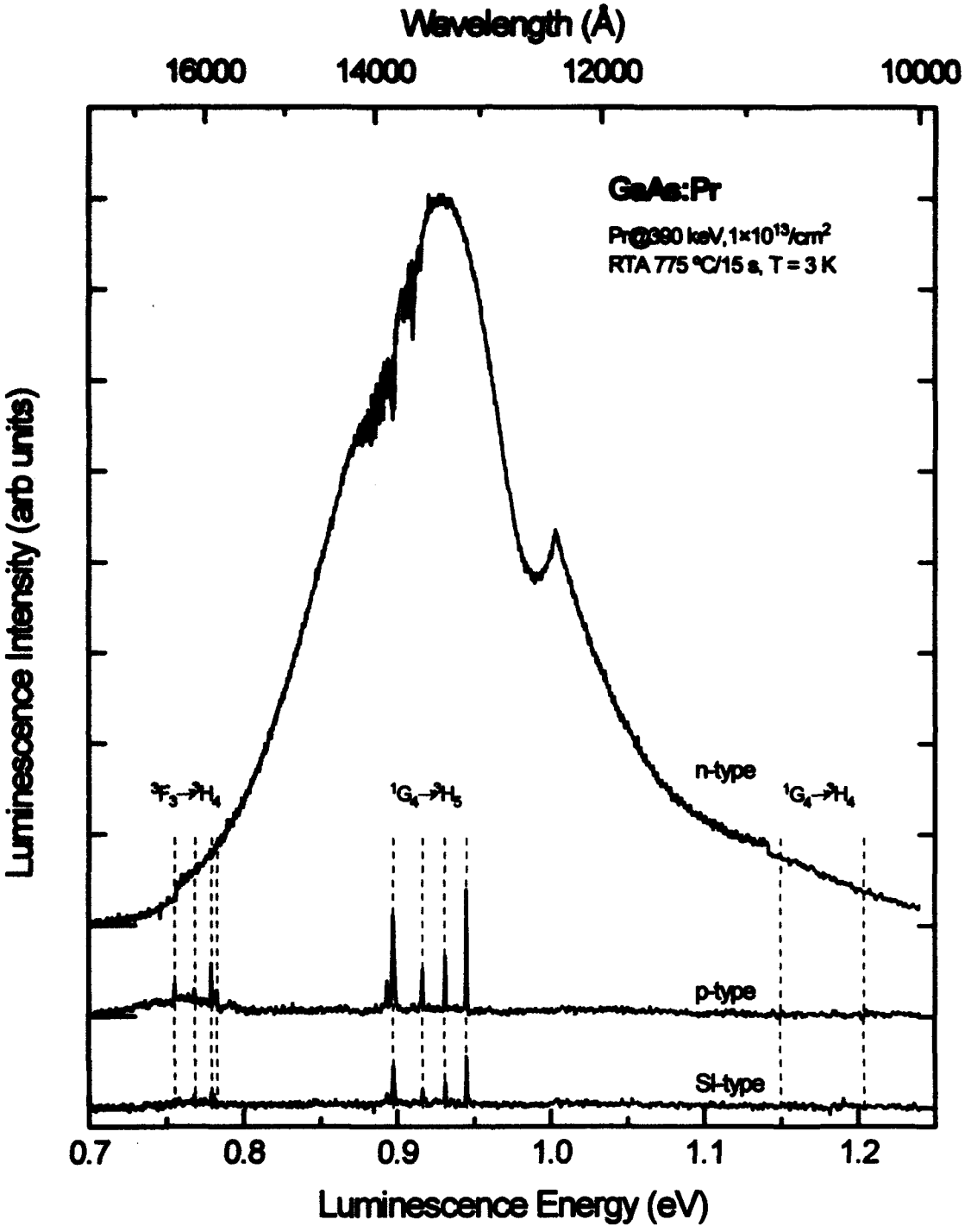

Figure 19. Photoluminescence spectra taken at 3 K for n-, SI-, and p-GaAs implanted with Pr at 390 keV with a dose of 1×10^{13} and annealed at 775 °C

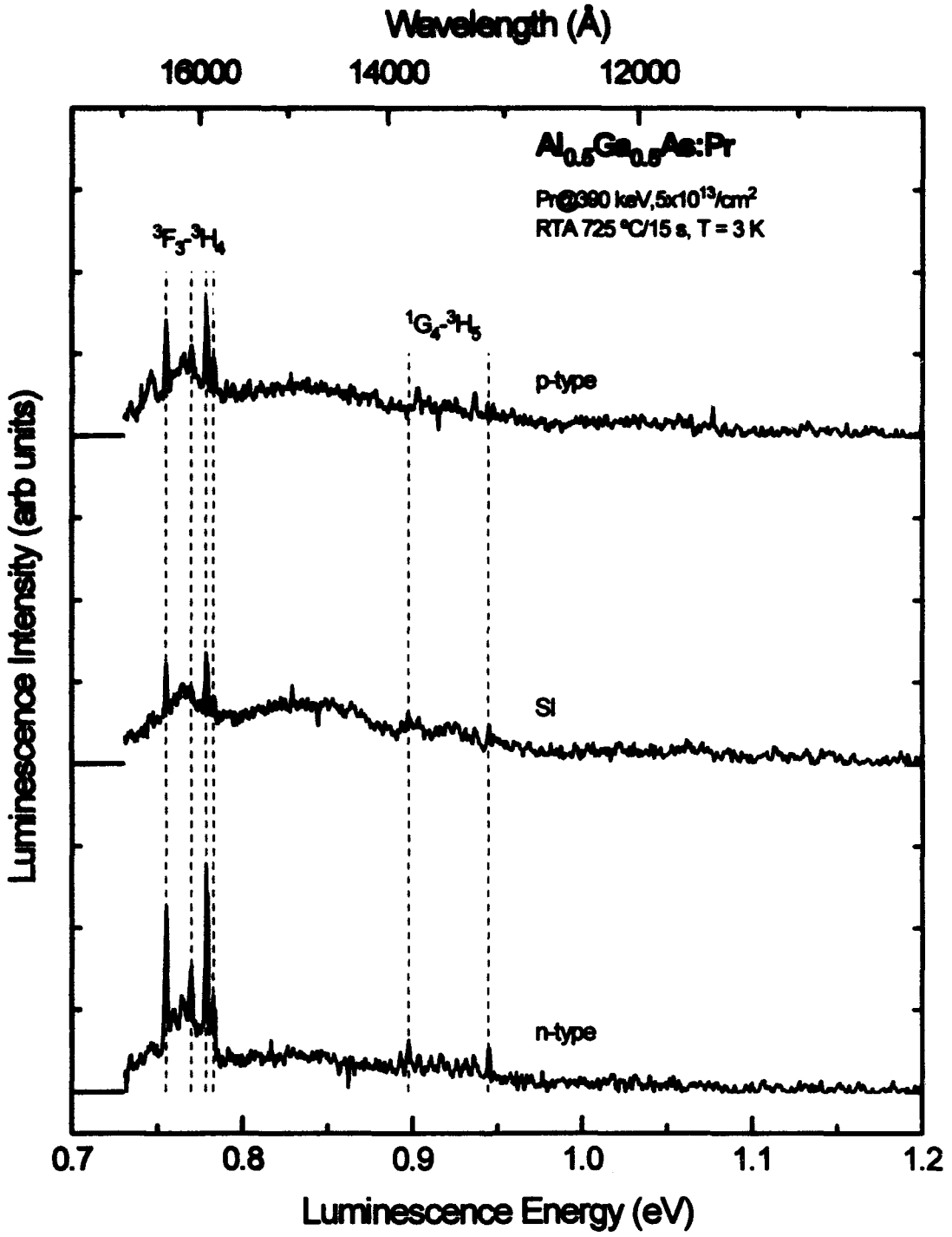

Figure 20. Photoluminescence spectra taken at 3 K for n-, SI-, and p-$Al_{0.50}Ga_{0.50}As$ implanted with Pr at 390 keV with a dose of 5×10^{13} and annealed at 725 °C

symmetry induced by the Al atoms, and 3) formation of Al-Pr complexes. For these hosts, the low temperature direct bandgaps are 1.519 eV (x=0), 1.733 eV (x=0.15), and 1.940 eV (x=0.30) (El Allai *et al.*, 1993:4403), while the x=0.50 case produces an indirect bandgap of about 2.07 eV (Alferov *et al.*, 1973:1622). Wider bandgaps create higher energy free excitons and span greater energy levels in the Pr ions, potentially producing a more diverse set of intra-4f transitions. Alteration of the crystal field and symmetry due to the presence of Al atoms in the lattice reduces the symmetry thus increasing the number of crystal field split states of all free ion energy levels. Increasing the aggregate levels available for transitions is likely to increase the number of emission lines, but concurrently may decrease the intensities. Finally, the presence of Al atoms in an otherwise GaAs lattice may be considered to be high density impurities which can form binary complexes with the Pr ions. Not enough is understood about RE-impurity complexes to predict whether the Pr luminescence from such a complex would be greater or lesser than that from an 'isolated' Pr ion.

In this study, Pr was implanted at 390 keV with a dose of $1\times10^{13}/cm^2$ in hosts consisting of SI-GaAs and SI-$Al_xGa_{1-x}As$ with x=0.15, 0.30, and 0.50. Annealing was conducted using the optimal temperature for each host. Low temperature PL data was collected on each sample under otherwise identical conditions.

It was found that changing the Al fraction in the hosts had a dramatic effect on the Pr luminescence as shown in Figure 21. While the 0.9 eV emission group is dominant in the PL from GaAs hosts, the 0.75 eV group is strongly dominant in all Al-bearing hosts with x≥0.15 and appears to be quite abrupt. In GaAs, the $^1G_4\rightarrow{}^3H_5$ Pr emission group intensity dominates that of the weak $^3F_3\rightarrow{}^3H_4$ emission group. In $Al_{0.15}Ga_{0.85}As$, this behavior is reversed with the $^3F_3\rightarrow{}^3H_4$ Pr emission group showing much stronger intensity than that of $^1G_4\rightarrow{}^3H_5$, which has intensity and peak profiles almost identical to those of GaAs:Pr. As the Al mole fraction in the host increases to

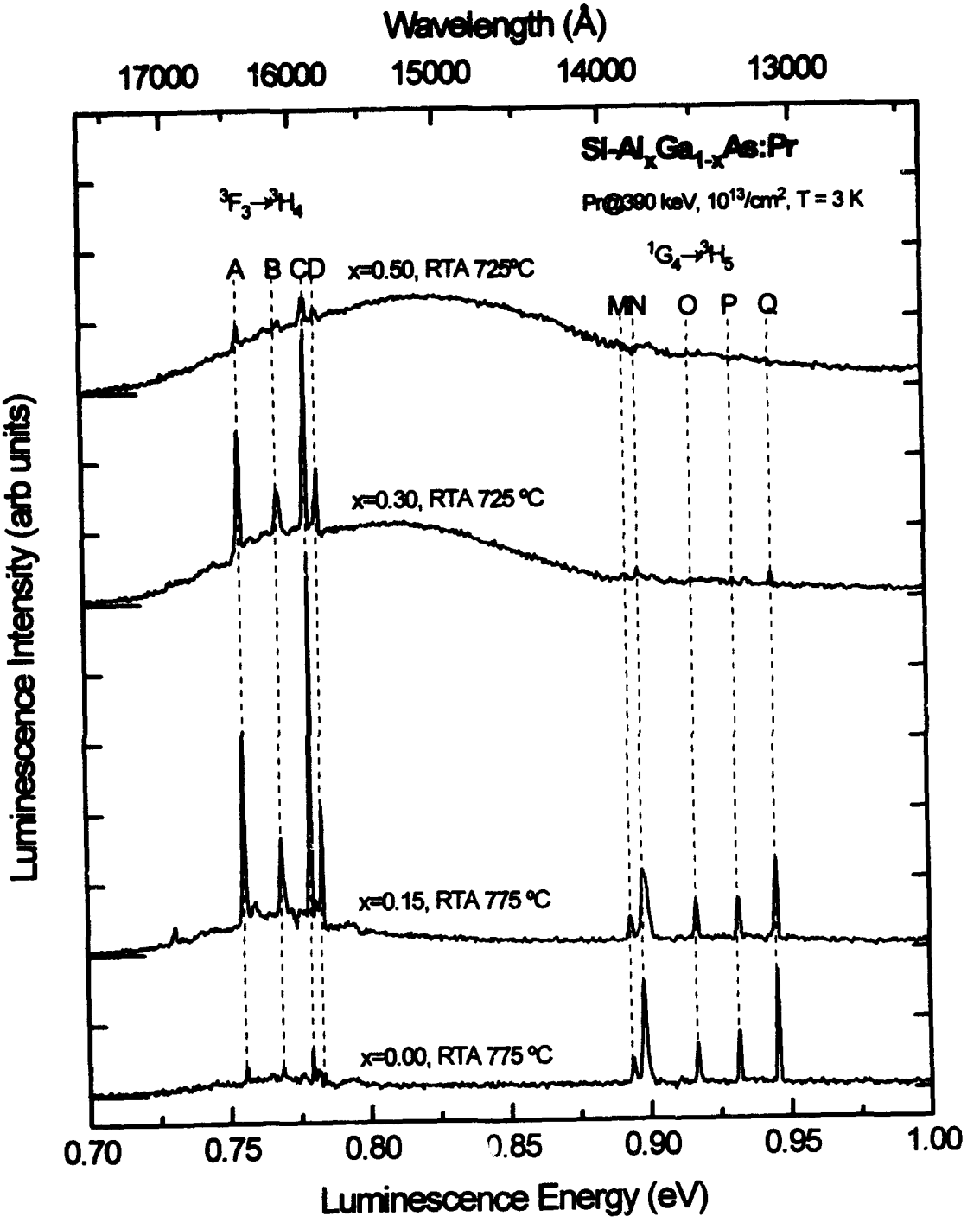

Figure 21. Photoluminescence spectra taken at 3 K for SI-GaAs, SI-$Al_{0.15}Ga_{0.85}As$, SI-$Al_{0.30}Ga_{0.70}As$, and SI-$Al_{0.50}Ga_{0.50}As$ implanted with Pr at 390 keV with a dose of $10^{13}/cm^2$ and annealed at various temperatures

0.30, and 0.50, the still dominant $^3F_3 \rightarrow {}^3H_4$ Pr emission group is significantly reduced and the $^1G_4 \rightarrow {}^3H_5$ group is almost undetectable. Clearly the Al somehow causes preferential de-excitation of the Pr through the $^3F_3 \rightarrow {}^3H_4$ transitions, but this effect does not follow the Al density in general since higher Al mole fractions reduce the absolute intensity.

Figure 21 also shows the consistent position of the emission lines across all hosts. To simplify reference to these many separate Pr emission lines, each of the main peaks was assigned a designator based on very close energy positions across all hosts and relative peak intensities within the emission groups. These letter designators are shown above their assigned peaks in Figure 21 and these energy assignments are summarized in Table 13 along with other strong lines. Table 13 lists the most exact position of each emission line determined in this study along with hot lines (shown in italics), which will be discussed in a later section on temperature behavior of the Pr PL. The emission lines labeled U and V are very weak (see Figure 11), but clearly visible in GaAs while U is only barely detectable in $Al_{0.15}Ga_{0.85}As$:Pr and not seen at all in $Al_{0.30}Ga_{0.70}As$:Pr or $Al_{0.50}Ga_{0.50}As$:Pr. In only Al-bearing samples an additional peak occurs at 0.778 eV (C0), which is not seen in GaAs hosts. This C0 peak is very near the C peak seen in all hosts and probably results from increased crystal field splitting of the energy levels due to the lower symmetry in $Al_xGa_{1-x}As$ compared to GaAs. The nearly identical energy positions and relative intensities of the remaining peaks within Pr emission groups in all hosts strongly implies that the Pr center responsible for luminescence is on the cation site. Only Ga or Al sites preserve local symmetry across all AlGaAs hosts because all four nearest neighbors are arsenic in all hosts. A centered interstitial position of a Pr^{3+} ion in T_d symmetry would likely include varying numbers of Al atoms as nearest neighbors. The average number of these neighboring Al atoms will increase with Al mole fraction, thus increasingly

TABLE 13

Main Pr^{3+} PL Emission Lines in SI-$Al_xGa_{1-x}As$

		Pr^{3+} Energy Transition Peak, Host (eV±0.0002)				
Designator	Transition	GaAs,LEC	$Al_{0.15}GaAs$	$Al_{0.30}GaAs$	$Al_{0.50}GaAs$	Wavelength (μm)
A	$^3F_3 \rightarrow {}^3H_4$	0.7557	0.7555	0.7555	0.7554,68	1.64
B	$^3F_3 \rightarrow {}^3H_4$	0.7688	0.7688	0.7693	0.7698 (?)	1.61
HL1	$^3F_3 \rightarrow {}^3H_4$	*0.7723*	*0.7726*	*0.7728*		
HL1a	$^3F_3 \rightarrow {}^3H_4$		*0.7750*	*0.7752*		
C0	$^3F_3 \rightarrow {}^3H_4$		0.7785	0.7786	0.7787	
C	$^3F_3 \rightarrow {}^3H_4$	0.7793	0.7794	0.7794	0.7795	1.59
D	$^3F_3 \rightarrow {}^3H_4$	0.7830	0.7833	0.7834	0.7830	1.58
HL2	$^3F_3 \rightarrow {}^3H_4$		*0.7893*	*0.7894*		
M	$^1G_4 \rightarrow {}^3H_5$	0.8933,36	0.8932	?	?	1.39
HL3	$^1G_4 \rightarrow {}^3H_5$	*0.8942*	*0.8945*			
N...	$^1G_4 \rightarrow {}^3H_5$	0.8976	0.8977,88	0.8977	0.8974	1.38
O	$^1G_4 \rightarrow {}^3H_5$	0.9166	0.9169	0.9165	?	1.35
P	$^1G_4 \rightarrow {}^3H_5$	0.9315	0.9320	0.9311 (?)	?	1.33
HL4	$^1G_4 \rightarrow {}^3H_5$	*0.9342*				
Q	$^1G_4 \rightarrow {}^3H_5$	0.9453	0.9455	0.9451	0.9452	1.31
U	$^1G_4 \rightarrow {}^3H_4$	1.150	1.15			1.08
V	$^1G_4 \rightarrow {}^3H_4$	1.204				1.03

distorting the local symmetry around As sites or interstitials, but not Ga or Al sites. This increased distortion should be manifest as increased numbers of crystal field split states with an accompanying increase in the number of PL transitions. This is simply not seen as the PL peaks are very consistent in energy position and group profile across the $Al_xGa_{1-x}As$ hosts. This is further evidence that luminescent Pr occupies a substitutional position in the host on the Al or Ga sites.

The assignment of these PL transitions to the states of specific levels allows construction of an energy level diagram for the Pr^{3+} ion in $Al_xGa_{1-x}As$. This diagram

is based on the common strong emissions identified in all hosts and depends on the assumption that low temperature de-excitation starts at the lowest state of the excited upper level. That is, after excitation to some arbitrary state in an upper level, the electron thermalizes to the lowest state in the level before making a radiative transition to any of the manifold of the crystal field split lower level states. Figure 22 shows the energy structure of those Pr^{3+} ion levels attributed to PL transitions observed in this study. Due to the weakness of all emissions in the higher Al mole fraction hosts, not all transition peaks can be identified, but emission peak energies and crystal field split widths are common throughout the series. The apparent full width of the crystal field split $^3H_4$ level is 28 meV with 3 to 5 identifiable peaks, while that of the $^3H_5$ level is 52 meV with 5 or fewer identifiable peaks.

Some previous reports provide instructive comparisons to these results. As was already noted and expected, the GaAs:Pr PL is virtually identical to that reported by Pomrenke *et al.* (Pomrenke *et al.*, 1991b:418-419) and Erickson *et al.* (Erickson *et al.*, 1993:2348). Although Er emissions display the same consistency of emission line energies independent of Al mole fraction in AlGaAs, the intensity increases with Al mole fraction at least from x=0.1 through x=0.4 (Colon, 1992a:66-68). Colon attributed this Er PL behavior to either formation of optically active Al-Er complexes or reduced thermal quenching as a by-product of the increased host bandgap. Thulium also exhibits stronger PL intensity in AlGaAs than GaAs (Pomrenke *et al.*, 1992:1925).

The evidence from this limited number of Al mole fraction samples is augmented by parallel behavior from older samples of AlGaAs which provide not only corroboration, but expanded information on the Al mole fraction behavior of the Pr emissions. SI-$Al_{0.10}Ga_{0.90}As$ and SI-$Al_{0.20}Ga_{0.80}As$ wafers were implanted with Pr at 390 keV with a dose of $1\times10^{13}/cm^2$ and annealed at 750 °C for 15 seconds. The Pr emissions displayed in Figure 23 for the x=0.10 sample are very similar to those of the

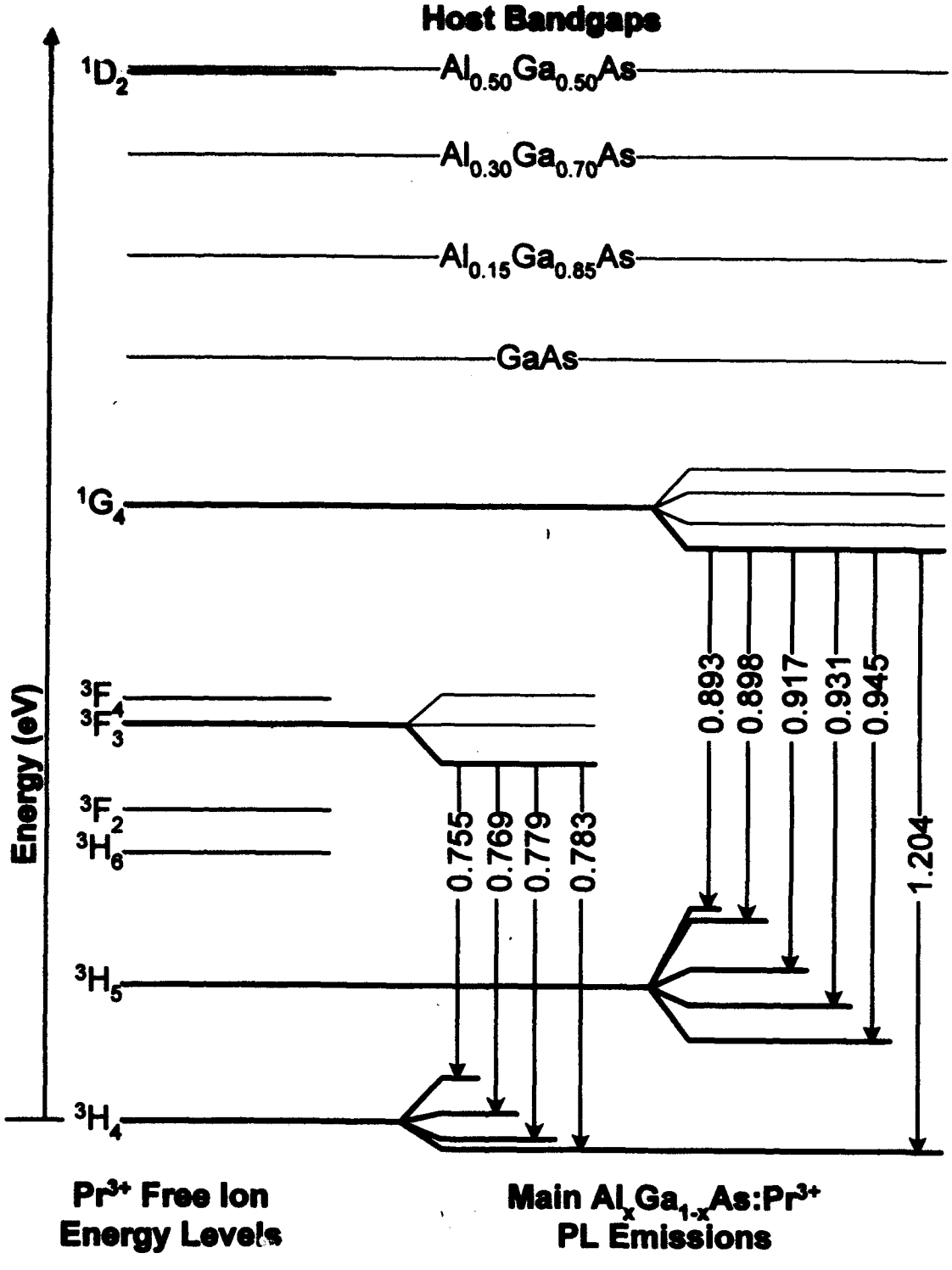

Figure 22. Energy levels and crystal field split states of Pr^{3+} in $Al_xGa_{1-x}As$ compared to semiconductor host bandgaps

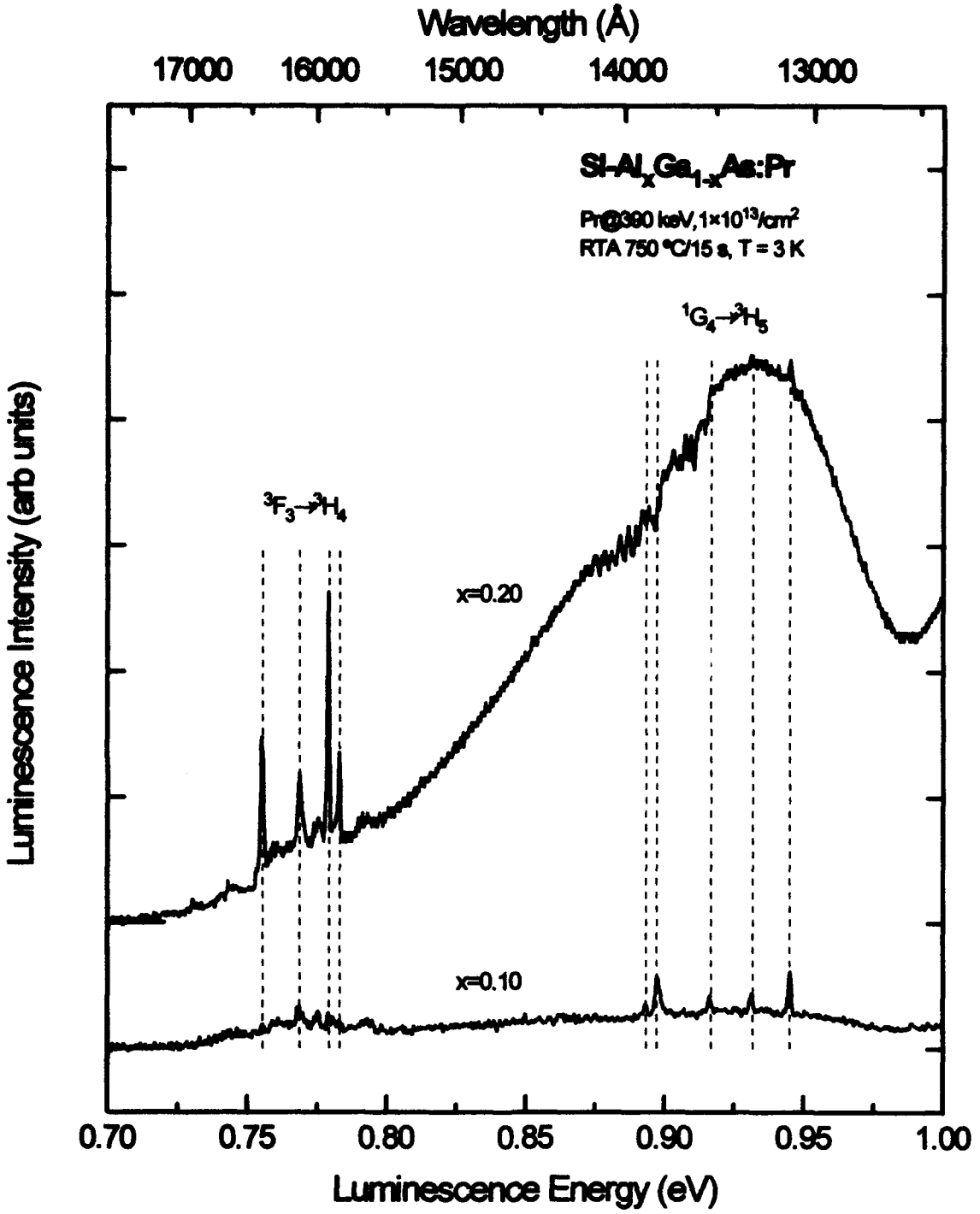

Figure 23. Photoluminescence spectra taken at 3 K for SI-$Al_{0.10}Ga_{0.90}As$ and $Al_{0.20}Ga_{0.80}As$ implanted with Pr at 390 keV with a dose of $1\times10^{13}/cm^2$ and annealed at 750 °C

GaAs shown earlier with the $^1G_4 \rightarrow {}^3H_5$ group intensity dominating the $^3F_3 \rightarrow {}^3H_4$ group, while the x=0.20 sample shows the opposite behavior. Although the x=0.20 sample spectra displays a broad defect emission near 0.92 eV and water absorption between 0.87 and 0.93 eV, the $^3F_3 \rightarrow {}^3H_4$ group of Pr^{3+} dominates the much weaker $^1G_4 \rightarrow {}^3H_5$ group which is characteristic of samples with Al mole fractions greater than 0.15. The Pr emission intensity behavior of these samples shows that the switch to stronger $^3F_3 \rightarrow {}^3H_4$ emissions occurs at an Al mole fraction above x=0.10. Combining this with earlier data, the Al mole fraction at which the Pr emission group intensity switch occurs is between x=0.10 and 0.15. This behavior also presents further evidence against Al atoms themselves as the cause for the intensity shift in Pr emission groups.

Pr Luminescence Dependence on Excitation Power

Determination of the behavior of Pr luminescence as a function of laser pumping power is a requirement to guarantee the reliability and consistency of results and can yield information on the excitation process as well. It is important to keep sample heating to a minimum, since the concurrent expansion of the lattice can alter the experimental results. Operation of the laser at a power below saturation of the Pr luminescence is desirable to minimize the effects of laser-induced sample heating. The PL intensity variance with laser power for the 0.779 eV peak of SI-$Al_{0.15}Ga_{0.85}As$:Pr is shown in Figure 24. This is representative of the behavior of all lines in all hosts. Three different laser apertures were required since no one aperture value can span the entire range of power. As seen, operation of the laser in the 100 to 300 mW range, which was used in all experiments in this effort, is well below any conceivable saturation point.

No saturation power point for the Pr PL was detected in this study. No power above 700 mW was attempted because of possible sample damage, but the steadily

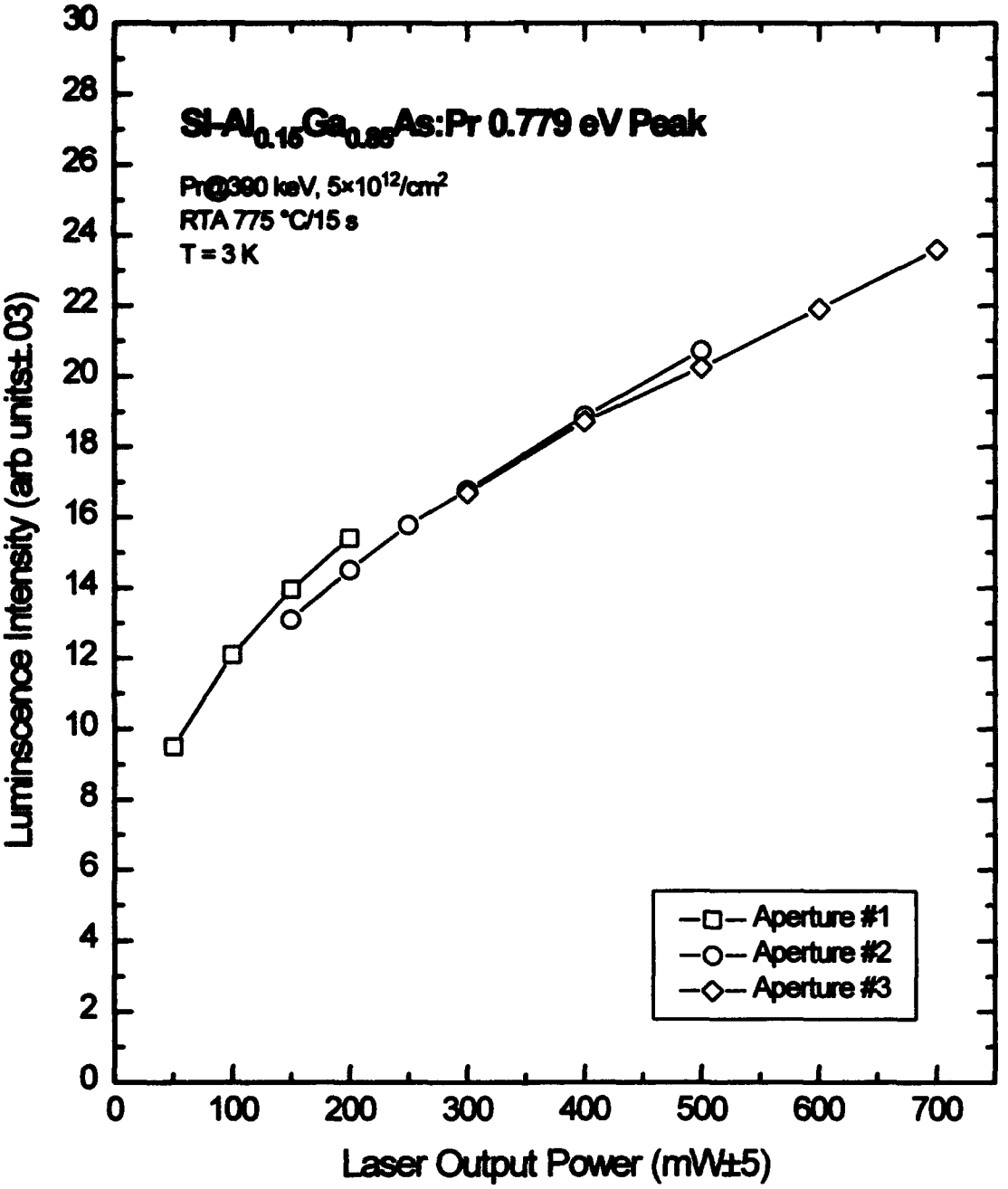

Figure 24. Behavior of the 0.779 eV peak of SI-$Al_{0.15}Ga_{0.85}As$:Pr with Ar^+ laser power

increasing intensity with power through 700 mW can be explained by paralleling the work of Benyattou *et al.* (Benyattou *et al.*, 1991:2133). These workers found a square root dependence of the PL intensity with laser power for the 1.54 μ emissions from $Al_{0.55}Ga_{0.45}As$:Er. Their explanation assumed the Er introduced an isoelectronic trap in the host bandgap which trapped excitons. The bound exciton recombination energy could then be transferred either to the Er atom or to a free carrier via an Auger process. The probability of this competing Auger process is then proportional to the density of free carriers. Defining the concentration of free carriers as n, then the likelihood of the bound exciton recombination energy transfer to a free carrier is Bn, where B is the transfer constant. The total probability for bound exciton energy transfer to the Er atom is given by (Benyattou *et al.*, 1991:2133)

$$\frac{P_e}{P_e + Bn}, \tag{9}$$

where P_e is the excitation rate of the Er atoms. The rate equation for Er excitation is then

$$\frac{dn_e^*}{dt} = A\phi \frac{P_e}{P_e + Bn} - \frac{n_e^*}{\tau_f}, \tag{10}$$

where n^*_e is the excited erbium concentration, $A\phi$ is the concentration of bound excitons proportional to the light flux ϕ, and τ_f is the Er fluorescence decay time constant. These workers further assumed a bimolecular recombination of the photogenerated carriers requiring that $n=B'(\phi)^{1/2}$ and that the Auger process dominates due to high flux rate. The steady state solution is then

$$n_e^* = \frac{\tau_f A P_e}{C} \sqrt{\phi}, \tag{11}$$

where $C=\hbar B'$. Thus the density of excited Er atoms, under these assumptions, is proportional to the square root of the pump power. This model can also be used to explain the behavior of the Pr intensity. The Pr PL intensities I in Figure 24 were fit to the equation

$$I = a + b\sqrt{P}, \tag{12}$$

where P is the laser pump power in milliwatts and a and b are the fitting parameters. A very good fit was obtained using $a=3.64\pm0.21$ and $b=0.84\pm0.02$ for the aperture 1 case, $a=3.88\pm0.13$ and $b=0.75\pm0.01$ for the aperture 2 case, and $a=3.74\pm0.45$ and $b=0.75\pm0.02$ for the aperture 3 case. The use of the simple offset parameter a was required for good fits and is justified as a correction factor corresponding to some background luminescence at this peak. The behavior of the Pr luminescence with laser power is well explained by this process showing that there is a substantial competition for the BE recombination energy between the Pr ions and Auger processes of free carriers.

Temperature Dependence of Pr Luminescence

In order to learn more about the nature of the Pr excitation mechanism, certain parameters of the photoluminescence experiment may be altered while examining the behavior of the Pr luminescence. One important parameter is the sample temperature. While the analysis of PL emission lines alone gives the transition energies, investigation of the temperature dependent changes in the PL spectra can give important information such as:

1) an expanded energy level structure via 'hot lines,'

2) the activation energies associated with the transitions corresponding to each spectral line or group, and

3) identification of different luminescent centers via distinct temperature dependent behavior of emission lines.

The expanded energy levels are determined through the rise of 'hot lines.' These are spectral lines not generally seen at very low temperature (<3 K), but which appear and grow as the temperature increases while the normal 'cold lines' are diminishing. Hot lines result from the thermal populating of higher than the lowest energy states in the upper level of an emissive transition. The energy state of the upper level can be assigned by assuming that the next lowest spectral line transitions to the same lower state or by using consistency between several hot lines.

The activation energy is more closely related to the excitation mechanism itself. The activation energy represents an energy step in the excitation mechanism responsible for the spectral line transition which is thermally deactivated as the temperature increases. This effect is manifest as the familiar decrease in cold line luminescence intensity as temperature increases. An example of a thermal depopulation mechanism is excitons bound to shallow impurity energy levels. As the temperature increases, the bound exciton eventually gains sufficient energy to break free from the impurity (dissociation). This temperature corresponds to the activation energy via the Boltzmann distribution. Another mechanism which thermally depopulates and is a plausible step in RE luminescence is electrons (or holes) bound to impurities (such as REs). These trapped carriers can form bound excitons and so represent another path to excitation. The activation energy in this case corresponds to the bound carrier ionization energy. Experimentally, luminescence which depends on bound exciton recombination at an impurity site would diminish substantially above this

temperature. By their very nature, hot lines also reduce the intensity of their accompanying emission group cold lines by decreasing the population of the lowest energy state in the upper transition level. The hot lines will then have an activation energy which will probably be different for each emission group since the crystal field splittings are probably not identically spaced.

Paralleling Bimberg *et al.* (Bimberg *et al.*, 1971:3451-3455), the activation energy (or energies) may be calculated by assuming a Boltzmann distribution for the exciton energy levels with ε_0 designated as the bound ground state and ε_1 as the single excited or dissociative energy state. (Note that there is no inconsistency in viewing the excitons or carriers in a PL-driven system as being in thermal equilibrium as distinct from the steady state excitation/de-excition processes. The only requirement which the excitons must meet is lifetimes sufficient for thermalization to equilibrium.) One next assumes a fixed total number of excitons $N_G(T)$ at a temperature T with $N_0(T)$ as the average number of bound excitons at T and $N_1(T)$ as the number of dissociated excitons. The conservation equation for this simple 2 level system is then given by

$$N_0(T) + N_1(T) = N_G(T). \tag{13}$$

The ratio of the Boltzmann distributed particles in energy levels ε_0 and ε_1 is

$$\frac{N_1(T)}{N_0(T)} = \frac{g_1}{g_0} e^{-(\varepsilon_1 - \varepsilon_0)/kT}, \tag{14}$$

where g_1 and g_0 are the degeneracies of the respective energy levels and k is Boltzmann's constant. Identical equations hold for the ratios of the populations of other energy levels if they are postulated. Combining these equations and assuming only 2 levels, the ground state ε_0 and the dissociative energy state ε_1, we obtain

$$N_G(T) = N_0(T)(1+\frac{g_1}{g_0}e^{-(\varepsilon_1-\varepsilon_0)/kT}). \tag{15}$$

The temperature dependence of $N_G(T)$ is not known and is taken to be a constant over the limited temperature range of interest. Actually, this assumption is valid for PL in which a constant laser power creates a constant density of electron-hole pairs forming excitons in the sample. This means that $N_G(T)=N_G(0)=N_0(0)$, so that

$$\frac{N_0(T)}{N_G(0)} = (1+c_1e^{-E_1/kT})^{-1}, \tag{16}$$

where $c_1=g_1/g_0$ and $E_1=\varepsilon_1-\varepsilon_0$. $N_0(T)/N_G(T)$ is thus the fractional number of excitons still bound and therefore available for the radiative recombination process. Thus the intensity of luminescence coupled to these bound excitons is proportional to the ground state population as a function of temperature is

$$\frac{I_T}{I_0} = \frac{N_0(T)}{N_G(0)} = (1+c_1e^{-E_1/kT})^{-1}, \tag{17}$$

where I_T is the luminescent intensity at temperature T and I_0 is the intensity at 0 K. Thus this equation relates the temperature dependence of the spectral line intensity to the activation energy E_1. The relative magnitude of the exponential coefficients represent the efficiency of the quenching mechanism corresponding to that activation energy.

Double activation energies are typically used in activation energy calculations for Er (Langer *et al.*, 1993, 19) and Yb (Thonke *et al.*, 1990:1128). These systems are considered to represent a three state process. Paralleling the previous derivation,

the behavior of the PL intensity resulting from a system with 2 activation energies is

$$\frac{I_T}{I_0} = (1 + c_1 e^{-E_1/kT} + c_2 e^{-E_2/kT})^{-1}, \tag{18}$$

where E_1 and E_2 are the activation energies and c_1 and c_2 are the corresponding degeneracy factors.

In practice, one records the integrated intensity of a specific peak at several temperatures and fits the data to Eq (17) or Eq (18) using I_T/I_0 and T as the independent variables with c_1 and E_1 (and c_2 and E_2) as the dependent variables. Computer programs such as Jandel's TableCurve can automatically find the best fit of the data to the exponential activation energy equation.

The primary thermal quenching mechanism which may be manifest as the activation energy for RE luminescence quenching is bound excitons dissociating from the Pr ion to free exciton states. This process deprives Pr ions of their localized energy source, thus quenching the luminescence. The actual energy E_X of a free exciton is based on a hydrogen-like model with the electron-hole pair orbiting their center of mass and is given by

$$E_X = \frac{-m_r^* q^4}{2\hbar^2 \varepsilon^2} \frac{1}{n^2}, \tag{19}$$

where m_r^* is the reduced mass of the electron and hole effective masses in the host, q is the unit charge, h is Planck's constant (here reduced by 2π), ε is the host semiconductor dielectric constant, and n is an integer ≥ 1 indicating exciton excited states (Pankove, 1971:12). Thus, the free excitons in a semiconductor have energies dependent on the host hole and electron effective masses and the material's dielectric constant. For $Al_xGa_{1-x}As$, these energies may be empirically described as a function of

the Al mole fraction x (Adachi, 1985:R18)

$$E_X(x) = 4.7 + 6.82x + 5.48x^2 \; meV . \tag{20}$$

Using this formula, one obtains free exciton energies of 4.7 meV for GaAs, 5.8 meV for $Al_{0.15}Ga_{0.85}As$, and 7.2 meV for $Al_{0.30}Ga_{0.70}As$.

Finally, the qualitative behavior of sets of emission lines within a single transition group can indicate the existence of multiple luminescent centers. A marked difference in the thermally-induced decay of intensity between two or more sets of lines in an emission group indicates differing excitation paths and correspondingly different centers. However, identical behavior of a set of lines is strong evidence for a common excitation mechanism.

For this study, Pr-implanted SI-GaAs, SI-$Al_{0.15}Ga_{0.85}As$, SI-$Al_{0.30}Ga_{0.70}As$, and SI-$Al_{0.50}Ga_{0.50}As$ hosts were optimally annealed as previously found. The temperature of each sample was varied and complete PL spectra were collected at each temperature. Normally filters are used to remove all but first order emissions to prevent obscuring the Pr luminescence. However, in this study the thermal behavior of the band-edge emissions is also of interest, so optical filters were used to allow second order band-edge emissions to be superimposed on the normal Pr spectra. Specifically, a 1000 nm long pass filter is normally used which should allow only first order emissions over the spectral range of 10000 to 20000 Å, whereas a 780 nm long pass filter was used in all temperature dependent runs allowing second order passage of the GaAs band-edge (8150 Å). An quantitative analysis of the emission peak intensity behavior will follow the review of temperature behavior for all hosts.

The temperature-dependant behavior of Pr photoluminescence for the SI-GaAs host is shown in Figure 25. Second order near-band-edge emissions are visible at energies of 0.729 eV and 0.747 eV. Because these emissions are second order, they

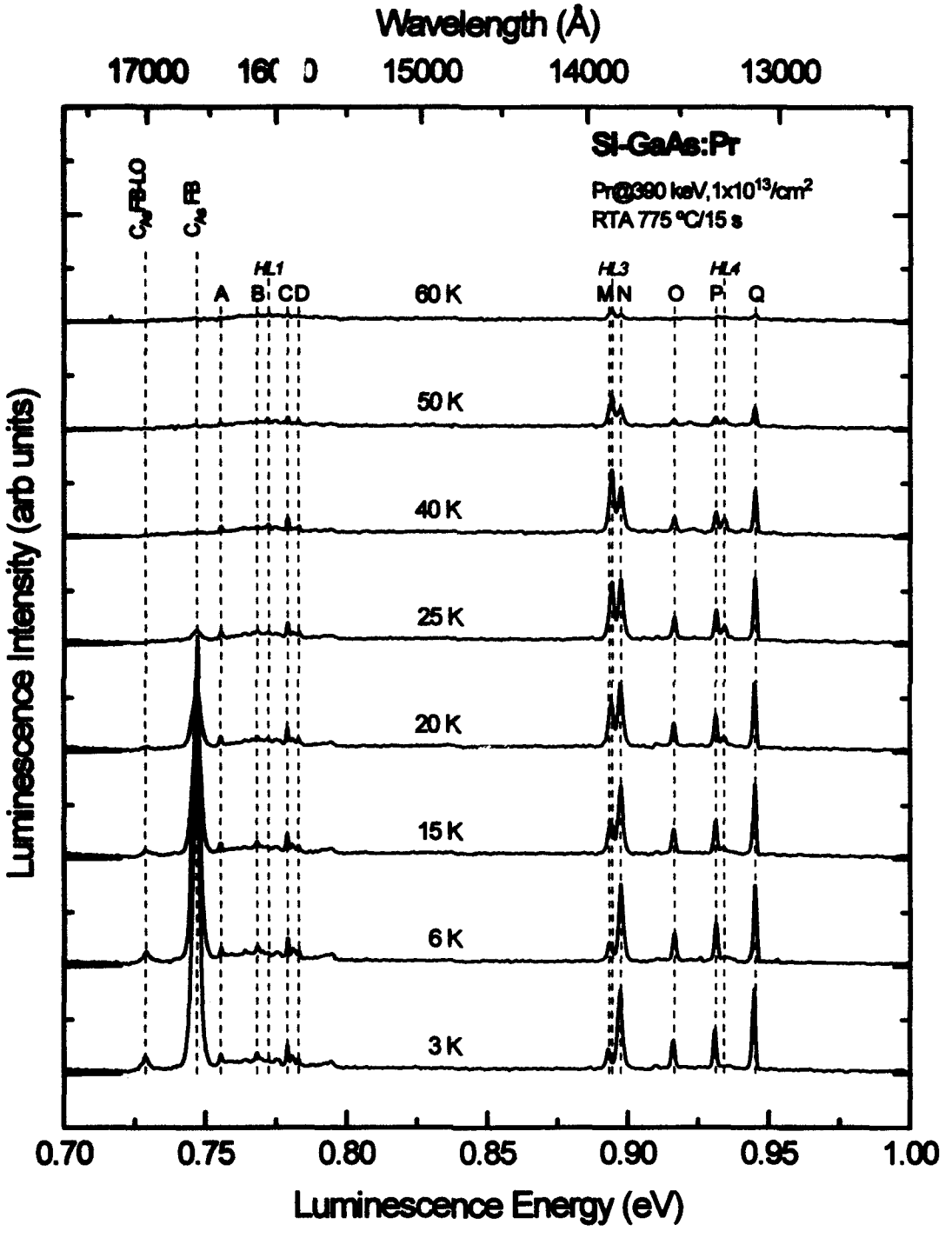

Figure 25. Photoluminescence spectra taken at various temperatures for SI-GaAs implanted with Pr at 390 keV with a dose of $1\times10^{13}/cm^2$ and annealed at 775 °C

are easily distinguished from the Pr emissions using appropriate long pass filters, but also by their much faster decay with temperature, although weak near-band-edge emissions are still clear even at 100 K. The 0.747 eV (1.494 eV/2) peak is commonly identified as emissions from the C on As site free-to-bound transition in GaAs, while the 0.729 eV (1.458 eV/2) corresponds to a GaAs LO phonon ($\sim$36 meV) replica of the 1.494 eV peak.

The now familiar 'cold' lines in each of the two main Pr emission groups, A, B, C, D, M, N, O, P, and Q are all distinct for sample temperatures of 3 through 50 K. Peaks in each of these emission groups decrease at the same rate while the 'hot' lines designated *HL1*, *HL3* and *HL4* all appear to increase intensity up through about 40 K. The exact energy position of all cold and hot lines was given in Table 13. *HL3* is very close to peak M with a separation of only 1 meV making resolution difficult at the slit widths required for a sufficient signal-to-noise ratio. The persistence of PL from Pr to temperatures higher than the temperature at which the band-edge emissions are completely quenched implies that the Pr trapping energy of an exciton is higher that the carbon acceptor level of 25 meV.

Like GaAs:Er, the Pr linewidths do not increase with T (within experimental resolution) or form phonon absorption-based emission lines (Favennec *et al.*, 1989:333). This suggests that the 4f intracenter transitions in the Pr-implanted material are not coupled to phonons. Additionally, the strong intensity of these suspected BE-related emissions at relatively high temperatures is not usually observed for BE transitions at donor/acceptor centers and is more typical of BE recombination at isoelectronic sites (Lozykowski, 1993:759). Upon this evidence, the optically active Pr sites are likely to be isoelectronic to the host lattice.

The stronger emissions of the SI-$Al_{0.15}Ga_{0.85}As$ samples allowed tracking of the luminescence of peaks A, B, C, and D as high as 100 K as displayed in Figure 26.

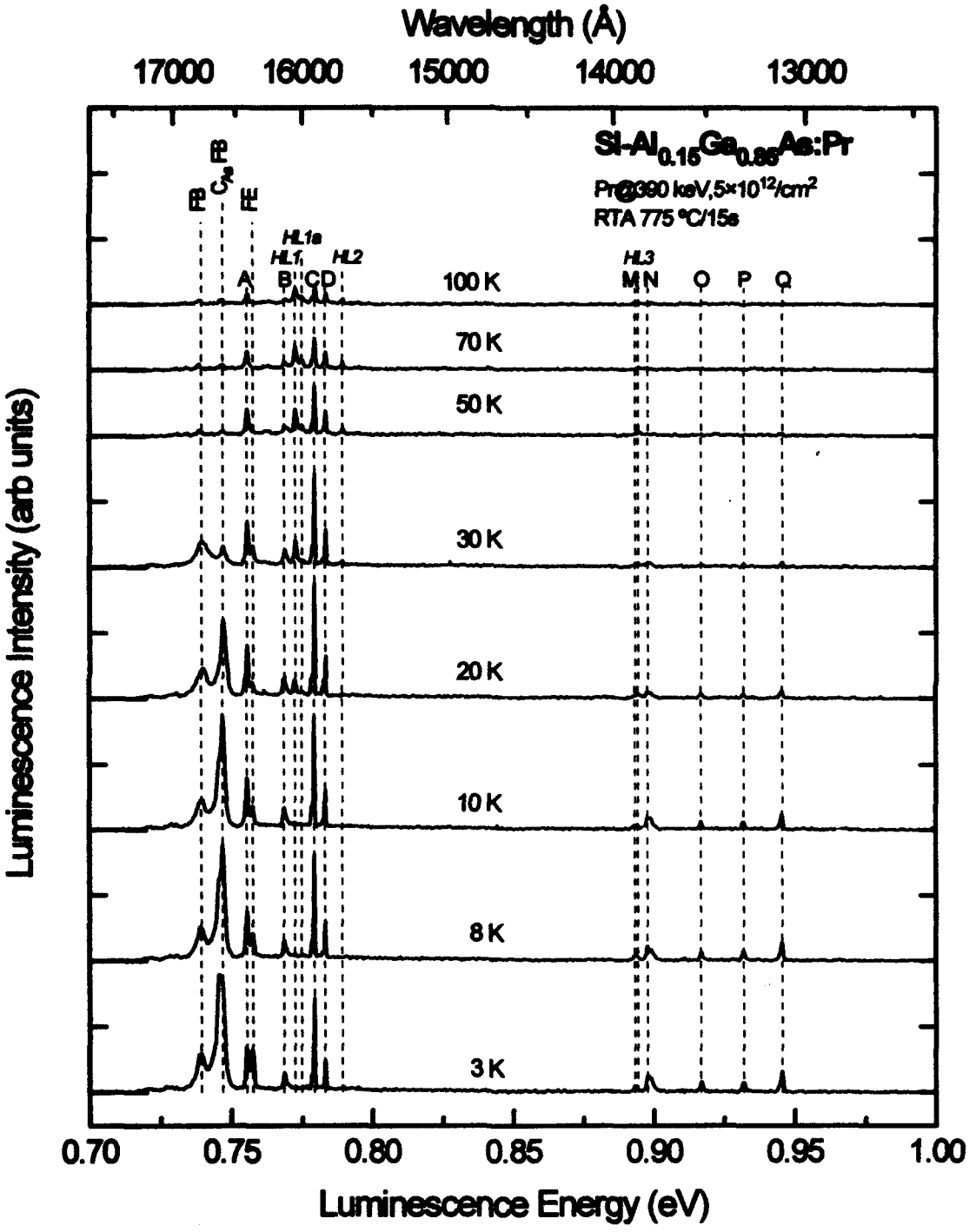

Figure 26. Photoluminescence spectra taken at various temperatures for SI-$Al_{0.15}Ga_{0.85}As$ implanted with Pr at 390 keV with a dose of $5\times10^{12}/cm^2$ and annealed at 775 °C

The weak peaks M, N, O, P, and Q were extinguished almost entirely above 30 K. More hot lines are evident than in the GaAs:Pr case. *HL1* peaks in intensity around 30 to 50 K, while the weaker *HL1a* and *HL2* grow up through about 70 K. *HL3* is weakly seen. The second order emission of the C_{As} FB 1.494 eV transition from the GaAs cap layer is again seen at 0.747 eV with no phonon replica, but the other near-edge PL differs from that of the GaAs case. The 0.739 eV peak (second order of 1.478 eV) is an undetermined FB or DAP emission, but the 0.758 peak (located next to peak A) corresponds closely to the second order of the low temperature FE transition of GaAs at 1.515 eV.

Temperature dependant PL of SI-$Al_{0.30}Ga_{0.70}As$:Pr shown in Figure 27 essentially mirrors that of SI-$Al_{0.15}Ga_{0.85}As$:Pr with much weaker intensity across the spectrum and with band-edge emissions similar to that of GaAs:Pr. This data is shown to emphasize the consistency of the Pr hot and cold lines in these Al-bearing hosts. In this host only peak C has sufficient intensity over the temperature range to allow meaningful quantitative analysis of the activation energy.

Theoretically, the identification of hot lines should allow assignment of excited energy states to the upper levels in the transitions. The difficulty in this instance is that very few hot lines were seen. This allows multiple different energy level assignments for each hot line making unique upper energy level assignments difficult. For example, *HL1* may be associated with excited upper level transitions of peaks A or B. Similarly, all hot lines in an emission group could correspond to excited upper level transitions from any lower energy transition in that group. What is needed, but not present, is a complete set of hot lines with energy spacing identical to those of the cold lines, but offset by the difference in energy between the lower and upper excited transition states.

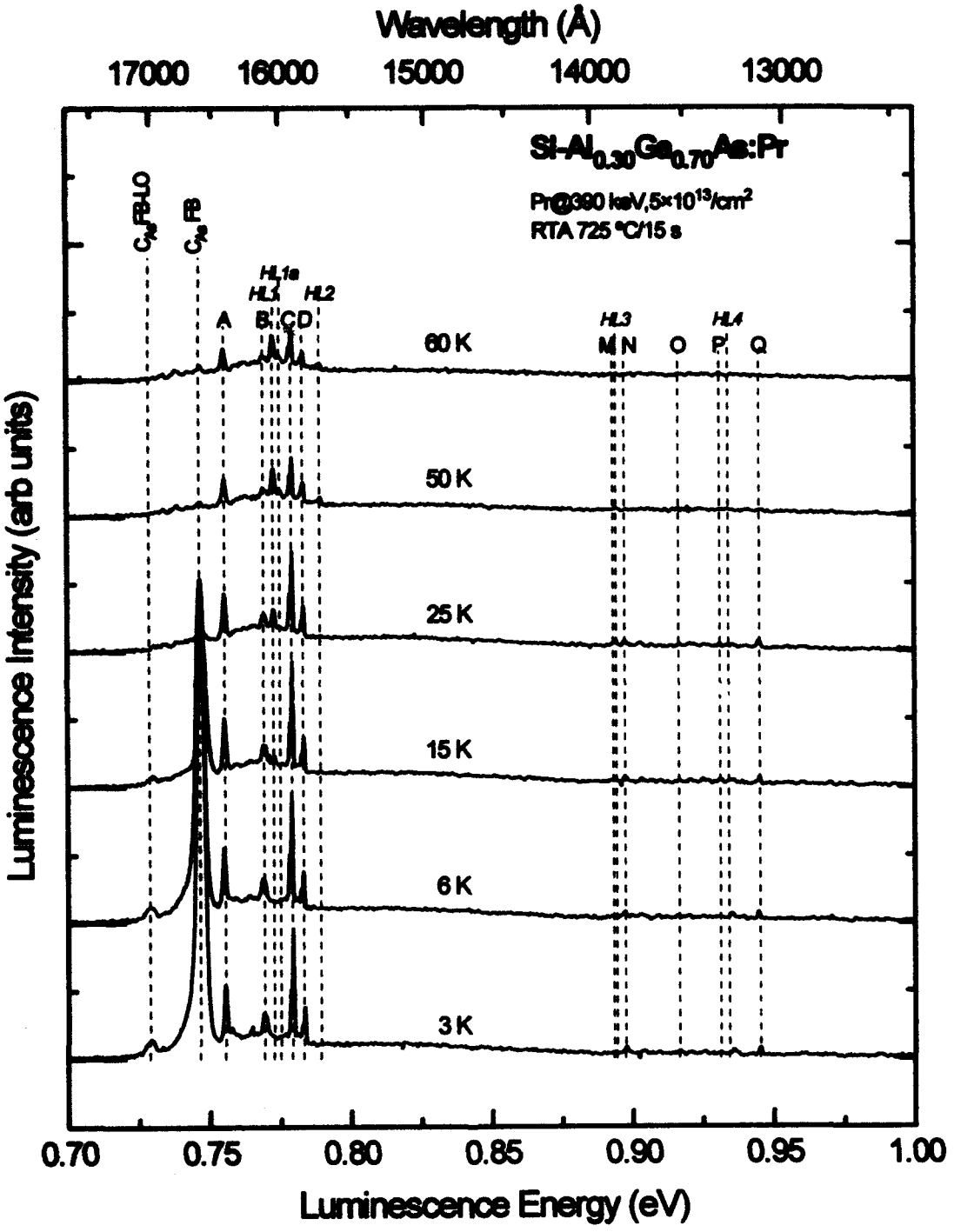

Figure 27. Photoluminescence spectra taken at various temperatures for SI-$Al_{0.30}Ga_{0.70}As$ implanted with Pr at 390 keV with a dose of $5\times10^{13}/cm^2$ and annealed at 725 °C

The integrated luminescence intensities of peak C, Q, and *HL1* obtained from SI-$Al_{0.15}Ga_{0.85}As$:Pr are plotted in Figure 28. The behavior of the peak C (0.779 eV line) and its accompanying emission group show a very interesting behavior of increasing intensity over the temperature range from 3 to about 15 K. However, this increase in intensity does not occur in other emission groups in SI-$Al_{0.15}Ga_{0.85}As$:Pr. Emissions described by the quenching model previously discussed should show only a continuing decrease in intensity with increasing sample temperature as with the peak Q in Figure 28 or should increase from essentially zero following a Boltzmann temperature distribution intensity like the 0.773 eV hot line *HL1*. However, peak C shows a strong intensity even at the lowest temperature, which is inconsistent with hot line behavior, and an increasing intensity with temperature over a limited range, which is inconsistent with normal temperature quenching associated with cold lines. A similar increase in peak intensity with temperature is seen from $Al_{0.45}Ga_{0.45}As$:Er emissions in figures from a paper by Benyattou *et al.*, but the authors make no mention of this behavior (Figures 2(a) and (b) in Benyatou *et al.*, 1992:351). The explanation of the temperature behavior of this peak is not well understood at present.

The strongest cold lines, peaks C and Q, were fitted to Eq (18) to determine activation energies intrinsic to the excitation mechanism. Since each emission line of the group varied intensity closely together, the peaks C and Q were chosen as representative. Single activation energy equation fits were used when an excellent fit was obtained, otherwise double activation energies were applied. Figure 29 shows the fit to peak Q in SI-$Al_{0.15}Ga_{0.85}As$:Pr for parameters corresponding to 2 activation energies of E_1=1.4±0.5 meV and E_2=6.0±1.6 meV and for the single activation energy of E_1=9.6±2.0 meV for peak C. Figure 30 shows the fit to peak C in SI-GaAs:Pr for parameters corresponding to activation energies of E_1=1.2±0.6 meV and E_2=22.5±9.0 meV, and to peak Q using E_1=2.2±0.4 meV and E_2=28.9±2.9 meV.

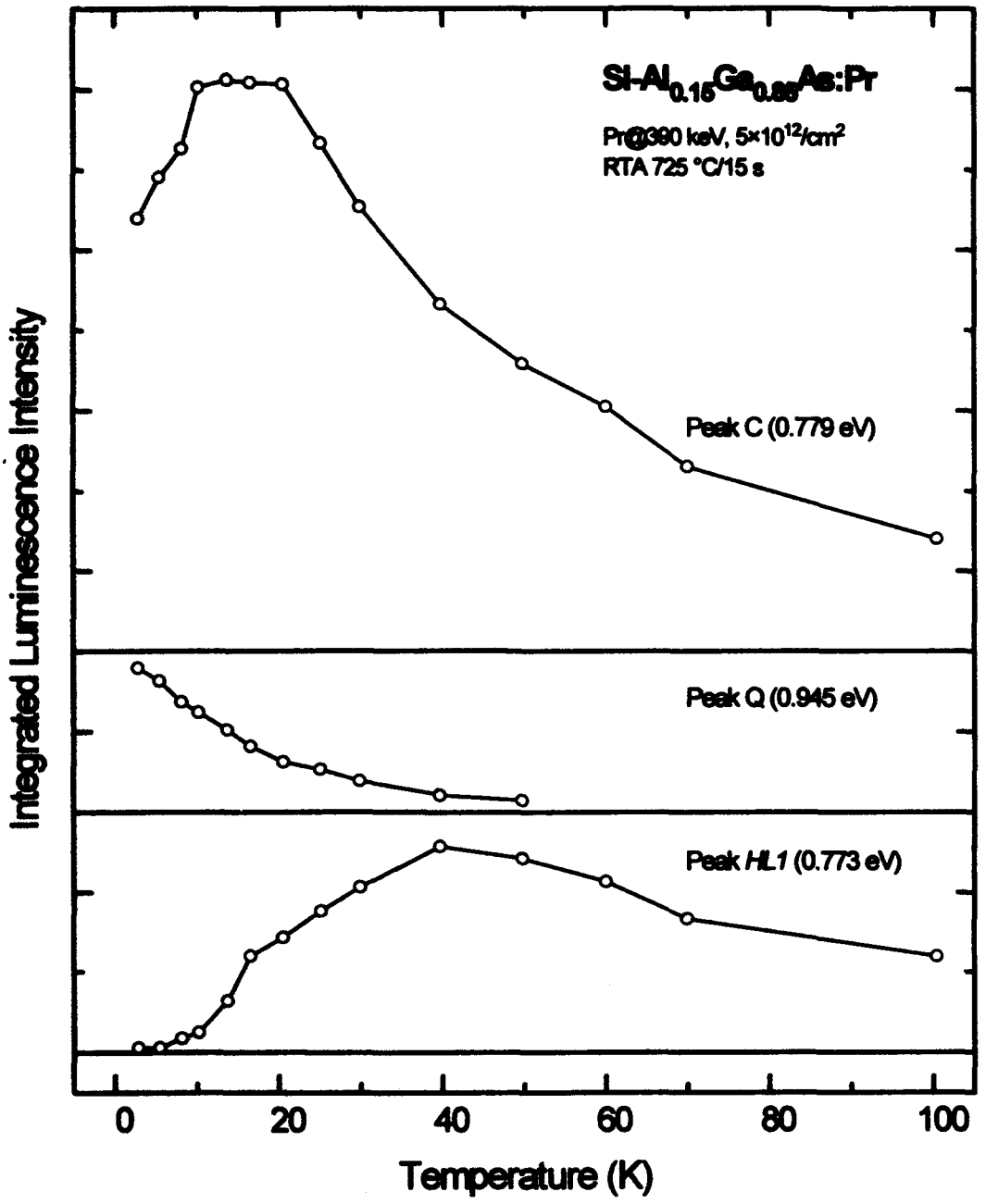

Figure 28. The temperature behavior of the integrated luminescence intensity of peaks C, Q, and *HL1* in SI-$Al_{0.15}Ga_{0.85}As$:Pr implanted with Pr at 390 keV with a dose of $5\times10^{12}/cm^2$ and annealed at 775 °C

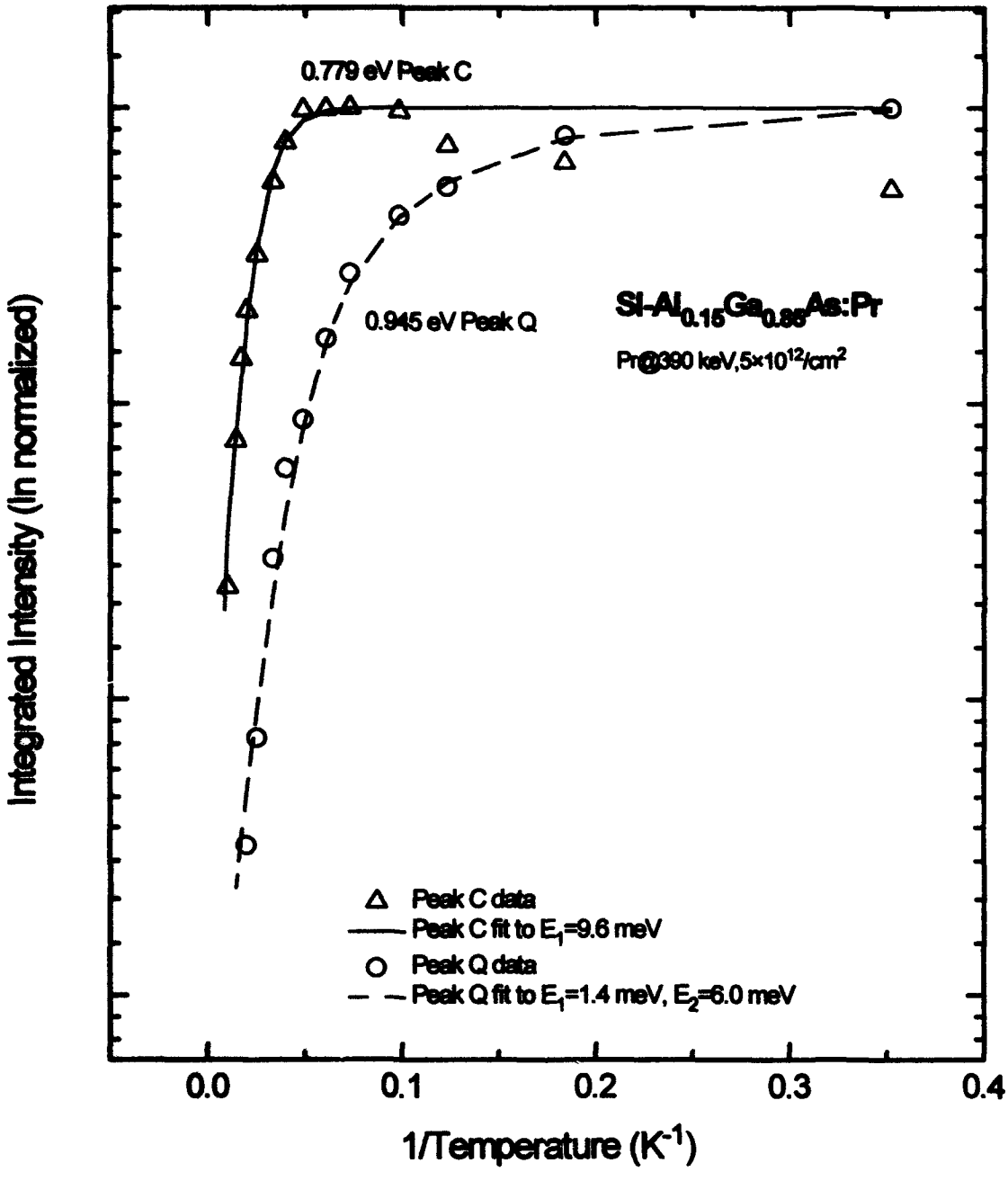

Figure 29. The temperature behavior of the integrated luminescence intensity of peaks C and Q in SI-$Al_{0.15}Ga_{0.85}As$:Pr with lines fitting to Eq (18) with E_1=9.6 meV for peak C, and with E_1=1.4 meV and E_2=6.0 meV for peak Q

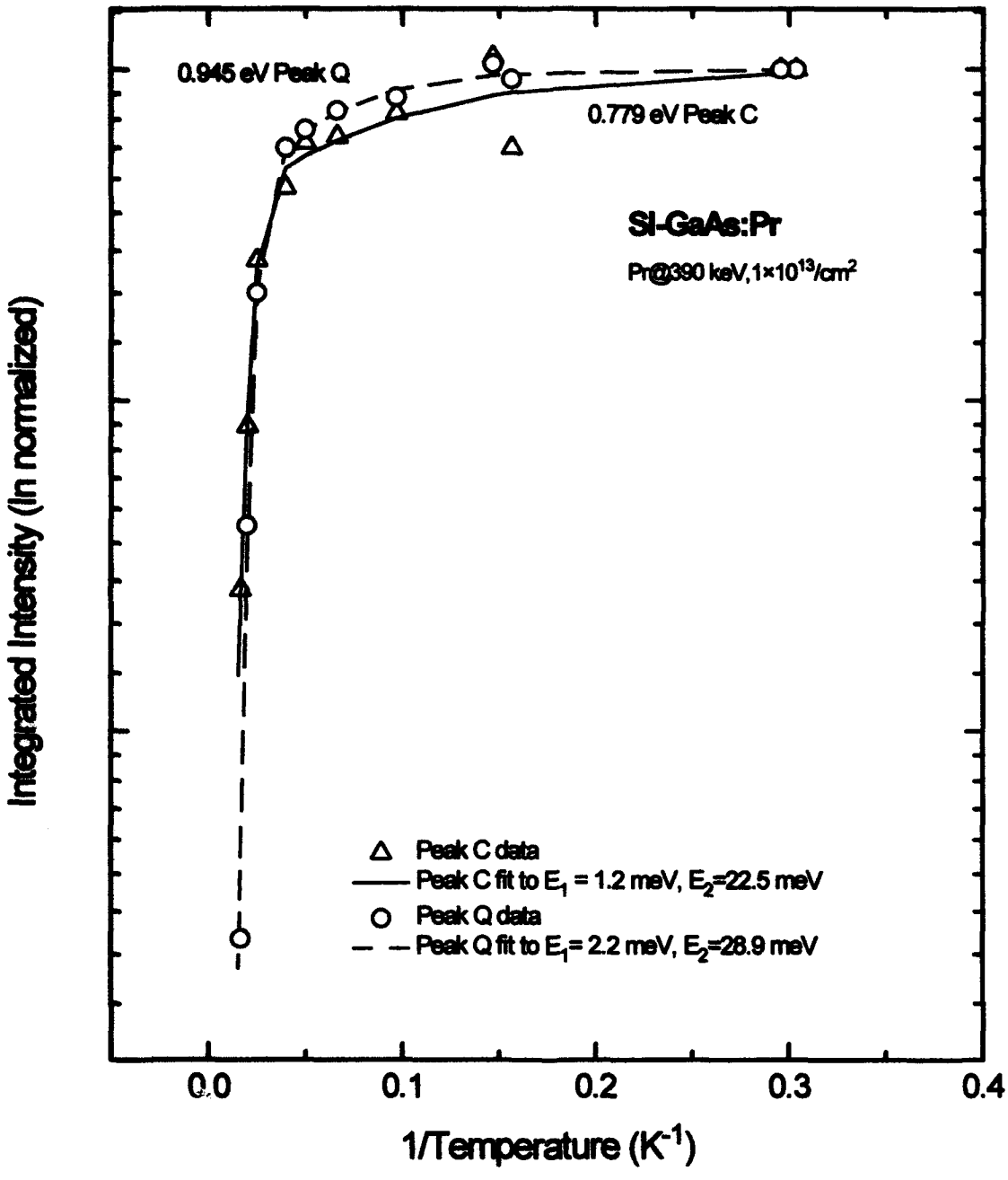

Figure 30. The temperature behavior of the integrated luminescence intensity of peaks C and Q in SI-GaAs:Pr with lines fitting to Eq (18) with E_1=1.2 meV and E_2=22.5 meV for peak C, and E_1=2.2 meV and E_2=28.9 meV for peak Q

Note that both peaks have the same activation energy pairs within the fitting parameter's standard errors. In SI-$Al_{0.30}Ga_{0.70}As$:Pr, only peak C was strong enough to conduct a temperature dependence study. This peak gives weak corroboration to the behavior of peak C in SI-$Al_{0.15}Ga_{0.85}As$:Pr, and the effect is small enough that a satisfactory fit to the simple activation energy Eq (18) could be obtained. Figure 31 shows the fit to peak C in SI-$Al_{0.30}Ga_{0.70}As$:Pr for parameters corresponding to Eq (18)'s activation energy $E_1=5.6\pm0.8$ meV.

Figures 29 through 31 conform to the typical plot format for PL temperature dependence. They are displayed using semi-natural logarithm intensity versus inverse temperature to aid in the quick visual confirmation of the semi-logarithmic linear behavior of the intensity at higher temperatures. This results from the increasing dominance of the inverse exponential terms in Eq (18) as T grows. Data from a sufficiently wide temperature range will include several points in this linear high temperature regime to unambiguously define the activation energy.

Table 14 summarizes the activation energies derived from Eq (18) and the temperature-dependent PL data for both of the representative peaks. The fits were determined using TableCurve (Jandel Scientific Inc) and verified using Origin (MicroCal Inc) or Mathcad (MathSoft Inc). The reported uncertainties correspond to the standard error reported by TableCurve, where, for a large sample set, about 68% of the data would fall within these values. The activation energy reported for Peak C for SI-$Al_{0.15}Ga_{0.85}As$ is that of the best fit using E_1 in Eq (18). The activation energies for each host are within fitting uncertainties of each other so no conclusive evidence for different luminescent centers or excitation paths for the different emissions groups is seen. Lacking other evidence, these emissions must be considered to emanate from a common Pr luminescent center through a common excitation process.

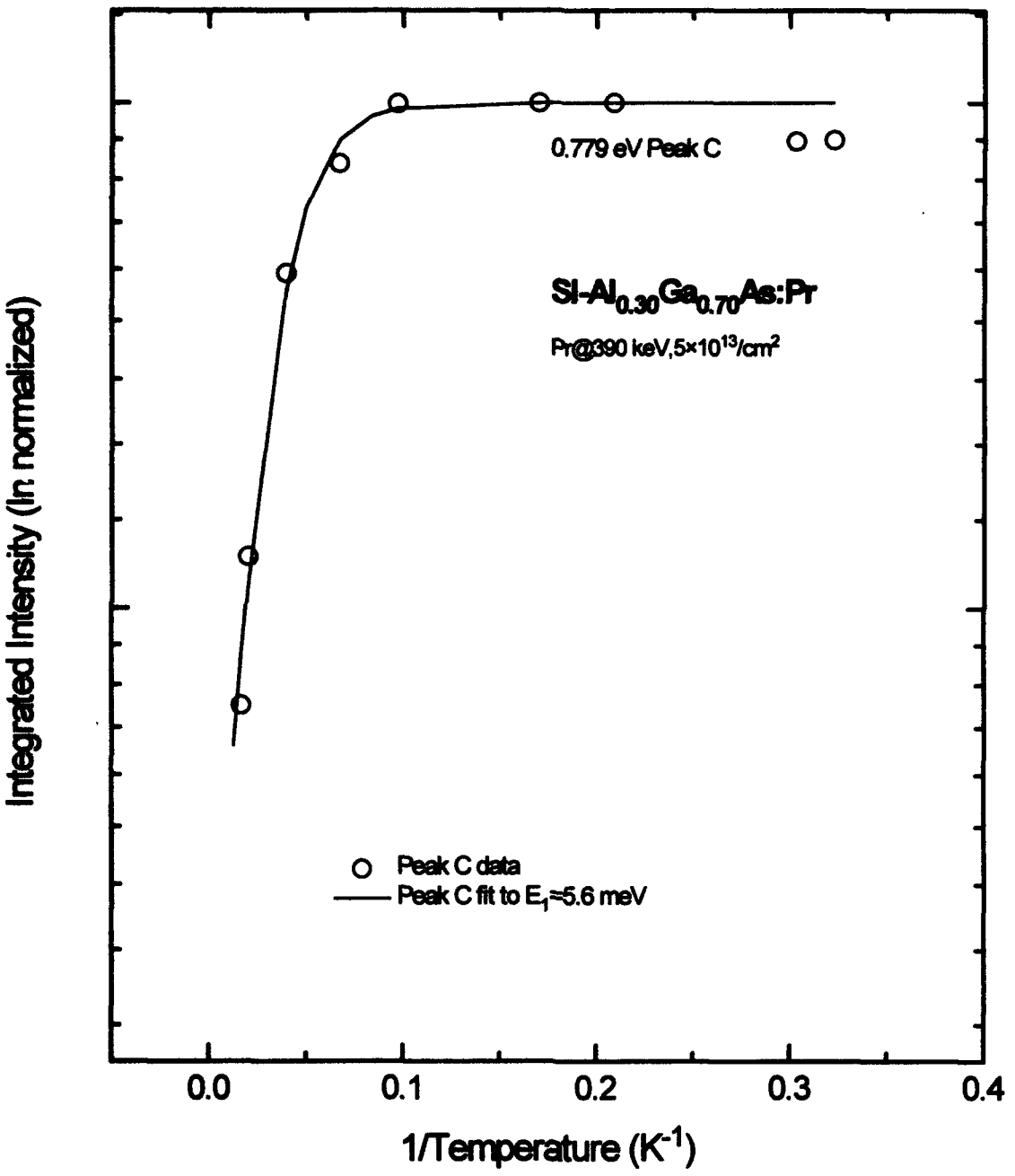

Figure 31. The temperature behavior of the integrated luminescence intensity of peak C in SI-$Al_{0.30}Ga_{0.70}As$:Pr with lines fitting to Eq (18) with $E_1 = 5.6$ meV

TABLE 14

Activation Energy Parameters for Pr PL in SI-$Al_xGa_{1-x}As$

	Peak C, 0.779 eV				Peak D, 0.945 eV			
Host:Pr	c_1	E_1 (meV)	c_2	E_2 (meV)	c_1	E_1 (meV)	c_2	E_2 (meV)
SI-GaAs:Pr	0.6	1.2±0.59	266.4	22.5±9.0	0.7	2.2±0.43	2389.9	28.9±2.9
SI-$Al_{0.15}Ga_{0.85}As$:Pr	9.9	9.6±2.0	-	-	2.0	1.4±0.45	30.9	6.0±1.6
SI-$Al_{0.30}Ga_{0.70}As$:Pr	5.8	5.6±0.8	-	-	too weak	too weak	too weak	too weak

Several other researchers have worked on the activation energies of the Er and Yb. For example, Benyattou and workers obtained activation energies for PL of SI-$Ga_{0.55}Al_{0.45}As$:Er, and found different activation energies for different Er emission energies (Benyatou *et al.*, 1992:351). These include 67 meV for the 0.9 micron emissions, 40 meV for the 1.54 micron emissions, and 25 meV for the 1.57 micron emissions. In explaining these data, they discounted multiphonon decay due to the large number of phonons required to bridge the energy gap. Instead they suggested that these energies could be related to a back transfer of energy from the Er excited state to the bound exciton level responsible for 4f excitation. Langer and coworkers proposed a pair of activation energies of 74 and 11 meV for the 1.54 micron emissions of GaAs:Er, and suggested that these correspond to, respectively, capture of electrons by excited RE ions from the conduction band at elevated temperatures and thermal ionization of bound excitons at the Er^{3+} centers (Langer *et al.*, 1993:19). Thonke *et al.* and Klein reported similar values for activation energies of InP:Yb of 12 and 118 meV for an n-type host and 10 meV for a p-type host (Thonke *et al.*, 1990:1127; Klein, 1988:1098-1099). Thonke made no specific proposal for the nature of the activated quenching mechanism and assumed a thermally activated dissociation of the luminescent complex in two steps (Thonke *et al.*, 1990:1127). Klein proposed that the

large activation energy was comparable to the binding energy of a hole to a neutral Yb acceptor and possible involvement of a population of non-equilibrium carriers which recombine with carriers trapped on defect centers (Klein, 1988:1098-1099).

With these past analyses in mind, the Pr activation energies may now be explained. The higher activation energies for each host (>4 meV) probably correspond to the dissociation of excitons bound to the Pr ions. The lower activation energies (<4 meV) are attributed to the effect of the hot lines of each group which depopulate the bottom most upper level states of the cold line transitions such as those monitored for these activation energy calculations. This implies that, for GaAs:Pr, the next higher state of the $^3F_3$ excited energy level is $\sim$1.2 meV above that from which the $^3F_3 \rightarrow {}^3H_4$ emissions emanate, while the next higher state of the $^1G_4$ level is elevated by $\sim$2.2 meV. A similarly small activation energy for the 0.945 eV peak from $Al_{0.15}Ga_{0.85}As$:Pr implies that the next upper state of the $^1G_4$ level is elevated by 1.4 meV which is consistent with the value 2.2$\pm$0.5 meV observed for GaAs. The previously discussed pronounced increase in Pr peak C up through 40 K no doubt overwhelmed any small hot effect on this peak, so no hot line-associated activation energy was found for this peak. These small implied crystal field splittings are similar to the splittings of PL lines as low as 4 meV and are near to the smallest hot line states of about 0.9 meV (peak *HL3* to M), 2.7 meV (peak *HL4* to P) and 3.5 meV (peak *HL1* to B) (for GaAs:Pr in Table 13). This hot line quenching effect will probably be much weaker than that of trapped carrier dissociation at Pr sites, which is confirmed by the smaller c coefficients for the smaller activation energies associated with the hot lines.

Selective Excitation of Pr Luminescence

The selective excitation experimental results gave direct insight into the excitation mechanism of Pr in $Al_xGa_{1-x}As$ hosts. After calibration of the tunable

Ti:Sapphire laser wavelength versus position, a computer program was coded to automatically control the output wavelength of the laser, collected data from the detector, calibrated and stored the data. The uncertainty of laser excitation energy measurements reported in this section stems from the standard error of the equation used to fit the laser calibration and is ± 3 meV. The laser was tuned from 7070 Å (1.75 eV) through 8600 Å (1.44 eV). The low temperature direct bandgap of $Al_xGa_{1-x}As$ was calculated from experimentally determined parameters reported recently. The direct bandgap as a function of the Al mole fraction x, $E_g(x)$, is defined by (El Allai *et al.*, 1993:4403)

$$E_g(x) = E_{g,GaAs} + ax + bx^2, \tag{21}$$

where $E_{g,GaAs}$ is the GaAs bandgap at T=0 K given as 1.519 eV, and a and b are fitting parameters which were determined to be a=1.447 eV and b=-0.15 eV for T=0 K. Since this empirical equation is valid only for direct gap material, the range for x is 0.0 to 0.4. This gives bandgaps of 1.52 eV for GaAs, 1.73 eV for $Al_{0.15}Ga_{0.85}As$, and 1.94 eV for $Al_{0.30}Ga_{0.70}As$ (2.07 eV for $Al_{0.50}Ga_{0.50}As$ as noted previously). Thus the selective excitation spanned from above to below bandgap energies in both low temperature GaAs and $Al_{0.15}Ga_{0.85}As$. For the other hosts the excitation energy ranged below gap from about 186 to 493 meV in $Al_{0.30}Ga_{0.70}As$ and about 316 to 623 meV in $Al_{0.50}Ga_{0.50}As$. For comparative uses, the values of the free excitons in these hosts is determined again from Eq (20). The strongest emission peak in each group was used as the monitor (0.779 eV peak C and 0.945 eV peak Q) and the intensity data for these peaks were collected at approximately 5 Å intervals of the excitation laser wavelength. Tests were run on optimally Pr-implanted and annealed SI-GaAs:Pr, SI-$Al_{0.15}Ga_{0.85}As$:Pr, SI-$Al_{0.30}Ga_{0.70}As$:Pr, and SI-$Al_{0.50}Ga_{0.50}As$:Pr, however tests of SI-$Al_{0.30}Ga_{0.70}As$:Pr and SI-$Al_{0.50}Ga_{0.50}As$:Pr revealed no Pr-related luminescence

whatsoever over the entire excitation energy range. This is due to the excitation energies of the laser which were well below bandgap for both.

Figure 32 shows the SEL luminescence behavior of peak C in the SI-$Al_{0.15}Ga_{0.85}As$:Pr host which was found to be identical to that of peak Q. The intensity of both peaks increase slightly as the laser energy moves below the bandgap of the host and starts to decrease sharply at a laser energy of about 11 meV below E_g. The luminescence was further monitored to over 280 meV below the bandgap energy, but no Pr luminescence was observed over this range. This common behavior of each emission group is evidence for a shared excitation mechanism step related to the free carriers, excitons, and near band-edge emissions. The PL intensity drop is very distinct, and occurs at 1.720 ± 0.003 eV which is about 11 meV below the band-edge which agrees well with the activation energy of 6.0 to 9.6 meV for these peaks (Table 14). The half-maximum point of the intensity drop off is shown to be 21 meV from the band-edge energy. Since energies near the free exciton energy are required for luminescence of Pr in these hosts, free carriers, excitons, and/or free-to-bound transitions must be considered essential for the Pr excitation process.

Figure 33 shows similar behavior from the SI-GaAs:Pr sample. The intensity drop of both lines is abrupt as the excitation energy dips below the exciton energy level of GaAs at 1.515 eV. The intensity drop occurs over a narrow range with the half-maximum point for this host being only 5 meV below the FE level (half that of SI-$Al_{0.15}Ga_{0.85}As$ case). Peak Q also has a clear, below bandgap energy maximum centered at 1.496 eV (24 meV below the bandgap energy) which appears to be about 20 meV wide. This peak may result from pumping directly to the BE energy level at the Pr ion site since 24 meV is close to the activation energies assigned to BE dissociation for SI-GaAs:Pr (22.5 and 28.9 meV). Thonke *et al.* reported similar photoluminescence excitation behavior of Yb^{3+} in InP with a very steep drop of Yb-

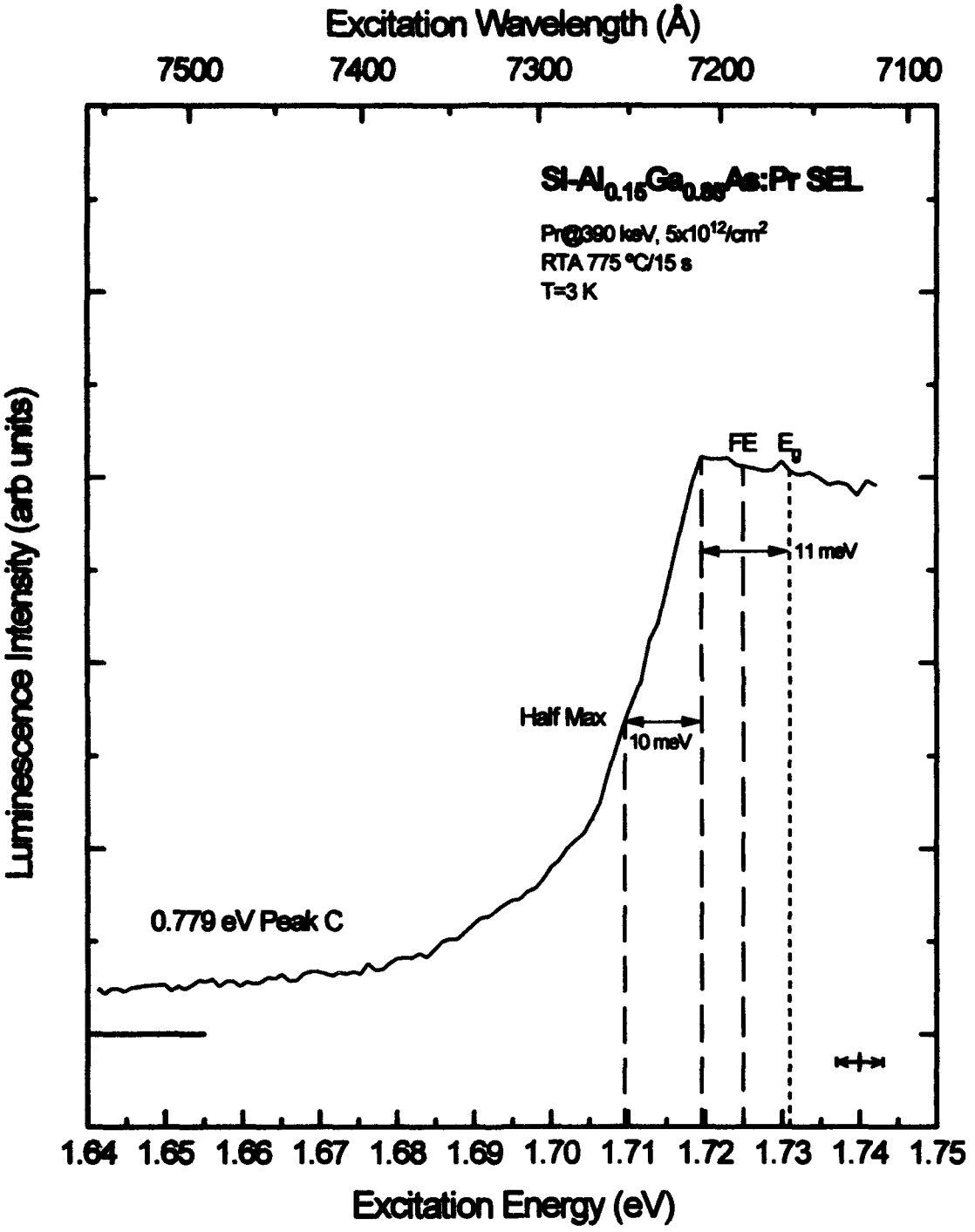

Figure 32. Selective excitation luminescence intensity at 3 K for peak C in SI-$Al_{0.15}Ga_{0.85}As$ implanted with Pr at 390 keV with a dose of $5\times10^{12}/cm^2$ and annealed at 775 °C

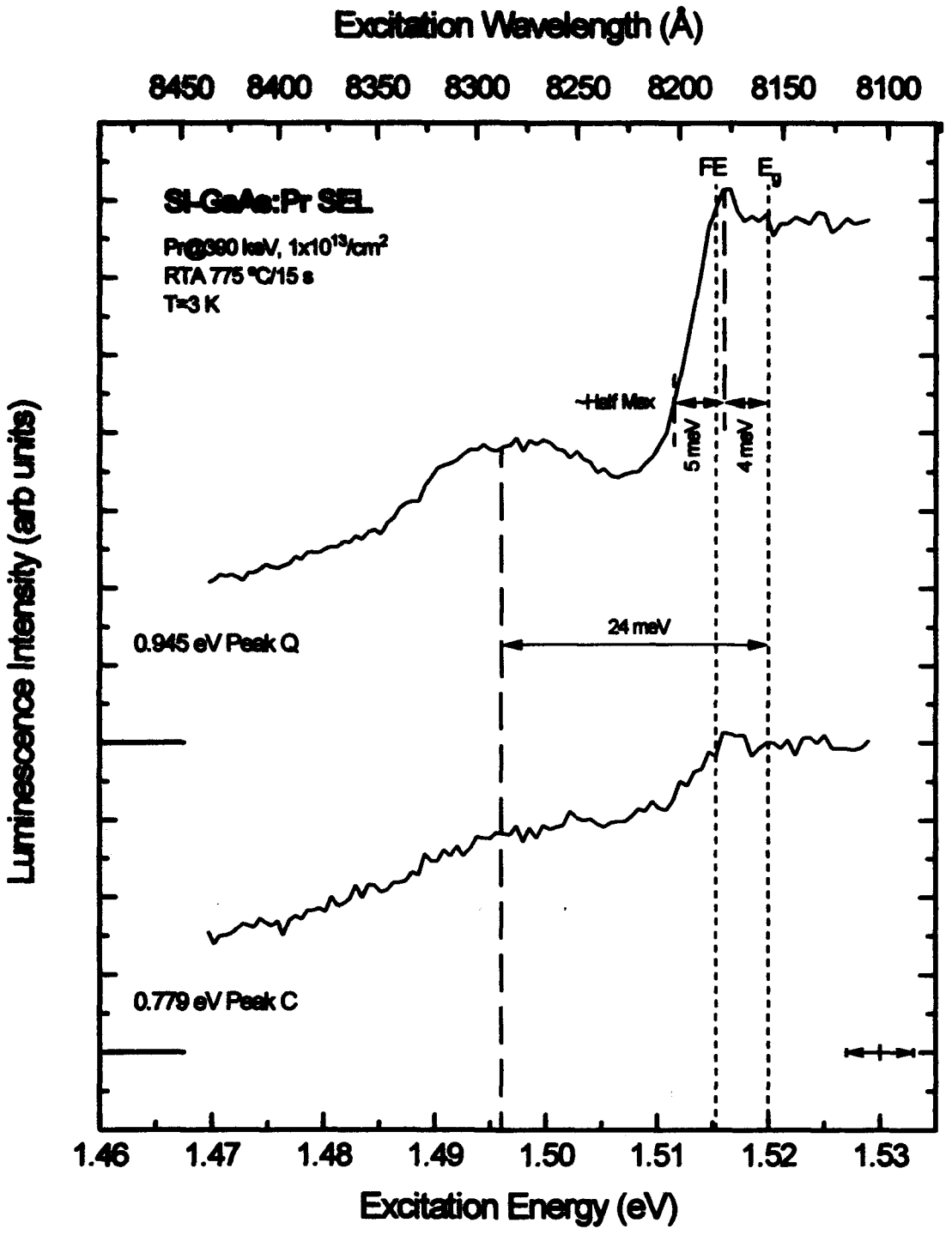

Figure 33. Selective excitation luminescence intensity at 3 K for peaks C and Q in SI-GaAs:Pr implanted with Pr at 390 keV with a dose of $1\times10^{13}/cm^2$ and annealed at 775 °C

related emissions below excitation at the FE energy and a small maximum at about 33 meV below the InP bandgap energy (Thonke *et al.*, 1990;1125). These workers concluded that this CB-33 meV peak could correspond to a process in which electrons trapped at the Yb ion (treated as a pseudodonor) are excited either to EMT states (still bound to the localized hole) or directly to the CB (Thonke *et al.*, 1990;1129).

Pomrenke *et al.* reported SEL results on GaAs:Pr, which were limited to fairly coarse excitation energy steps due to the use of a tunable dye laser (Pomrenke *et al.*, 1990:333-334). They reported that the luminescence of a 1320 nm line (0.939 eV) drops in intensity near the free exciton energy, however the coarseness of the excitation energy steps also jumped over the below gap maximum at 1.497 eV. They did not report SEL for the 1592 nm line (0.779 eV) for any excitation energies less than 1.51 eV, which were seen in this study down to 1.47 eV (Figure 33). However, for an excitation energy of 1.386 eV, they reported a spectra with weak, sharp Pr lines quite dissimilar to those found for above gap excitation. These different Pr lines are attributed to multiple Pr centers, but the possibility of some sharp lines emanating from residual transition elements and other impurities was not excluded.

The lack of Pr luminescence for excitation energies less than about 25-30 meV below the host bandgap is in striking contrast to the behavior of Er in GaAs. Colon *et al.* reported strong Er PL from the 1.538 micron line for laser excitation energies as low as 960 nm (1.29 eV or 228 meV below GaAs bandgap) along with Er-related deep hole traps (Colon *et al.*, 1992b:673). These researchers proposed that the below-gap excitation ionized electrons from these Er-related hole traps into the CB and the remaining bound hole recombines with an electron, thus pumping the Er luminescence. In this present study, the lack of any below-gap excitation-based luminescence ranging from 186 to 623 meV below the gap of hosts examined gives evidence to infer then that no such Pr-related deep hole traps exist in the hosts tested here.

The common characteristics of each of these SEL data sets is the sufficiency of pumping at or slightly below the FE energy of the host for inducing Pr luminescence. It is apparent that Pr luminescence in these hosts can only be pumped with energies capable of creating free carriers or free excitons, with the singular possibility of direct pumping to the BE energy levels at the Pr ion.

Photoluminescence of Dual-doped Pr and Er

In order to evaluate the effect of introducing 2 different RE elements into a semiconductor, both Pr and Er were implanted into $Al_xGa_{1-x}As$ hosts. It was hoped that the energetic interaction between the two ions might serve to facilitate stronger near IR emissions than either would produce separately. There are 2 competing mechanisms which affect luminescence of REs in the same host. First, separately, both REs compete for available free excitons for their energy source. Second, the ions may pair up, forming heterogeneous rare earth complexes. These complexes may facilitate the transfer of BE recombination energy by providing energy level combinations which are well matched to BE energy.

For this study, Er was implanted with an energy of 1 MeV at doses of 1×10^{13} and $5\times10^{13}/cm^2$. Host semiconductors included SI-GaAs, and SI-$Al_xGa_{1-x}As$ with x=0.15, 0.30, and 0.50. Portions of these hosts were implanted with Er only, with both Er and Pr, and with Pr alone. All samples implanted with Pr were at 390 keV with a dose of $1\times10^{13}/cm^2$. The implant depth of Er peak concentrations into these hosts spans a range of 1833 Å in GaAs to 2048 Å in $Al_{0.50}Ga_{0.50}As$ as shown in Table 15. Although these implant depths are roughly twice their Pr counterparts (Table 8), this is actually advantageous when combined with the dosages used. For the low Er dose, the Er and Pr implant profiles are essentially separate as shown in Figure 34. The corresponding results may be viewed as nearly independent luminescence from

TABLE 15

Erbium Implant Characteristics (1 MeV)

Host	Range, Rp (Å)	Straggling, ΔRp (Å)
SI-GaAs	1833	527
SI-$Al_{0.15}Ga_{0.85}As$	1879	534
SI-$Al_{0.30}Ga_{0.70}As$	1948	545
SI-$Al_{0.50}Ga_{0.50}As$	2048	561

each RE. The high Er dose caused the Er density profile to almost completely envelop the Pr implants (Figure 34), so Pr luminescence in these samples would have the maximum 'Er effect,' if any. By then comparing PL spectra from samples of both Er doses, the effect of Er collocated with Pr at similar densities can be seen.

As was previously reviewed (Table 5), Er has been very widely studied, and is characterized by near-IR emissions which peak in a narrow range at 1.54 μm. A limited RTA study was conducted on all samples with temperatures of 700, 750, 800, and 850 °C for a duration of 15 seconds. The highest Er PL emission intensities were found to occur for an RTA temperature of 750 °C for the SI-GaAs and SI-$Al_{0.15}Ga_{0.85}As$ hosts, and 700 °C for the SI-$Al_{0.30}Ga_{0.70}As$ and SI-$Al_{0.50}Ga_{0.50}As$ hosts. These RTA characteristics were used for all subsequent samples, both with and without Pr and Er. In all cases, the Er emissions were significantly stronger for the higher dose although never more than a factor of two.

Figure 35 shows the PL of identically annealed samples of SI-GaAs implanted with Er only, Pr only, and Er and Pr together. As annealed for optimal Er PL, the SI-GaAs host implanted with both Pr and Er showed virtually no Pr emissions in either of the main emission groups. This was true for both high and low doses of Er. However, very weak, but distinct Pr emissions in the 0.9 eV range emerged for an

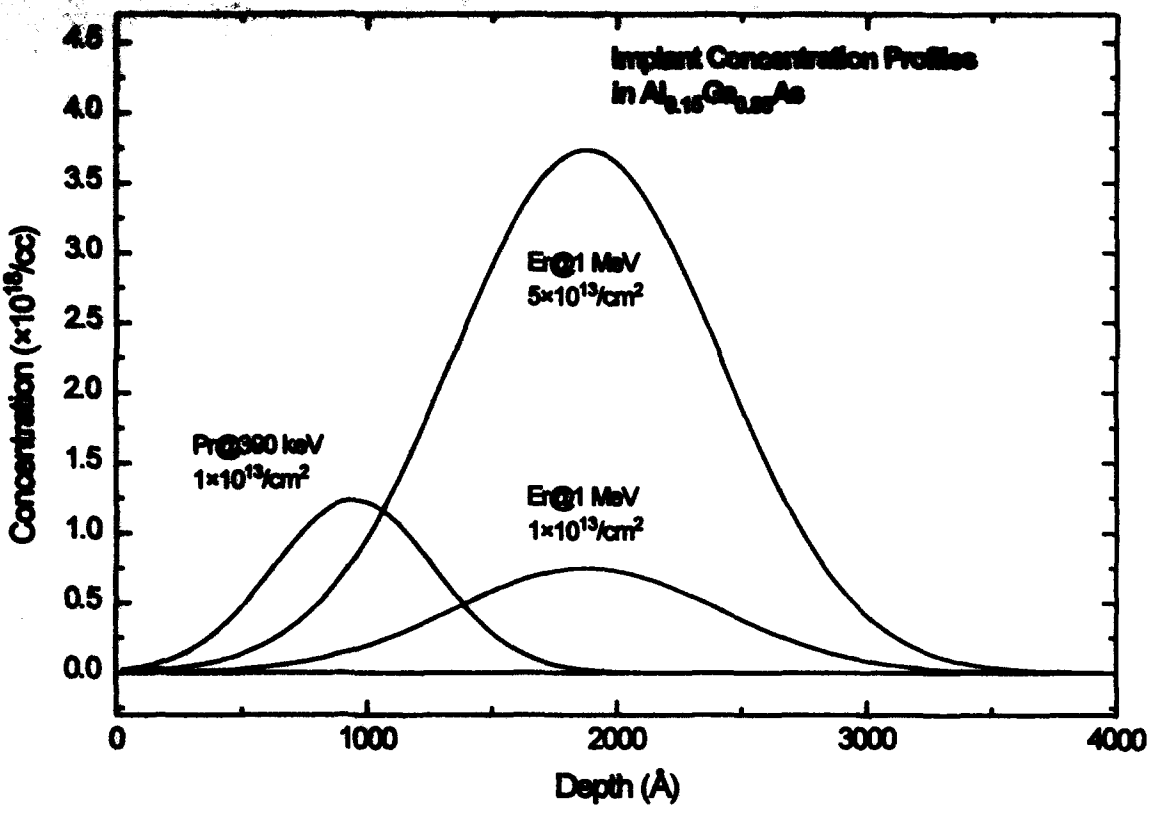

Figure 34. Concentration profiles of Er and Pr implanted into $Al_{0.15}Ga_{0.85}As$ as used in the dual-doping study

RTA temperature of 800 °C (higher than the optimal temperature for Er) as shown in Figure 36. Dotted guidelines are displayed to distinguish the major emission lines from each RE. The Er $^4I_{13/2} \rightarrow {}^4I_{15/2}$ transition emissions are only slightly decreased by the presence of Pr, while the Pr emissions are seen to be completely extinguished by the presence of Er.

The intrinsically stronger Pr emissions from $Al_{0.15}Ga_{0.85}As$ allowed a more interesting investigation of the emissions from this dual-doped host. The upper traces in Figure 37 show typical Er-only luminescence, which is very similar to that of the SI-GaAs host, however the PL from a host containing both of Er and Pr depends on the comparative doses of the implants (Figure 37 lower traces). For equal doses, here $1\times10^{13}/cm^2$, the Pr emissions are stronger than those of Er, but with the Er dose

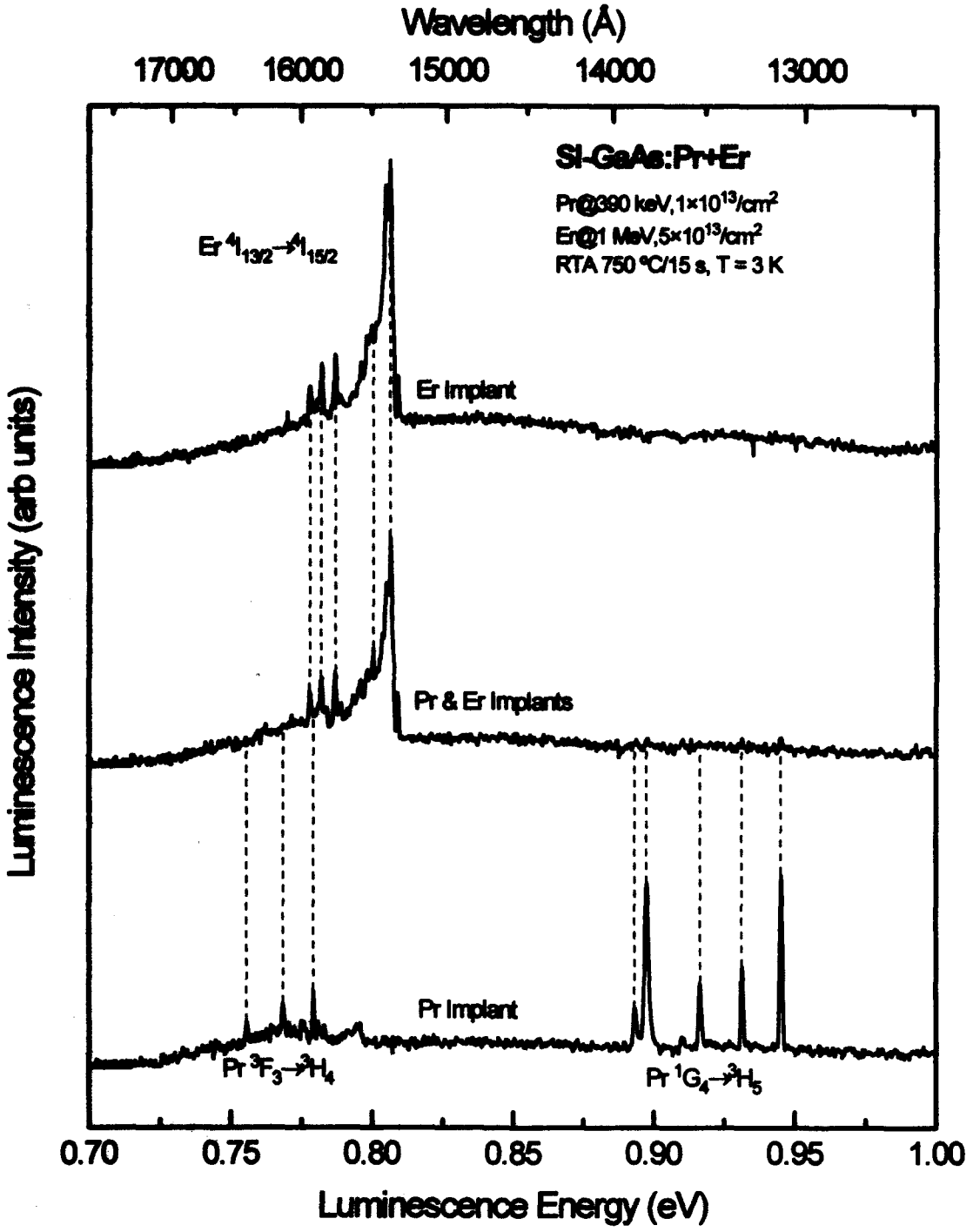

Figure 35. PL spectra taken at 3 K from SI-GaAs implanted with Pr at 390 keV with a dose of $1\times10^{13}/cm^2$, Er at 1 MeV with a dose of $5\times10^{13}/cm^2$, and both Pr and Er and annealed at 750 °C

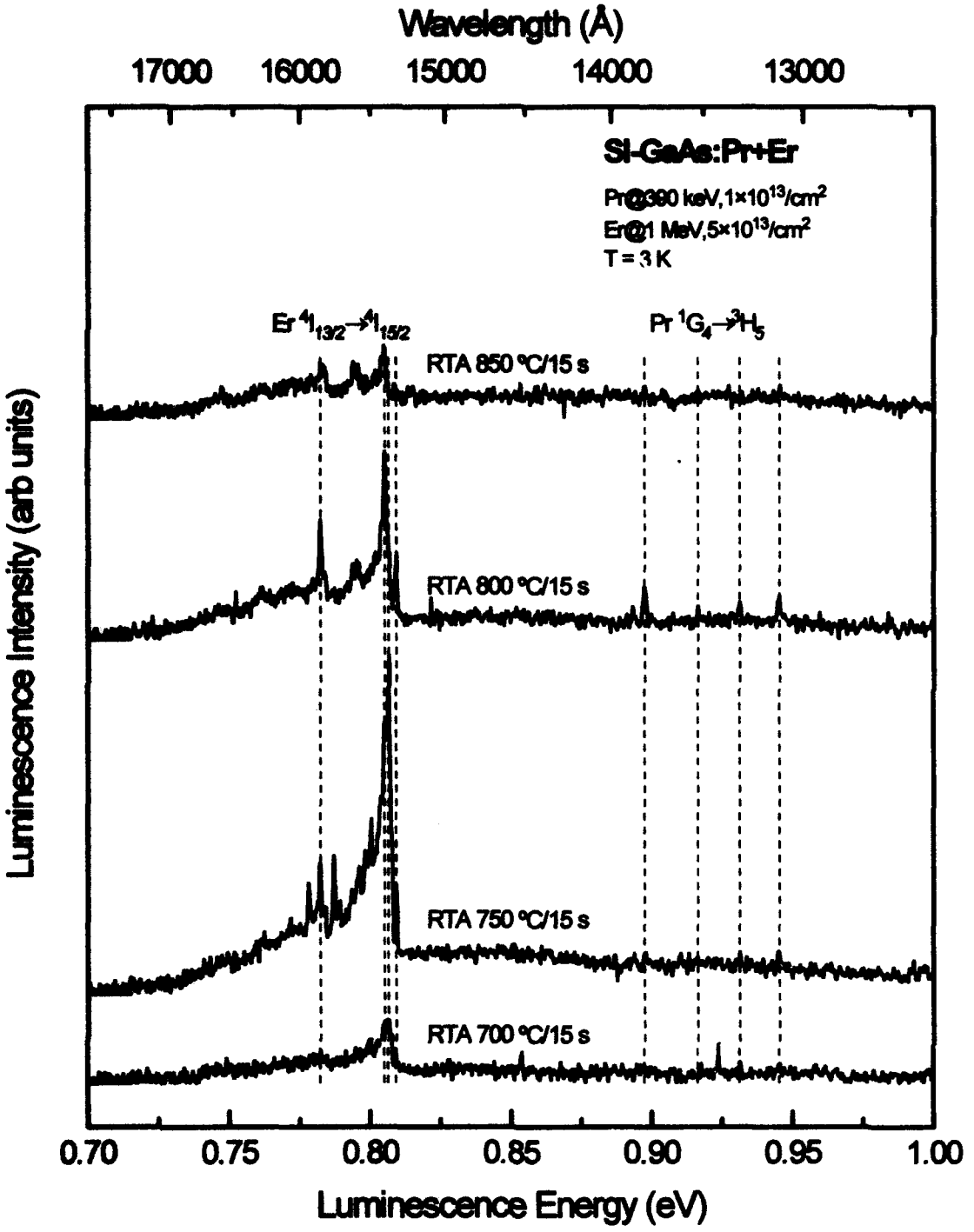

Figure 36. PL spectra taken at 3 K from SI-GaAs implanted with Pr at 390 keV with a dose of $1\times10^{13}/cm^2$ and Er at 1 MeV with a dose of $5\times10^{13}/cm^2$ and annealed at various temperatures

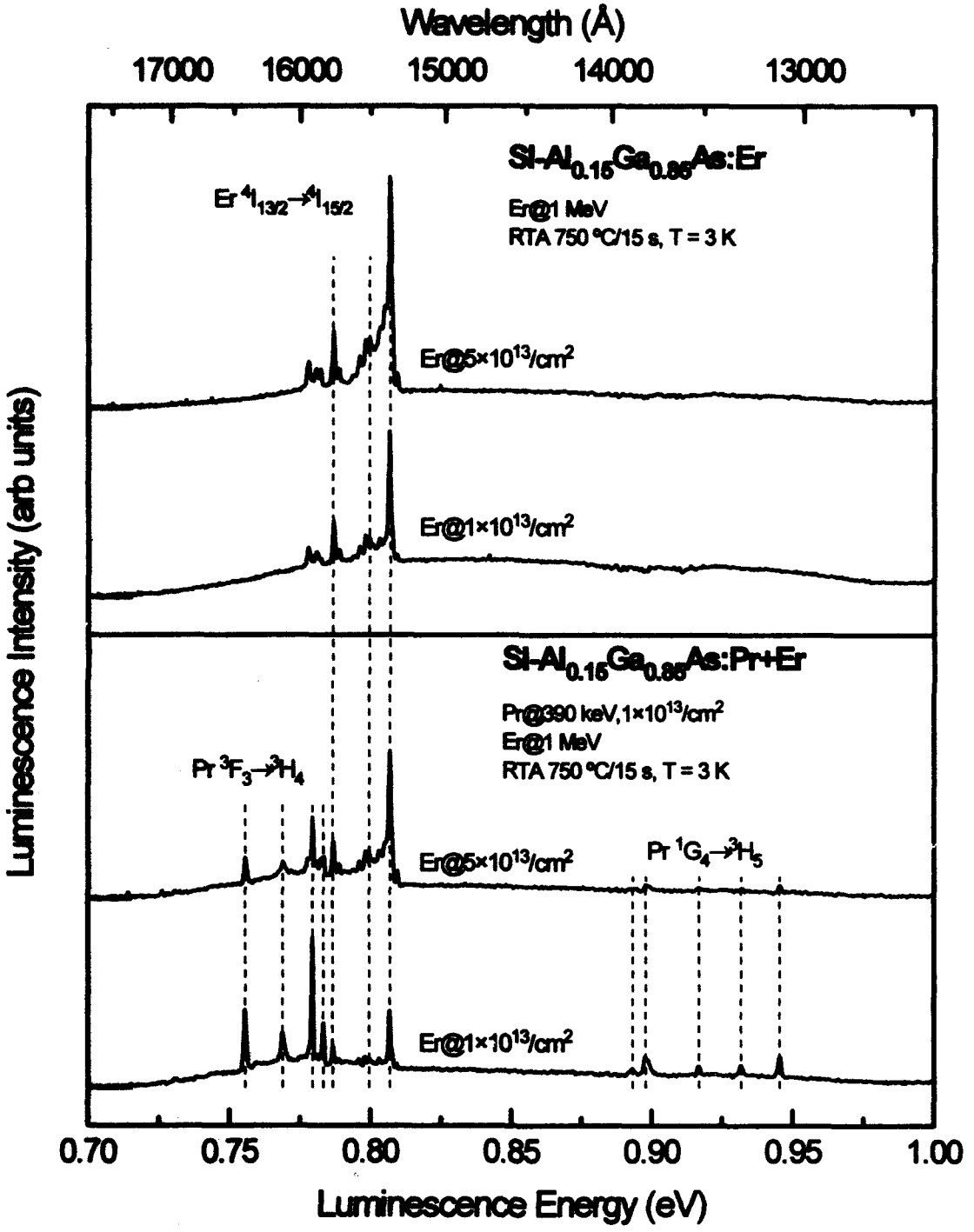

Figure 37. PL spectra taken at 3 K from SI-$Al_{0.15}Ga_{0.85}As$ implanted with Er at 1 MeV with a doses of $1\times10^{13}/cm^2$ and $5\times10^{13}/cm^2$ with and without Pr at 390 keV with a dose of $1\times10^{13}/cm^2$ and annealed at 750 °C

increased by a factor of five, the Er emissions increase strength at the cost of the Pr intensity. This implies that no luminescence enhancement is occurring, and that the two REs are competing for pumping energy from the lattice. The higher density RE will capture a greater percentage of the available free carriers and excitons. If any Pr-Er complexes are forming, they are not significantly affecting the luminescent behavior compared to the corresponding singly implanted hosts. This effect is demonstrated again by comparing the three variants in this study as shown in Figure 38. The sample with pure Pr shows the familiar pair of strong emission groups, while the Er-only sample shows similarly strong emissions albeit with a higher dose. When these REs are combined, as shown by the center trace in Figure 38, both RE emissions are strongly diminished.

Figure 39 displays the PL spectra of SI-$Al_{0.30}Ga_{0.70}As$ implanted with Er only, Pr only, and both Pr and Er. Both RE emissions decreased slightly when they were dual-implanted, but the effect is not as dramatic as in the earlier two cases. Figure 40 displays the PL spectra of SI-$Al_{0.50}Ga_{0.50}As$ implanted with Er only, Pr only, and both Pr and Er. This host exhibits different behavior in that the Pr emissions, although weak, seem slightly enhanced by the presence of Er, while the Er emissions are essentially unchanged. This increase in Pr intensity is also accompanied by a decrease in the broad-band defect emissions centered near 0.82 eV in the dual implant case. With both of these apparent effects, it is difficult to assign a specific reason for the enhancement of the Pr emissions, especially when it is so contrary to the results of Pr PL from the other three dual-doped cases in this study.

Figure 41 shows graphs of the PL spectra from each of the SI-$Al_xGa_{1-x}As$ hosts implanted with Pr at a dose of $1\times10^{13}/cm^2$ and Er at a dose of $1\times10^{13}/cm^2$, while Figure 42 shows the results of duplicated experiments for an increased Er dose of $5\times10^{13}/cm^2$. For this case of equal amounts of Pr and Er in the lattice, neither RE PL

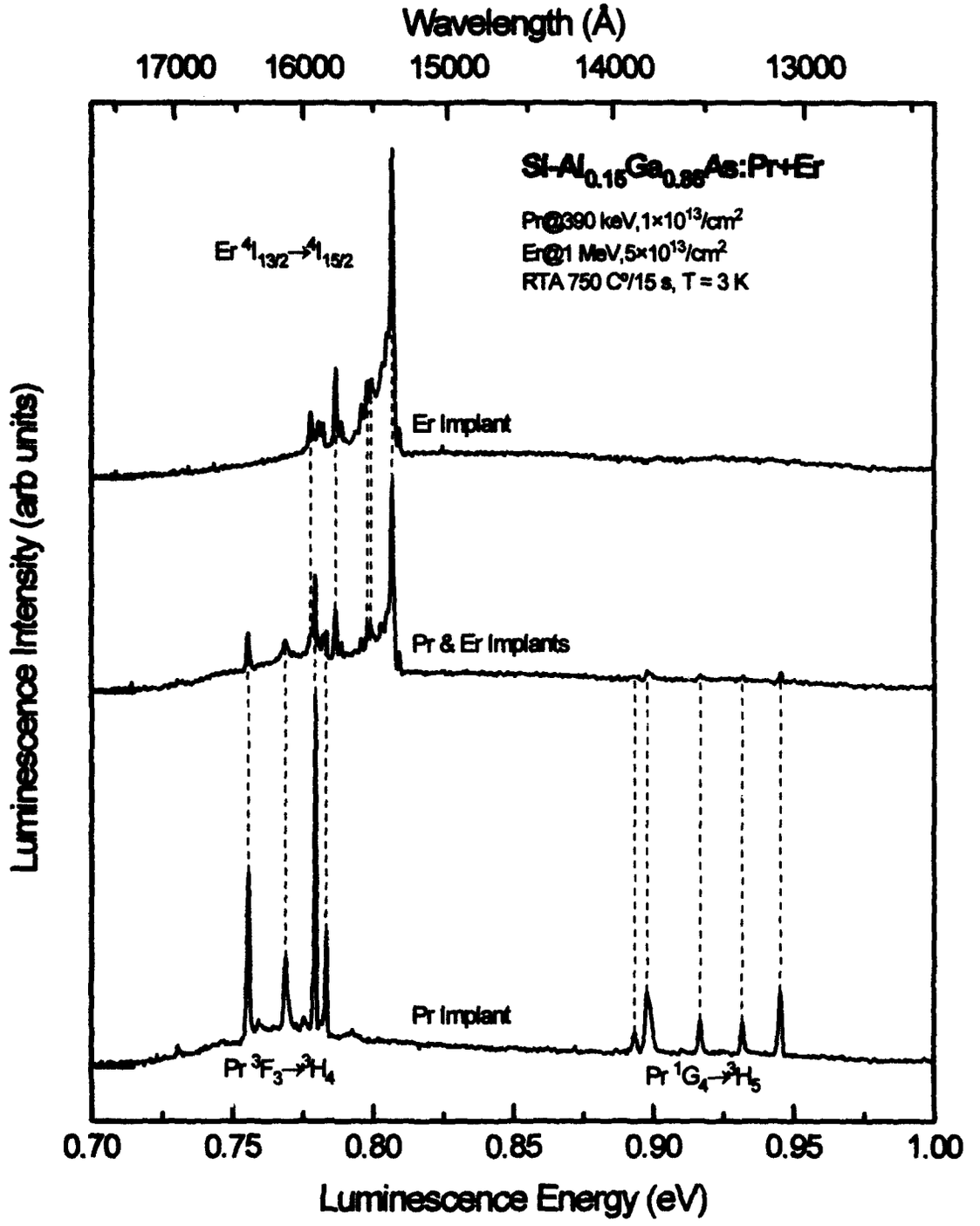

Figure 38. PL spectra taken at 3 K from SI-$Al_{0.15}Ga_{0.85}As$ implanted with Pr at 390 keV with a dose of $1\times10^{13}/cm^2$, Er at 1 MeV with a dose of $5\times10^{13}/cm^2$, and both Pr and Er and annealed at 750 °C

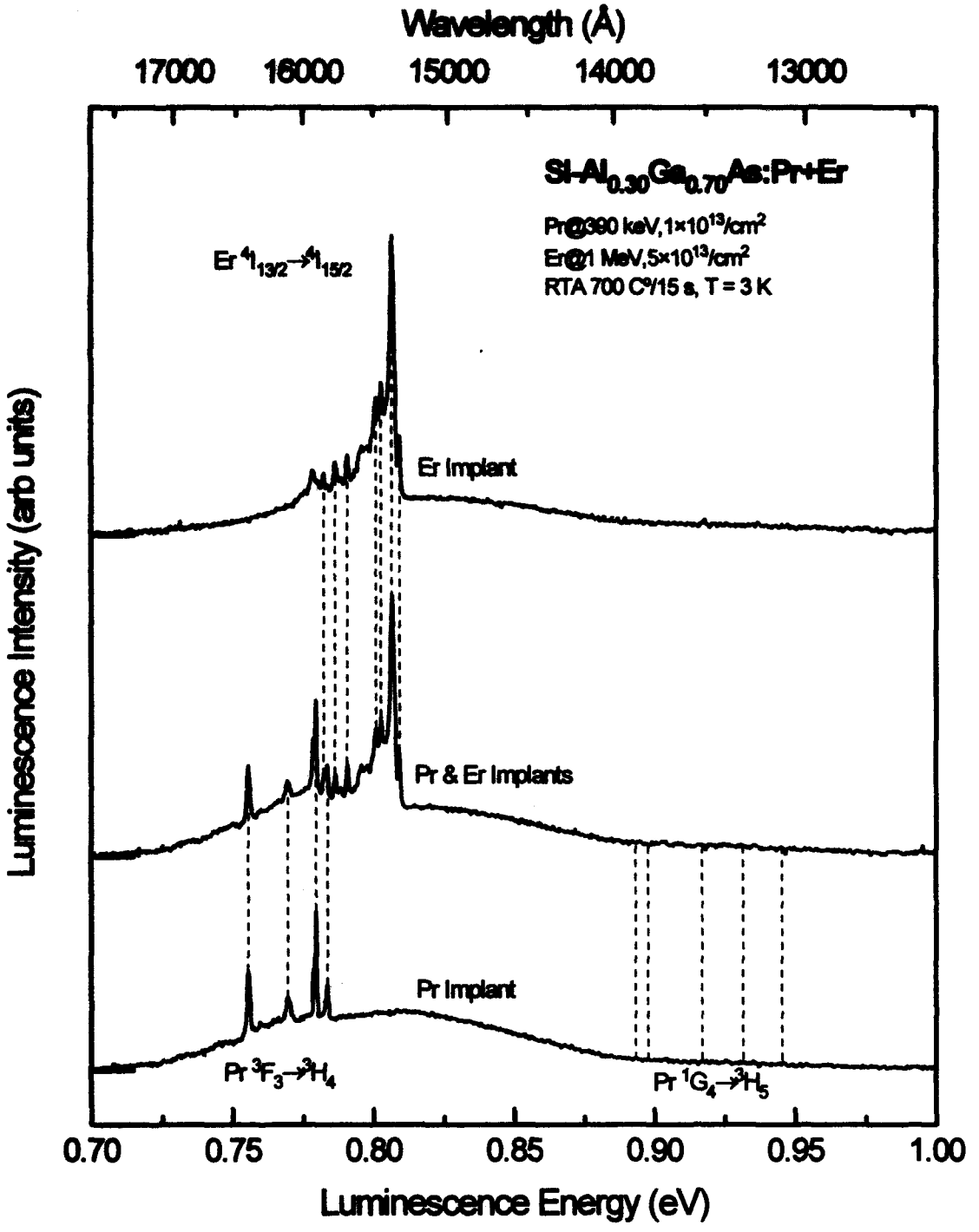

Figure 39. PL spectra taken at 3 K from SI-$Al_{0.30}Ga_{0.70}As$ implanted with Pr at 390 keV with a dose of $1\times10^{13}/cm^2$, Er at 1 MeV with a dose of $5\times10^{13}/cm^2$, and both Pr and Er and annealed at 700 °C

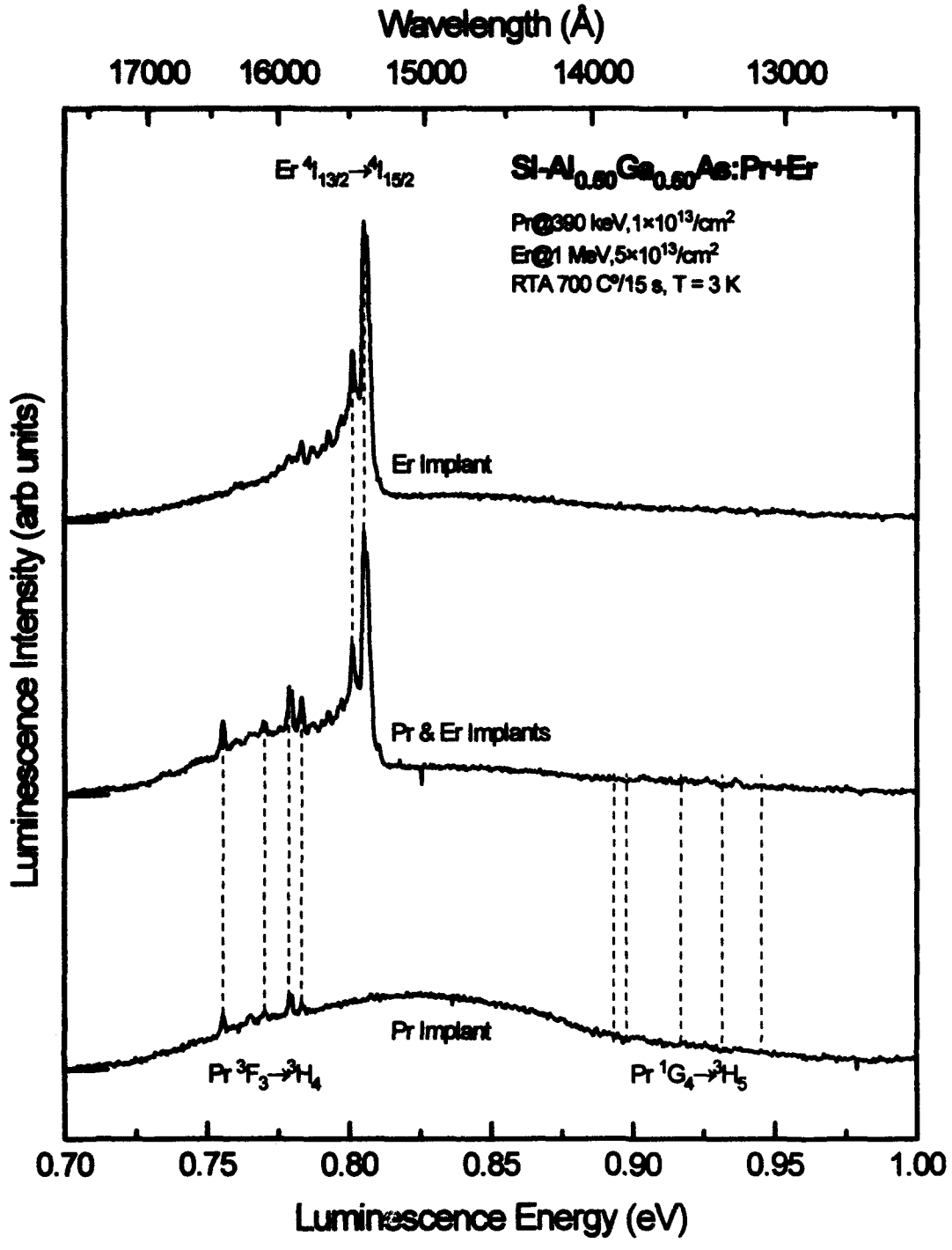

Figure 40. PL spectra taken at 3 K from SI-$Al_{0.50}Ga_{0.50}As$ implanted with Pr at 390 keV with a dose of $1\times10^{13}/cm^2$, Er at 1 MeV with a dose of $5\times10^{13}/cm^2$, and both Pr and Er and annealed at 700 °C

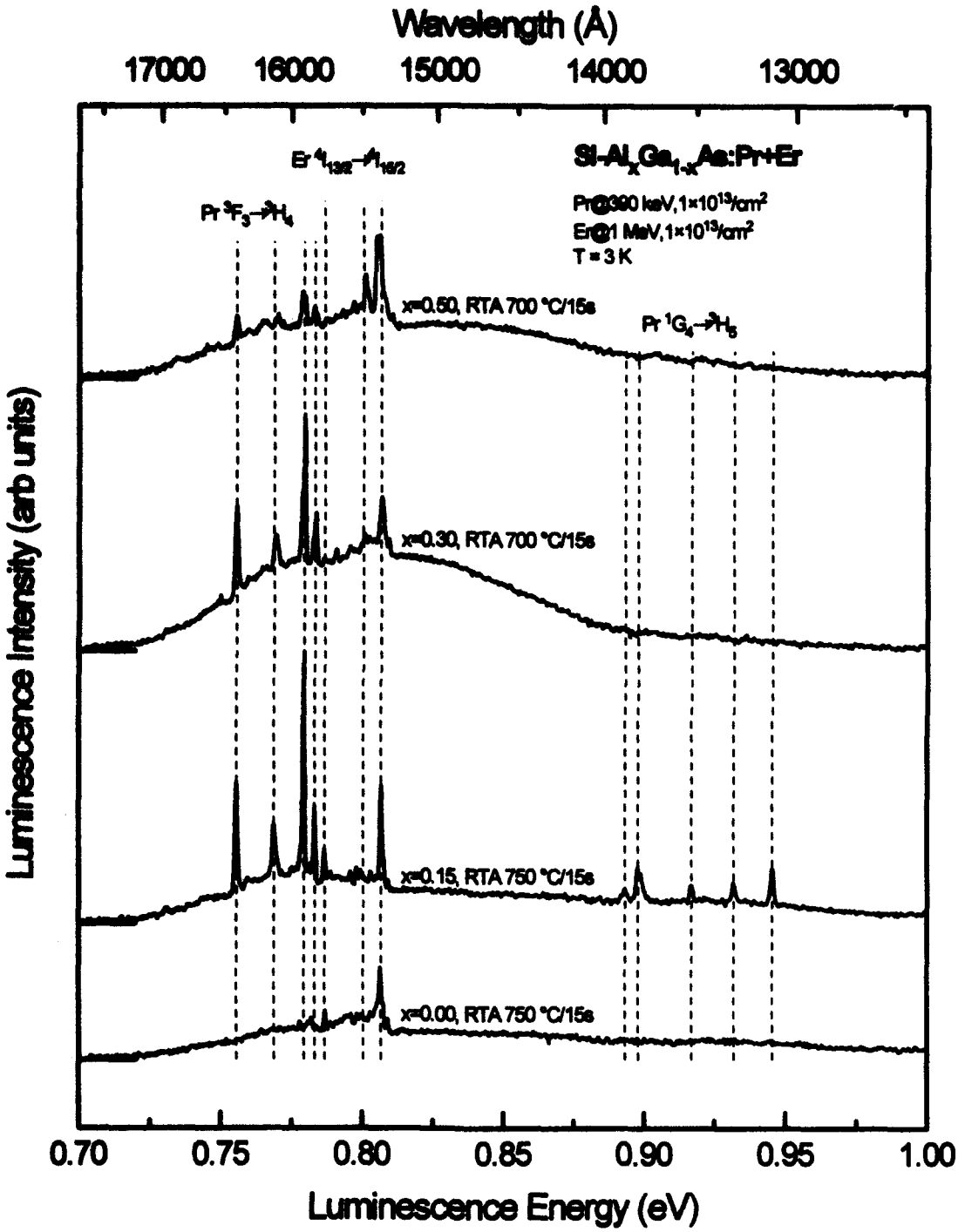

Figure 41. PL spectra taken at 3 K from SI-$Al_xGa_{1-x}As$ with x=0.00, 0.15, 0.30, and 0.50 implanted with Pr at 390 keV with a dose of $1\times10^{13}/cm^2$ and Er at 1 MeV with a dose of $1\times10^{13}/cm^2$ and annealed at various temperatures

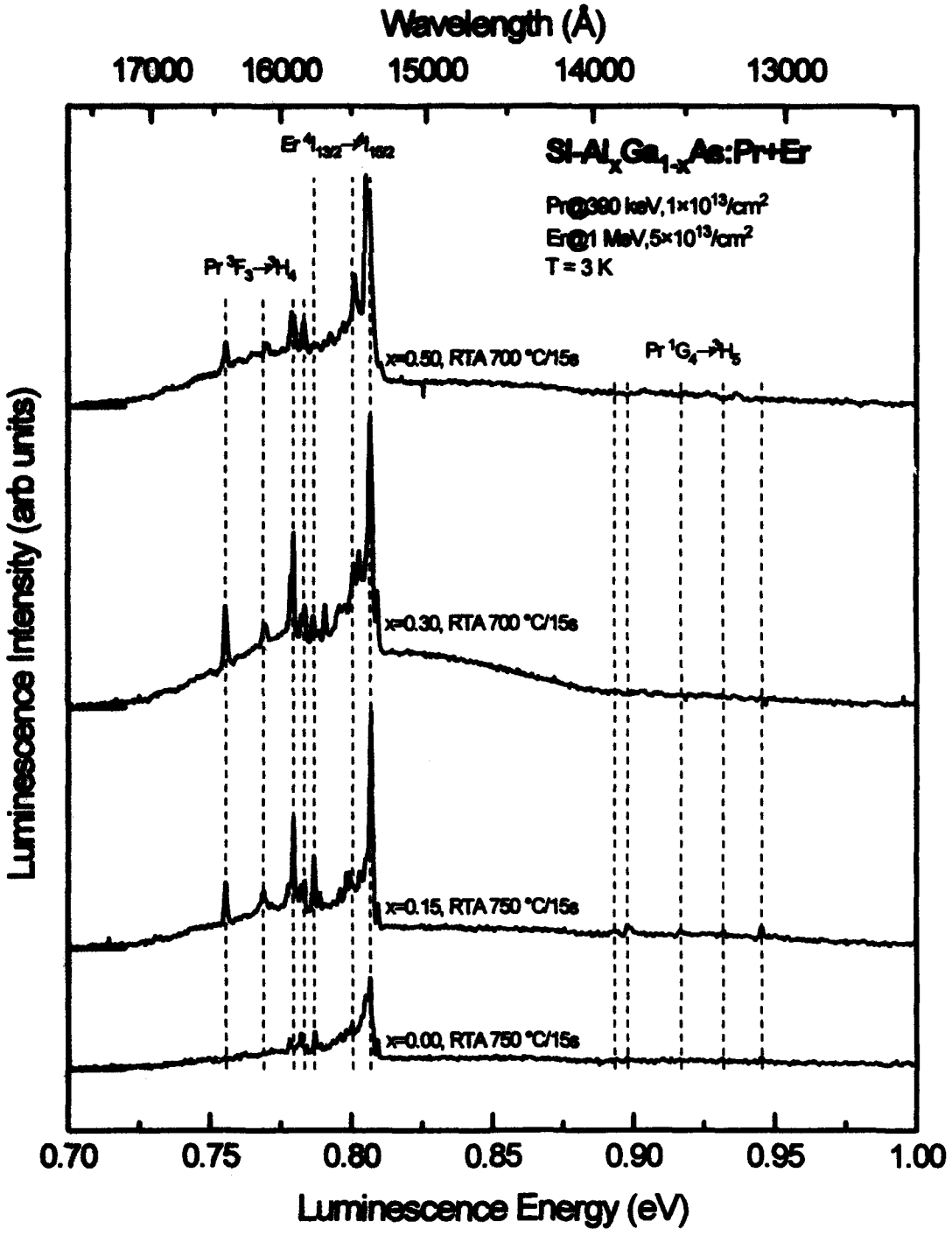

Figure 42. PL spectra taken at 3 K from SI-$Al_xGa_{1-x}As$ with x=0.00, 0.15, 0.30, and 0.50 implanted with Pr at 390 keV with a dose of $1\times10^{13}/cm^2$ and Er at 1 MeV with a dose of $5\times10^{13}/cm^2$ and annealed at various temperatures

seems to be dominant. The greater Er atom depth (due to higher implant energy) should not affect the Er PL intensity with respect to increased absorption of the exiting Er luminescence, but the laser excitation energy will be reduced at the greater depths. Thus direct comparison of the intensities is inconclusive. However, for the case of the high Er dose with a five-fold increase in atoms over Pr, the Er PL is increased at the expense of the Pr PL (Figures 35, 38, 39 and compare Figures 41 and 42), since there is a much greater number of Er atoms in the implant region.

The significant decrease in Pr PL in the presence of even the low dose Er (bottom spectrum in Figure 41), where the Pr and Er are mostly separated in the lattice, suggests that the apparently shared energy source (free carriers/excitons) is mobile at least within the 2000 Å implant region. If the free carriers/excitons were created by the laser and immediately absorbed only by local RE atoms, then no decrease in luminescence from either RE should have been observed.

Although the dual-doping of Er and Pr did not increase the luminescence intensity as hoped, important information can be gleaned from this data. Summarizing the results from this dual Pr and Er implantation study, the PL intensity from each RE in dual-doped samples was reduced compared to their singly doped counterparts. The energy positions and relative intensity of the PL emissions are essentially unchanged within each of the RE emission groups. Thus, no discernible interaction between the 2 different RE ions is occurring and their luminescence processes are essentially independent, although apparently competing for the same energy source. This is attributed to a failure of the Er and Pr to couple energetically, either because they are generally too distant in the lattice or an intrinsic inability of Pr-Er pair complexes to be excited simultaneously by Auger energy transfer.

Photoluminescence of Pr Codoped with Other Elements

Adding additional elements to the host:Pr compound, such as lighter atoms, is hoped to enhance the Pr emissions. These extra elements may enhance emissions through formation of complexes with Pr. These complexes may then (1) have a greater probability of binding an exciton, or (2) make the transfer of exciton recombination energy more likely. The formation of these complexes is especially likely due to the gettering effect of REs in general.

Since no codoping studies have ever been reported on Pr, the codope elements for this effort were chosen based on elements shown to enhance Er PL in Si (Michel *et al.*, 1991:2675). These include B, C, N, O, and F, which were implanted at doses of 1×10^{14} and $1\times10^{15}/cm^2$ into semiconductor hosts both without and with Pr implantation at 390 keV with a dose of $1\times10^{13}/cm^2$. The larger doses for the codope elements were chosen to increase the possibility of interaction with the Pr ions. The host semiconductors used in this study include SI-GaAs and SI-$Al_{0.14}Ga_{0.86}As$. In addition, SI-$Al_{0.15}Ga_{0.85}As$:Pr was implanted with oxygen as a consistency check between host wafers from different growth dates. The implantation energies for each of the codope elements were carefully chosen to closely align the peak implant densities of all codope implants with that of the Pr density profile. Since, for practical economic reasons, only one implant energy had to be selected for each element, the profile of Pr in $Al_{0.15}Ga_{0.85}As$ was chosen as the benchmark. Slight differences in the Pr depth profiles in the other hosts should make no significant difference in the resultant luminescence. Table 16 shows the implant energy used for each of the codope elements along with the implant depth information supplied by the PROFILE code. Comparison to Table 8 shows the difference in depths from Pr to be minor, especially compared to the projected straggling ranges. Figure 43 shows a representative comparison of the concentration of Pr and C atoms for the implantation parameters

TABLE 16

Pr and Codope Element Implantation Characteristics in $Al_{0.15}Ga_{0.85}As$

Element	Energy (keV)	Range, R_p (Å)	Straggling, ΔR_p (Å)
Boron	35	949	678
Carbon	46	953	610
Nitrogen	54	951	586
Oxygen	60	957	589
Fluorine	65	952	582
Praseodymium	390	947	323

used in this study. Note that the straggling ranges projected for the codopes are about twice that of Pr. This means that the codoped element density is spread over a wider volume of the host, thus even though the implant doses are 10 and 100 times that of the Pr, the samples implanted with a dose of $1\times10^{14}/cm^2$ have only 5 times the peak implant density as the Pr and the higher codope doses provide about 50 times the density profile of Pr. After both implantations, the samples were rapid thermal annealed at optimal temperatures previously determined.

Figures 44 and 45 show the respective results of this codoping study for SI-GaAs:Pr and SI-$Al_{0.14}Ga_{0.86}As$:Pr coimplanted at the lower dose of $1\times10^{14}/cm^2$. The higher dose evidenced identical results. The obvious and completely general effect of these codopes is to quench very effectively the Pr luminescence while increasing band-edge emissions in the host and cap layer. For GaAs:Pr shown in Figure 44, increased band-edge emissions (in second order) were seen at 1.458, 1.491, and 1.494 eV. The 1.494 eV peak is the common C_{As}-FB transition while the 1.458 eV peak is the phonon replica of the 1.494 eV peak and the 1.491 eV peak is either the Mg-FB or C_{As} DAP transition. Figure 45 shows second order band-edge emissions from the $Al_{0.14}Ga_{0.86}As$ host at 1.719 and 1.694 eV. The FE emission from the GaAs

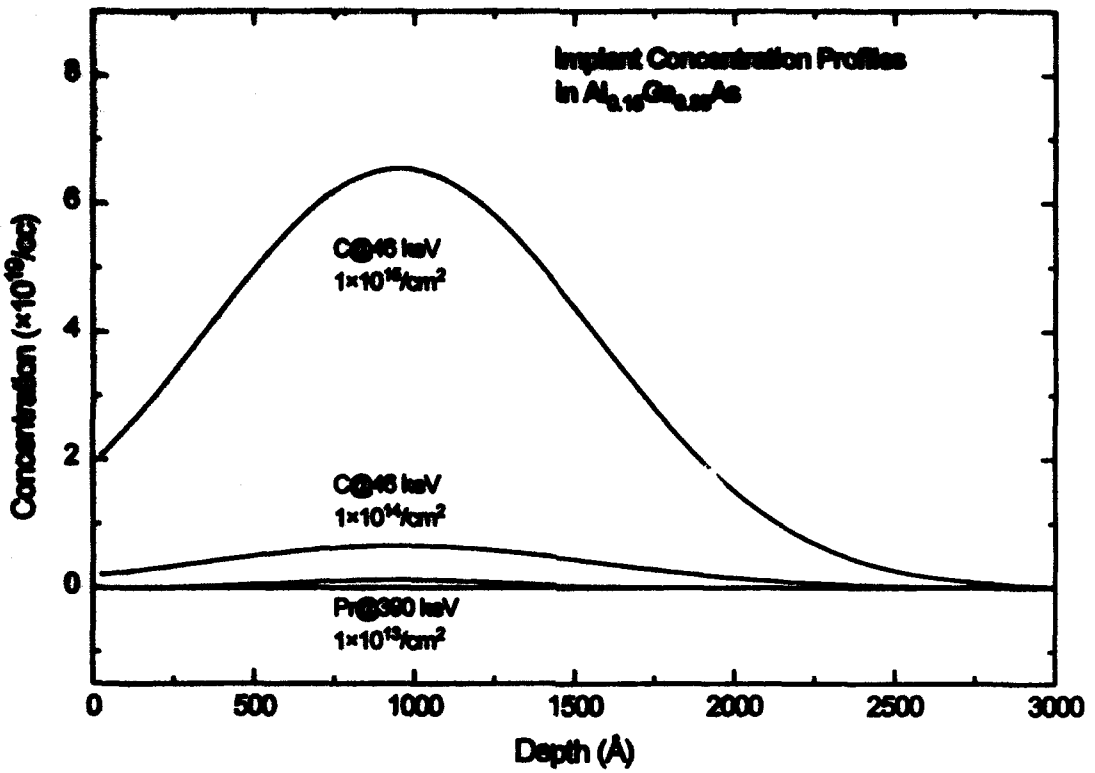

Figure 43. Concentration profiles of C and Pr implanted into $Al_{0.15}Ga_{0.85}As$ as used in the codoping study

cap layer is also seen at 1.513 eV along with the C_{As}-FB emission at 1.494 eV. The GaAs emissions differ slightly due to the different growth methods of the two samples with an LEC-grown GaAs substrate used in Figure 44 and MOCVD-grown GaAs in Figure 45. The $Al_{0.15}Ga_{0.85}As$:Pr sample is implanted with oxygen behaved exactly as the SI-$Al_{0.14}Ga_{0.86}As$:Pr+O sample with complete quenching of the Pr PL for both high and low oxygen doses.

The effect of the codope elements is likely to be either competition for the available free carriers/excitons or de-activation of the luminescence Pr ions through formation of non-luminescent Pr-codope complexes. Again, the results of Pr and O codoping show the strong contrast with Er and O codoping for both GaAs and AlGaAs which showed strong enhancement of the Er-related emissions (Colon *et al.*, 1993b:216; Colon *et al.*, 1993a:169).

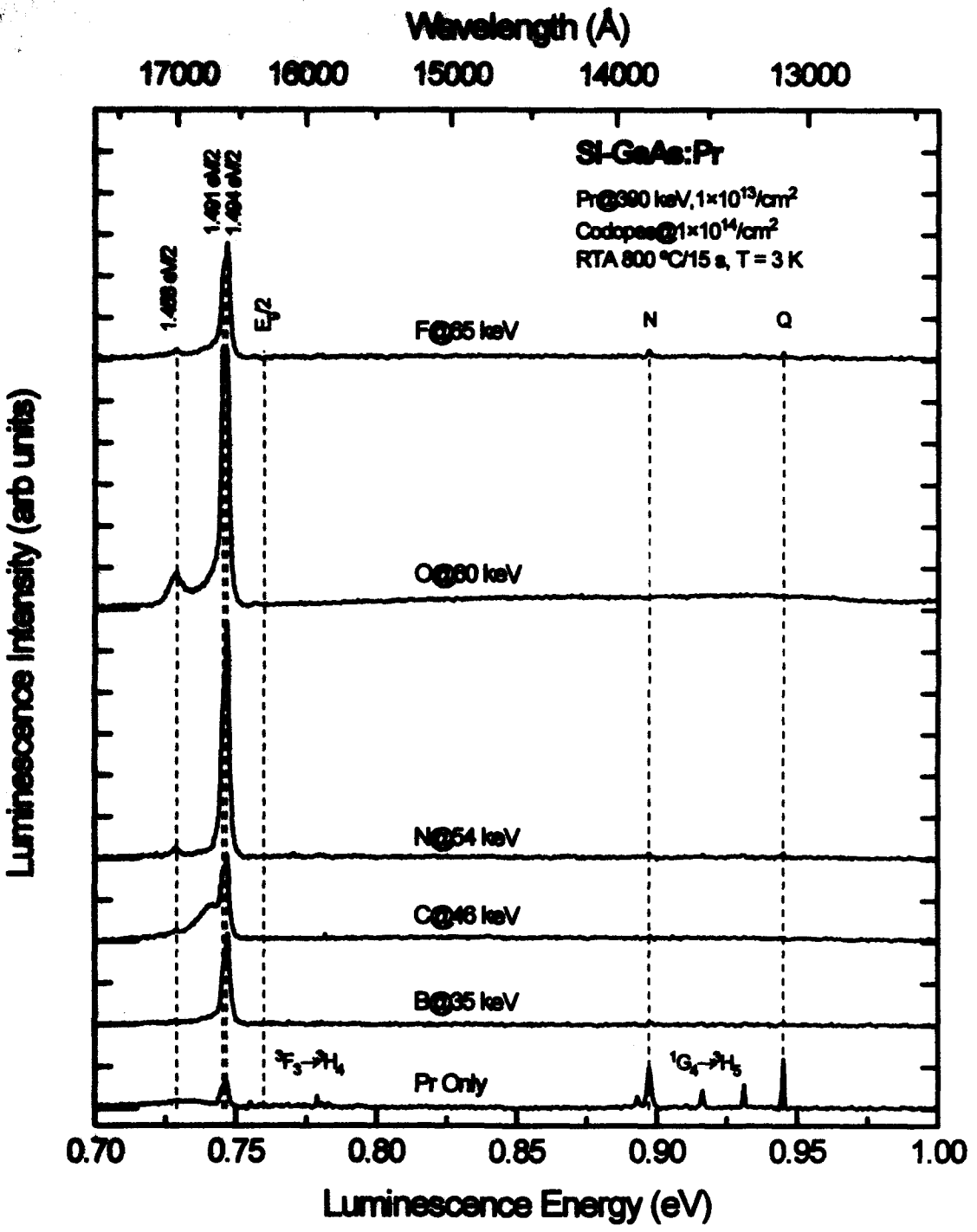

Figure 44. PL spectra taken at 3 K of SI-GaAs implanted with Pr at 390 keV with a dose of $10^{13}/cm^2$ and codoped with B, C, N, O, or F at energies indicated with a dose of $10^{14}/cm^2$ and annealed at 800 °C

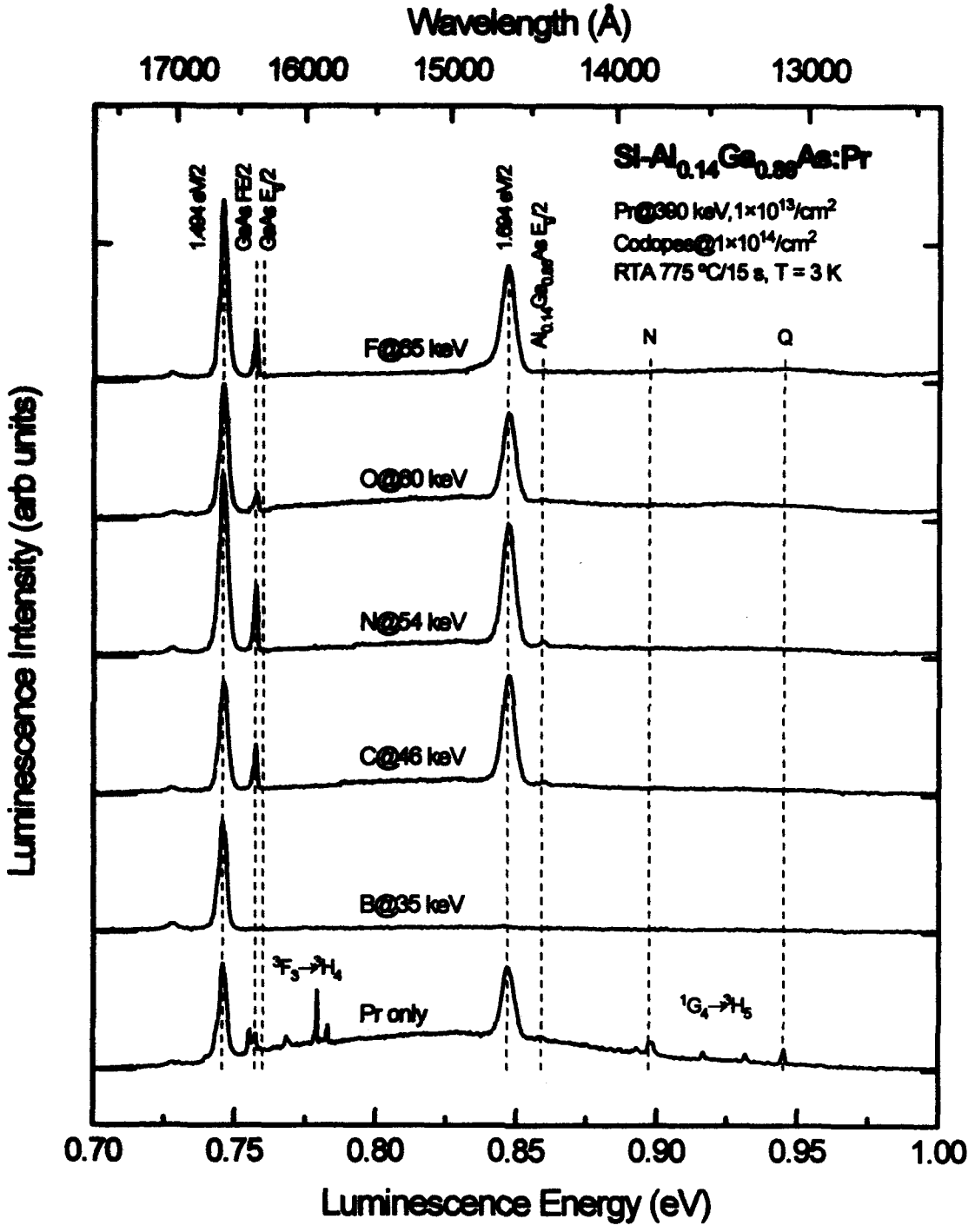

Figure 45. PL spectra taken at 3 K of SI-$Al_{0.14}Ga_{0.86}As$ implanted with Pr at 390 keV with a dose of $10^{13}/cm^2$ and Pr codoped with B, C, N, O, or F at energies indicated with a dose of $10^{14}/cm^2$ and annealed at 775 °C

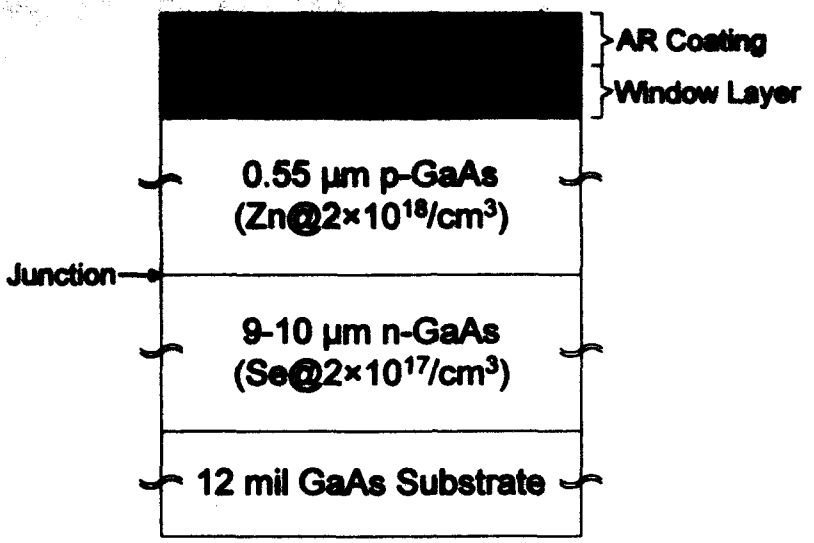

Figure 46. ManTech GaAs Solar Cell Structure used for Electroluminescence

Electroluminescence of Pr

To fabricate Pr-luminescent diodes, Pr was implanted into a p^+n GaAs junction at various depths on the p-side of the depletion region. The p-side was chosen since injection of free carriers occurs on the p-side of a junction because the density of states is more shallow in the n-type conduction band (Pankove, 1971:181).

The diodes used for this study were modified from solar cell junctions grown for the AFWAL ManTech Program ("Manufacturing Technology for GaAs Solar Cells", PO#F33615-81-C-5150). These MOCVD-grown solar cell structure is shown in Figure 46, and had an anti-reflective coating along with a window layer which were etched off using the following sequence:

1) Buffered Oxide Etchant (BOE) dip at room temperature longer than 60 seconds to remove the two surface oxide layers,
2) Deionized water (DI) rinse and dry, and
3) HCL:HNO_3:DI (10:1:9) dip at room temperature longer than 90 seconds to remove the AlGaAs window layer without etching the underlying GaAs.

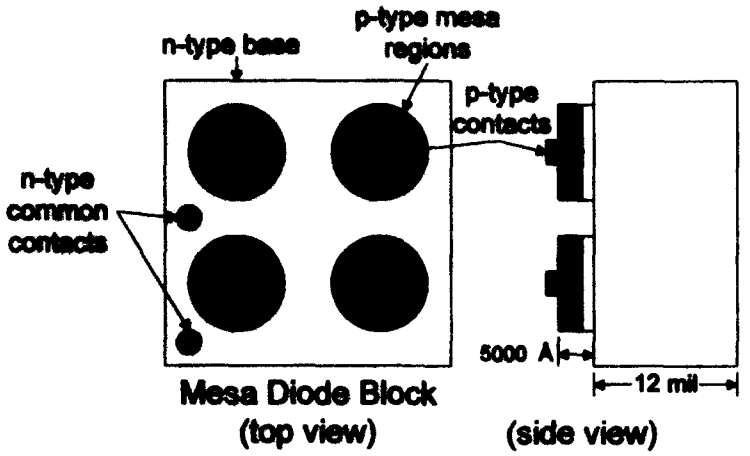

Figure 47. Mesa Diode Structure for GaAs:Pr Electroluminescence Experiments

Since the implantation depth of 390 keV Pr into GaAs is about 1000 Å and the best position of the Pr with respect to the depletion region was unknown, several wafers were etched to partially remove the original 0.55 μm GaAs layer to controlled depths. By etching the GaAs to desired depths, the Pr implant peak was positioned in four wafers from about 2000 Å from the depletion region on the p-side to about 500 Å into the n-side. This has the additional advantage of compensating for any errors in the depths of the originally grown wafers. The etch depths of actual wafers were monitored with a TENCOR Alpha-Step 250 profiler. The wafers were then all implanted with Pr at 390 keV at a dose of $1\times10^{13}/cm^2$, and rapid thermal annealed at 775° C for 15 seconds. Mesa diodes were then fabricated from these wafers in blocks of 4 (Figure 47) with 2 of these blocks mounted on a 16-pin DIP. The ohmic contacts used were Ni:Ge:Au (50:200:5000Å, RTA 425 °C/30 s) and Au:Zn:Au (50:250:5000 Å, RTA 375 °C/30 s) for the p-type.

Four devices were fabricated with p-type region depths of 2980±250 Å (Cell #1), 1809±250 Å (Cell #4), 783±250 Å (Cell #7), and 530±250 Å (Cell #10). Cell #4 was damaged during mounting and was unusable, while the others had 4 to 8 of the

diodes functional. For the electroluminescence experiments, all of the functional diodes on both blocks were connected in parallel and voltages of 1.88 to 5.46 V (with corresponding currents of 98 to 999 mA) were applied with the resulting emission spectra collected exactly as in the PL experiments. Unfortunately, none of the diodes displayed Pr luminescence, but all diodes showed near band-edge luminescence of the GaAs. Figure 48 shows the electroluminescence from Cell #1 along with photoluminescence from the surface of the diodes and from a bulk sample of the wafer from which Cell #1 was fabricated. These results are typical of those found for Cells #7 and #10. All of spectra showed clear GaAs band-edge-related luminescence in both first and second order, however none showed any evidence of Pr luminescence. The PL from the bulk samples displayed defect emissions which are very similar to the PL obtained from n-GaAs:Pr (Figure 19), but the Pr-bearing region in the diode contains a concentration of dopants an order of magnitude higher than that of the samples used in the host conductivity type study. Apparently, the dopants present in all diodes quenched the Pr luminescence. It was also possible that procedures used to fabricate the device from the junction material hindered the Pr luminescence. The metallization procedure used to attach contacts may introduce impurities such as gold into the Pr implanted region, and this may also reduce Pr luminescence. However, even the bulk material implanted with Pr was not capable of Pr luminescence. Possibly, lower doping of the host may yet allow Pr electroluminescence to be achieved.

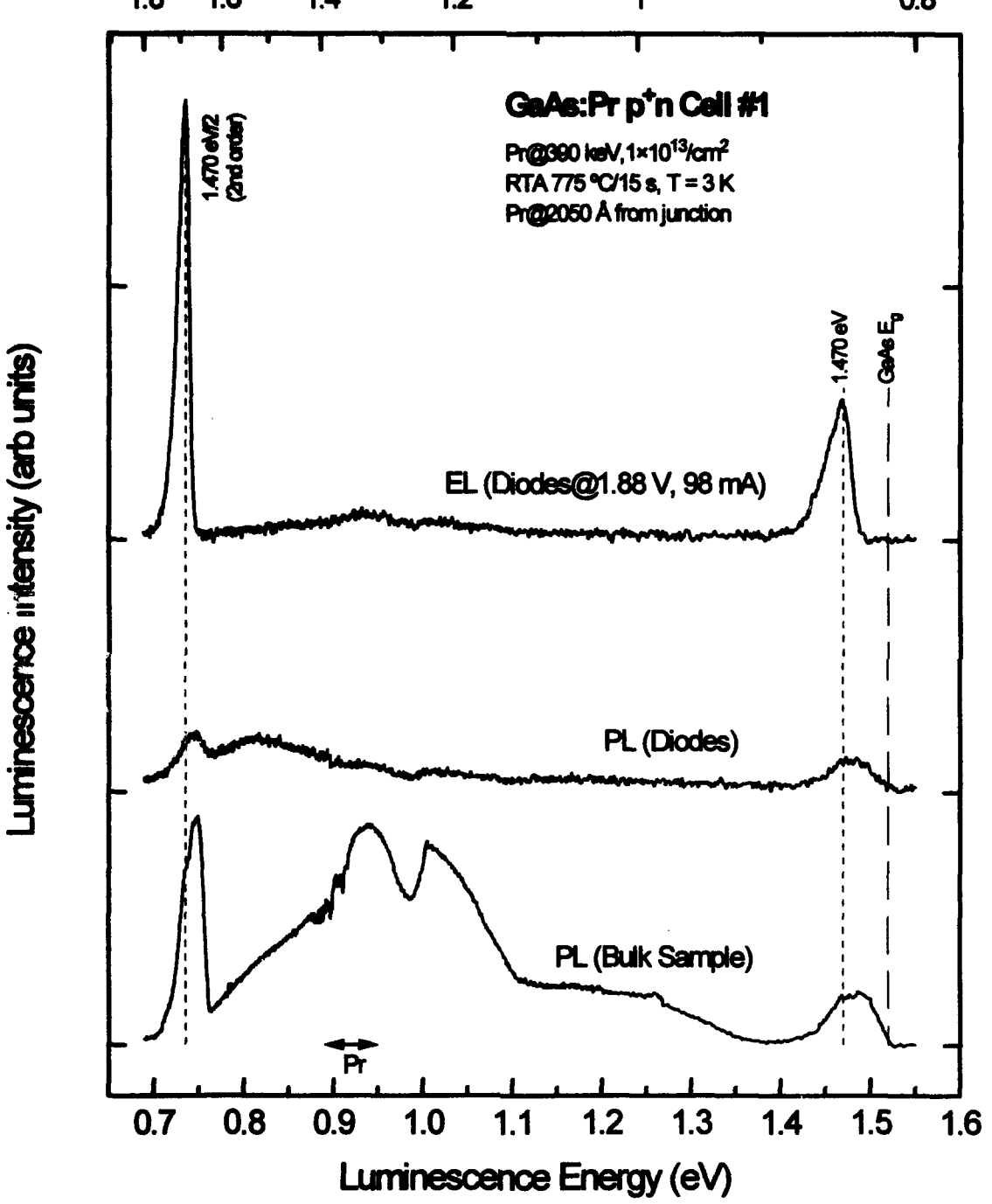

Figure 48. Electroluminescence and Photoluminescence from GaAs:Pr Cell #1

VII. CONCLUSIONS AND RECOMMENDATIONS

Summary

Each of the studies detailed in the previous chapter contributes information from which a portrait of the excitation mechanism for Pr in $Al_xGa_{1-x}As$ can be constructed. Table 17 contains a summary of important findings in this work. Since Pr emissions from $Al_{0.14}Ga_{0.86}As$ and $Al_{0.15}Ga_{0.85}As$ were nearly identical, but sufficient quantities of both were not available for a complete study, their results are reported together.

The following conclusions may be drawn from the data thus far presented:

1) The behavior of the Pr PL in the RTA studies including thermal stability and number of crystal field split emission lines argues that the Pr ions occupy Ga substitutional sites although the local site symmetry may be less than T_d.

2) The SEL study showed that excitation energy as low as that of free-to-bound transitions or bound excitons is sufficient for excitation of Pr in any of the studied hosts. Pr-related luminescence can be excited with a narrow range of laser excitation energies centered at 24 meV below the band-edge in GaAs. This may indicate direct pumping to the Pr-BE energy level. For $Al_{0.15}Ga_{0.85}As$, the SEL drop-off was broader and no below-gap maximum was observed over the range of over 280 meV below the band-edge.

3) The temperature-dependence study gave an activation energy for Pr lines in GaAs (22.5-28.9 meV) corresponding to the dissociation energy of bound excitons from the Pr sites. The smaller activation energies found for the $Al_{0.15}Ga_{0.85}As$ and $Al_{0.30}Ga_{0.70}As$ hosts probably correspond to dissociation energy of excitons which are less strongly bound to the Pr ion. Small activation energies of less than 4 meV may correspond to thermal excitation of the lower cold line level to the upper level. No evidence of different Pr luminescent centers was found.

TABLE 17

Summary of Significant Findings

Pr Luminescence	Host Semiconductors				
	GaAs	$Al_{0.14/0.15}GaAs$	$Al_{0.30}GaAs$	$Al_{0.50}GaAs$	Silicon
PL, $^3F_3 \rightarrow {}^3H_4$ group intensity	weak	very strong	strong	weak	none
PL, $^1G_4 \rightarrow {}^3H_5$ group intensity	medium	medium	very weak	none	none
PL, Optimal Dose ($/cm^2$)	$1\times10^{13}/cm^2$	$0.5,1\times10^{13}/cm^2$	$\geq5\times10^{13}/cm^2$	$\geq5\times10^{13}/cm^2$	
PL, Optimal RTA (±25 °C)	775-800 °C	750-775 °C	725 °C	725 °C (?)	
PL, Strongest in n/p/SI Host	p	SI	SI	n/p	
PL Intensity Power Dependence		square root			
SEL Drop off Energy (±3meV)	E_g-4 meV	E_g-11 meV			
SEL Below Gap Peak (±3 meV)	E_g-24 meV	none			
T-dep. Peak C, Act. En. E_1, E_2	1.2, 22.5 meV	9.6 meV	5.6 meV	too weak	
T-dep. Peak B, Act. En. E_1, E_2	2.2, 28.9 meV	1.4, 6.0 meV	too weak	too weak	
Er Dual-doping effect	quenched Pr PL	quenched Pr PL	quenched Pr PL	quenched Pr PL	
Codoping Effect (B,C,N,O,F)	quenched Pr PL	quenched Pr PL	not tested	not tested	
Electroluminescence	no Pr PL				

4) The square root dependence of the intensity on excitation laser power indicates that the bound exciton recombination energy may be transferred either to the Pr ion or a free carrier via an Auger process.

5) The reduction of Pr PL in hosts occurs when the hosts are doped with donors or acceptors, or they are codoped with other impurities is probably due to competition with other impurities for the available exciton recombination energy. The doping or codoped impurities were:

a) carrier-type impurities like Si and Zn,

b) other RE elements like Er, and

c) codoped impurities including B, C, N, O, and F.

6) The intensity of Pr emission groups varies strongly with Al mole fraction of $Al_xGa_{1-x}As$. The $^3F_3 \rightarrow {}^3H_4$ emissions are strongest in $Al_xGa_{1-x}As$ hosts with $x \geq 0.15$,

while for GaAs and $Al_{0.10}Ga_{0.90}As$, the strongest Pr emissions are the $^1G_4 \rightarrow {}^3H_5$ transition group. This behavior is abrupt, showing no gradual change. The change in relative PL intensities between the emission groups with different hosts is attributed to the differing bandgaps of those hosts and the interaction of these bandgaps with the internal 4f energy states of Pr^{3+}.

These pieces of information and their interpretation may now be assembled to propose an excitation mechanism for Pr in the succeeding sections.

Unfortunately, the potential application of Pr luminescence in GaAs, $Al_xGa_{1-x}As$, and Si technology appears to be no greater than that of other REs. Although Pr emissions at low temperatures are sharp and relatively strong, they still fall far short of the intensity and efficiency required for use in an LED. Attempts to increase the luminescent intensity through codoping with B, C, N, O, and F and dual-doping with Er were not successful and, although these tests are not completely definitive, there do not appear to be any obvious methods to achieve strong enhancement of Pr PL. The lack of any Pr-related electroluminescence was attributed to the impurities in the diode, but if Pr ions are, in general, poor competitors for absorption of exciton recombination energy, then the very impurities required to create the p-n junction may quench the Pr luminescence. Recommendations for further research presented at the end of this chapter do, however, present some areas for exploration, which may contribute to the further understanding of RE luminescence.

Excitation Mechanism Models

The excitation mechanism model must account for all of the data presented in this research effort as summarized above, both for the behavior of the Pr-related luminescence in the $Al_xGa_{1-x}As$ hosts and lack of the Pr-related luminescence in the silicon hosts. Examination and development of excitation mechanism models can be

divided into the bound exciton formation process and the bound exciton recombination process. These processes will be treated separately.

Bound Exciton Formation Process. The phenomenological model presented in Figure 49 shows the general overview of the proposed semiconductor host to Pr energy transfer process for above bandgap host excitation. This model is entirely consistent with the empirical data presented in this work and the conclusions drawn thus far. The excitation and luminescence process sequence is proposed as follows in 6 separate steps:

1) Free Carrier Formation Free carriers and free excitons are formed in the host material via an external pumping process such as a laser with a photon energy greater than the host bandgap.

2) Carrier/Exciton Trapping These free carriers can be trapped at the Pr sites which exist as isoelectronic traps (either for electrons or holes). The exact nature of this trap can not be conjectured until experiments are conducted to determine whether this is a hole or electron trap (such as DLTS). The trapping of free carriers by isoelectronic impurities (such as REs on group III sites in III-V semiconductors) is well established. Allen's atomic potential calculations showed that semiconductor isoelectronic bound states are probable when a large, heavy atom replaces a lighter one (Allen, 1971:1936). Several workers have reported experimental evidence of trapping of free carriers by REs in semiconductors including Yb and Er electron traps in InP (Whitney *et al.*, 1988b:2074; Lambert *et al.*, 1990:479), Yb electron traps in GaAs (Taguchi *et al.*, 1990:3390), and Er hole traps in GaAs (Colon *et al.*, 1992b:671). It is also possible that free excitons are themselves trapped at the Pr sites and this has also been proposed previously for RE excitation mechanisms (Lozykowksi, 1993:17760). Quenching processes are possible in this step which compete with the Pr ions for the

supply of free carriers. These include other trapping by other impurities, band-to-band recombination, free exciton formation and recombination, and other defects which allow free carriers to de-excite.

3) Bound Exciton Formation The carrier trapped at the Pr site attracts another oppositely charged carrier, forming a bound exciton. This step also depends on the concentration of free carriers in the host for the supply of oppositely charged carriers to form the bound exciton. Quenching effects for this step include ionization or dissociation of the bound exciton through thermal energy, impact ionization by other free carriers, or absorption of photon energy.

4) Bound Exciton Recombination This bound exciton has a finite lifetime and recombines releasing energy at the Pr ion site.

5) Energy Absorption The recombination energy is absorbed by the local Pr atom (or other particles). The energy conservation in this transfer is completed by another particle which may even be another, nearby Pr atom. This other particle may also be a carrier excited via an Auger process. Again, the energy transfer rate to the Pr ion may not be high. The bound exciton recombination energy may also be transferred entirely to an Auger process.

6) Pr Luminescence The excited Pr atom decays, radiating light.

This process is valid for all GaAs:Pr and $Al_xGa_{1-x}As$:Pr samples for above-gap excitation. A microscopic description of the Pr luminescence intensity can be constructed for this model with terms for each step in the excitation mechanism, which also accounts for each of the quenching processes listed above. A process diagram corresponding to this complete model is shown in Figure 50 along with associated equations and variables accounting for each step. First, above bandgap excitation depends on free carriers which have a concentration n described by the rate equation

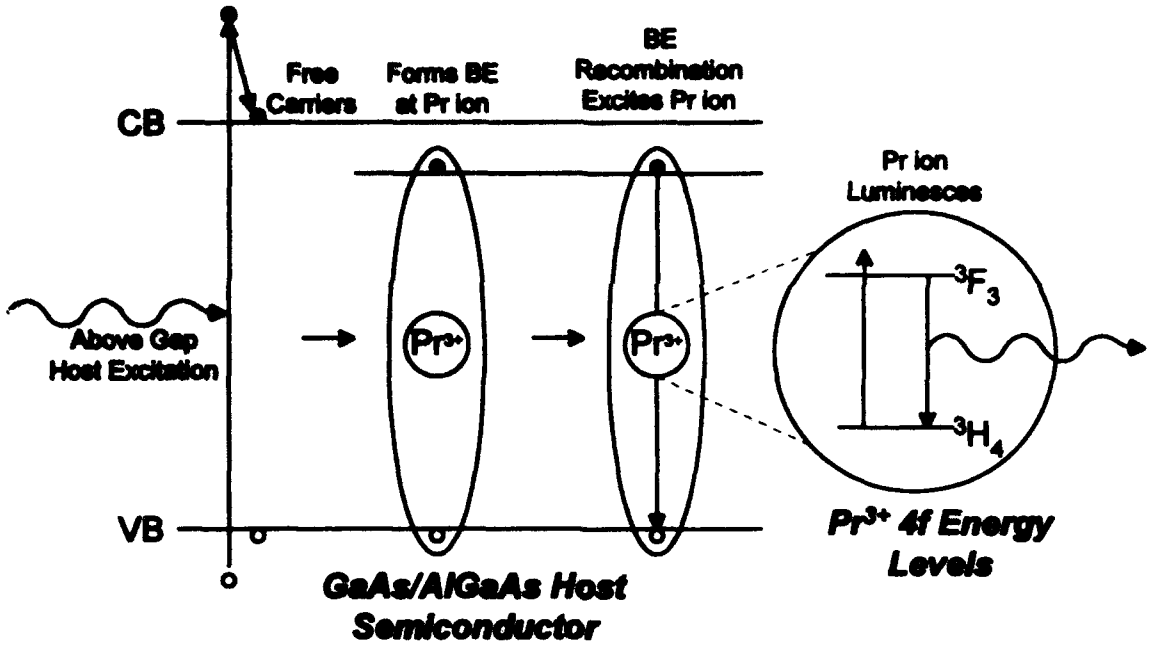

Figure 49. Above Bandgap Excitation Process of Pr Luminescence in $Al_xGa_{1-x}As$

$$\frac{dn}{dt} = G_l - \frac{n}{\tau_{tr}} - an^2 - cn^3, \tag{22}$$

where G_l is the pump generation rate, τ_{tr} is the carrier lifetime due to deep trap recombination, an^2 is the recombination rate through exciton formation, and cn^3 is the recombination rate via Auger processes (Coffa *et al.*, 1993:11787). Simple steady state solutions to three limiting cases of this rate equation exist. At low temperatures in good crystals, exciton recombination prevails giving (Coffa *et al.*, 1993:11787)

$$n = \left(\frac{G_l}{a}\right)^{1/2}. \tag{23}$$

Pr Excitation & Luminescence Process

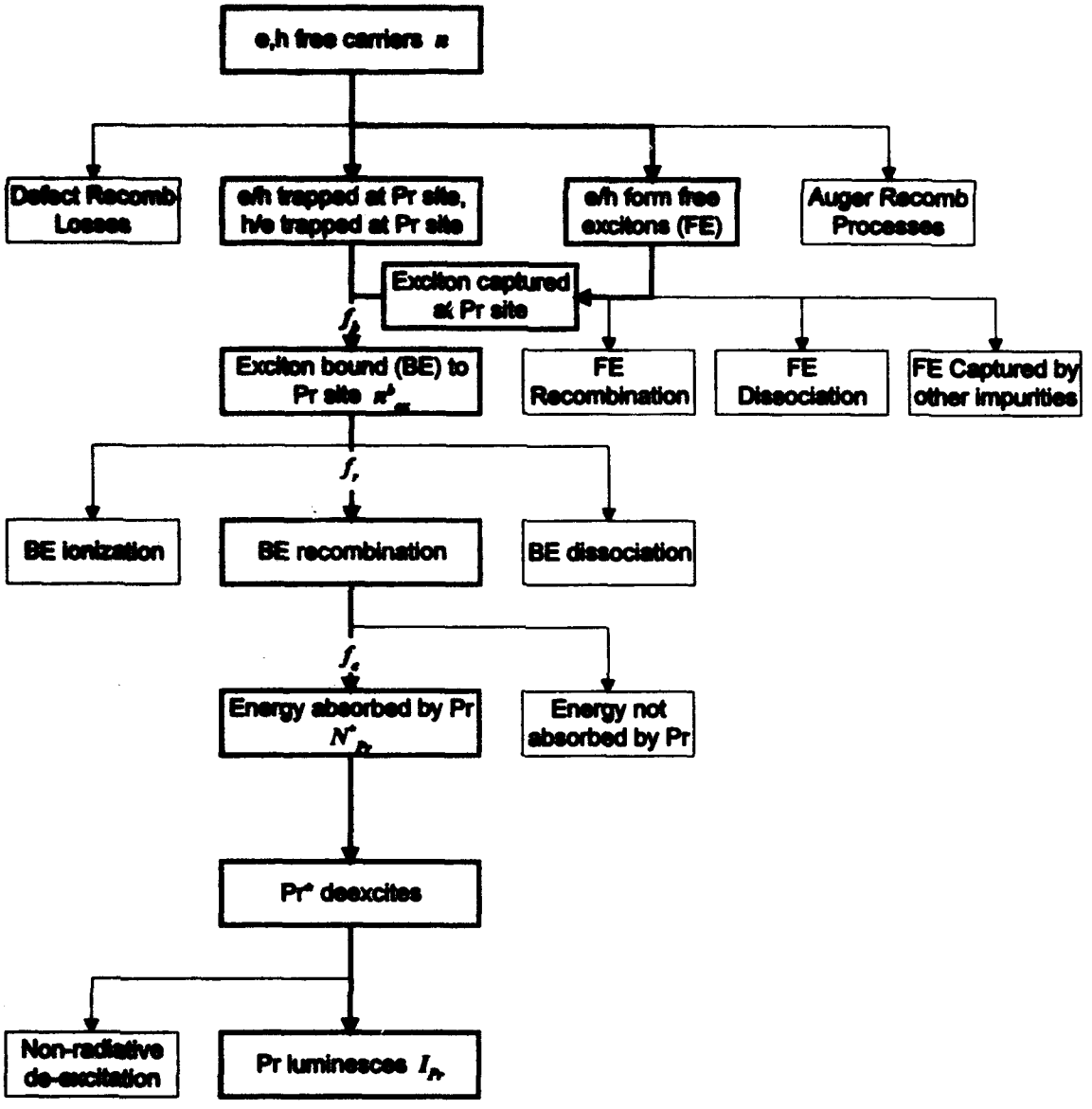

Figure 50. Process Diagram for the Pr Excitation Mechanism in $Al_xGa_{1-x}As$

For high temperatures, deep trap recombination dominates giving (Coffa *et al.*, 1993:11787)

$$n = G_l \tau_{tr}. \tag{24}$$

Finally, for high pump rates G_l, Auger processes dominate because of the large n^3 dependence giving

$$n = \left(\frac{G_l}{c}\right)^{1/3}. \tag{25}$$

Since the spectra in this effort were taken at low temperature with potentially high pump rates, a combination of exciton and Auger processes probably dominates. The square root power dependence of the PL intensity supports the strength of the Auger processes in these materials. Coffa *et al.* also give a rate equation for excited Er concentration, which may be adapted to describe the Pr luminescence process. The rate equation for excited state Pr ion concentration N^*_{Pr} is given by

$$\frac{dN^*_{Pr}}{dt} = f_r f_e \frac{n^b_{ex}}{\tau^*}\left(1 - \frac{N^*_{Pr}}{N_{Pr}}\right) - \frac{N^*_{Pr}}{\tau_d}, \tag{26}$$

where n^b_{ex} is the concentration of bound excitons at Pr ions, τ^* is the bound exciton recombination lifetime, N_{Pr} is the total concentration of optically active Pr, f_r is the fraction of BE at the Pr ions which do not ionize or dissociate prior to recombination (dependent on the temperature), f_e is the fraction of recombining bound excitons which excite the Pr ion (due to competition from photon emission and Auger processes), and τ_d is the decay time of the Pr ions whether radiative or non-radiative. The first term in Eq (26) is the rate of excitation events which is limited by the number of already

excited Pr ions; this is taken into account by the $(1-N^*_{Pr}/N_{Pr})$ factor. The second term represents the de-excitation process. Eq (26) depends on the free carrier concentration n through the bound exciton concentration n^b_{ex} in the form

$$n^b_{ex} = f_b n^2, \tag{27}$$

where f_b is a factor accounting for other processes competing for free carriers (such as defects, other impurities, or free exciton formation). If Pr binding of excitons is not a dominant process in the sample, then Eq (26) may be considered independent of Eq (22) in terms of the number of carriers n. Thus, assuming a steady state solution to Eq (26) and that Pr luminescence is proportional to the concentration of excited Pr ions, the intensity of the Pr luminescence I_{Pr} is given by

$$I_{Pr} \propto \frac{N^*_{Pr}}{\tau_{rad}} = \frac{1}{\tau_{rad}} \frac{f_r f_e n^b_{ex}}{\frac{f_r f_e n^b_{ex}}{N_{Pr}} + \frac{\tau^*}{\tau_d}}, \tag{28}$$

where τ_{rad} is the lifetime of the radiative decay for the excited Pr ion. The controllable conditions which maximize this luminescence include increasing the n^b_{ex} factor through increasing the free carrier concentration or reduction of impurities which compete for the free carriers. Also increasing N_{Pr} will enlarge I_{Pr}, but practical limits on the solubility of Pr ions in the lattice constrain this enhancement method.

Bound Exciton Recombination Process. The previous model explains the method for Pr excitation through bound exciton recombination at the Pr site. However, the BE energies are much greater than any single energy level of Pr, so the energy transfer process still requires a complete rigorous explanation of energy conservation. A review of the data suggests two possible explanations. The first is an Auger-assisted

process (Figure 51a), while the second is a novel Pr dual resonance process (Figure 51b). These will be examined in the context of the primary BE excitation-based model.

Pr luminescence has been observed over a wide range of host bandgaps (1.5-2.1 eV) which correspond to similarly large BE recombination energies. This shows a wide BE recombination energy to Pr energetic coupling range. Since the BE energies are all much greater than the excited states of Pr^{3+}, a process must exist which absorbs the remaining energy difference after exciting the 4f electrons to complete energy conservation for this transfer. Thus, there must exist a corresponding energy conservation process which is capable of absorbing a continuum of energies. A possible process which fits these requirements is a transfer of the energy difference between the BE and the Pr levels to free carriers via an Auger process (Figure 51a). This requires yet another particle to participate in this excitation process. The energy conservation for this model is described by

$$E_{BE} = E_{Pr^*} + E_{Auger}, \tag{29}$$

where E_{BE} is the bound exciton recombination energy which is divided between the Pr excited state energy E_{Pr^*} and the energy transferred to a carrier via an Auger process E_{Auger}. This process must allocate sufficient energy (E_{Pr^*}) to the Pr ion of at least 0.783 eV to allow the $^3F_3 \rightarrow {}^3H_4$ transition and about 1.2 eV to excite the Pr ion from the $^3H_4$ ground state to the $^1G_4$ state allowing the $^1G_4 \rightarrow {}^3H_5$ or $^1G_4 \rightarrow {}^3H_4$ emissions. These then require Auger transfer energy E_{Auger} of at least 0.32 eV in GaAs (using approximately E_g-1.2 eV) up to 1.287 eV in $Al_{0.50}Ga_{0.50}As$ (using approximately E_g-0.783 eV). This is indeed a very wide range of energies required for Auger-assisted energy conservation from the BE recombination energy. This Auger-assisted process also does not explain the switch in relative luminescence intensity between the $^3F_3 \rightarrow {}^3H_4$ and $^1G_4 \rightarrow {}^3H_5$ emission groups as the Al mole fraction x changes from

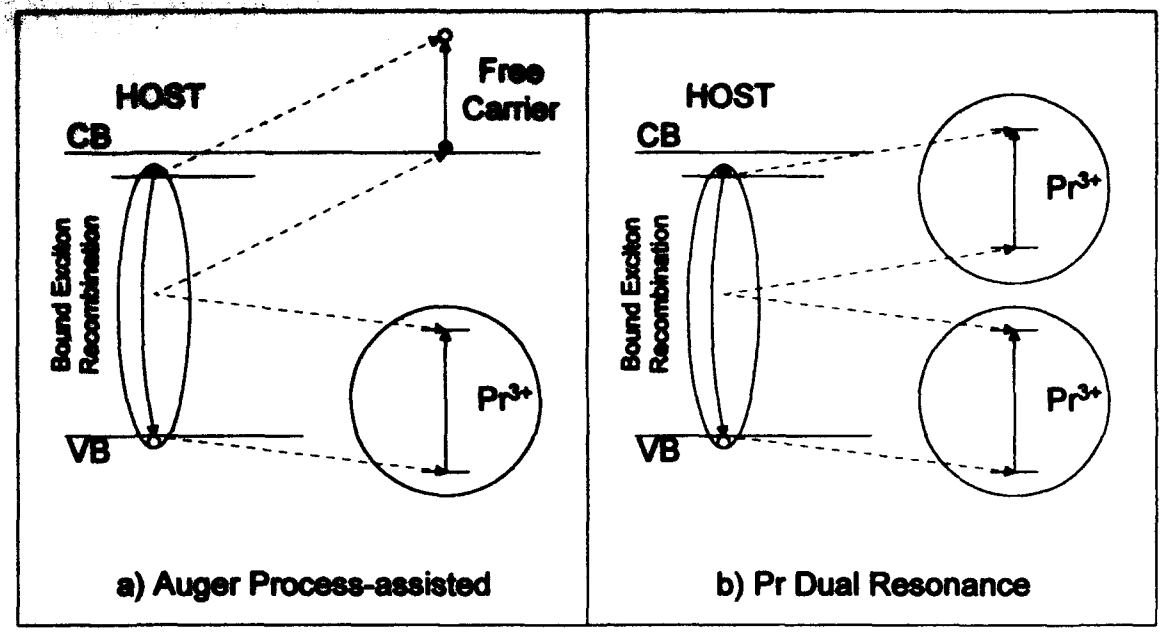

Figure 51. Bound Exciton Recombination Energy Transfer Processes

x=0.10 to 0.15 unless there is some preferred Auger transfer mechanism. This problem with the Auger-assisted explanation prompted the next possible model.

The dramatic change in relative Pr luminescence intensities between the two emission groups with Al mole fraction needs another explanation and forms the basis for the second explanation for BE energy transfer mechanism. In the former explanation, the BE recombination energy is split between the Pr ion and the Auger process particle. It is also possible that the recombination energy from the bound exciton is split between two different, but closely located Pr ions (Figure 51b). Examination of the Pr energy levels compared to the BE energies for each host reveals a very interesting correlation. When taken as pairs representing double resonance of the Pr ion energy levels, the sum of the two values of certain combinations of excited Pr energies are close to the BE recombination energy which may explain the luminescent behavior observed. In other words, the Pr^{3+} energy level pairs which are

best energetically matched to the BE recombination energy seem to correlate with the observed changes in emission group intensity. Table 18 shows Pr^{3+} paired excited energy sums which are near the bandgap energies (and presumably the BE energies) for the hosts in this study. The difference in the Pr energy sums and the BE energies are small enough that lattice phonons can complete the energy conservation during the process. Since so few of the Pr^{3+} energy levels are involved in the IR emissions studied here, the energy levels are based on the comprehensive studies of Pr^{3+} energy levels in $LaCl_3$ summarized in Dieke's book (Dieke, 1968:196). The energy conservation of this model is described by

$$E_{BE} = E1_{Pr^*} + E2_{Pr^*}, \tag{30}$$

where $E1_{Pr^*}$ and $E2_{Pr^*}$ are excited states of the two Pr^{3+} ions which split the available bound exciton recombination energy E_{BE}. For example, the Pr-bound exciton recombination energy in GaAs would be slightly less than the 1.52 eV bandgap, which would be sufficient and energetically well-matched to either the $^1G_4$ + $^3H_5$ (1.466 eV) or the $^3F_4$ + $^3F_2$ (1.430 eV) excitation sums. Since no $^3F_4$-based transitions were seen in this study or have been reported, it is likely that the $^3F_4$ state may be thermalized to the next lowest level $^3F_3$ which is only $\sim$54 meV lower in energy than the $^3F_4$ level. Also, no $^3F_2 \rightarrow {}^3H_4$ emissions were seen in this study, nor have any been reported in other Pr studies (Erickson *et al.*, 1993). This implies that the transition from $^3F_2$ to $^3H_4$ may be a forbidden transition, or, at best, a very weak transition. Thus, although emissions from $^1G_4$, $^3H_5$, and $^3F_3$ to $^3H_4$ are all possible from GaAs:Pr under this model, the $^1G_4$- and $^3H_5$-based emissions are expected to be strongest because they have the closest energy match to the BE energy, while the $^3F_3$-based emissions will be weaker because they are less well energetically matched to the BE energy. In fact,

TABLE 18

Pair Sums of Pr^{3+} Energy Levels

Pr^{3+} Energy Levels	Energy Sum (eV)
$^1G_4 + {}^3F_4$	2.032
$^1G_4 + {}^3F_3$	1.978
$^1G_4 + {}^3F_2$	1.804
$^1G_4 + {}^3H_6$	1.737
$^3F_4 + {}^3F_4$	1.658
$^3F_4 + {}^3F_3$	1.604
$^3F_3 + {}^3F_3$	1.550
$^1G_4 + {}^3H_5$	1.466
$^3F_4 + {}^3F_2$	1.430
$^3F_3 + {}^3F_2$	1.376
$^3F_4 + {}^3H_5$	1.092
$^3F_3 + {}^3H_5$	1.038

weak $^3F_3$- and strong $^1G_4$-based emissions were observed in GaAs:Pr. However, the transition of $^3H_5 \rightarrow {}^3H_4$ has not been experimentally confirmed yet.

Similarly for $Al_{0.15}Ga_{0.85}As$:Pr, the bound exciton energy is believed to be slightly less than the 1.73 eV band gap, thus the $^3F_4 + {}^3F_4$ (1.658 eV), $^3F_4 + {}^3F_3$ (1.604 eV), $^3F_3 + {}^3F_3$ (1.550 eV), and $^1G_4 + {}^3H_5$ (1.466 eV) sums are all energetically possible. The most likely of these excitations are $^3F_4 + {}^3F_4$ and $^3F_4 + {}^3F_3$ because these are the closest matches to the bound exciton recombination energy of $Al_{0.15}Ga_{0.85}As$. As mentioned above, the $^3F_4$ state may be thermalized to $^3F_3$. Then in this case, strong $^3F_3$-based transitions are expected. Also, the pair excitations of $^3F_3 + {}^3F_3$ could be strong, although the energy match is slightly worse than the above two cases. On the other hand, the pair excitation of $^1G_4 + {}^3H_5$ may not be strong because of a poor energy match to the recombination energy of bound excitons. Thus, weak $^1G_4$-based transitions are expected. Indeed, this is exactly what is observed from

$Al_{0.15}Ga_{0.85}As$:Pr. Note that the $^3F_4 + {}^3F_4$, $^3F_4 + {}^3F_3$, and $^3F_3 + {}^3F_3$ energetic combinations produce a total of six excited Pr ions which will likely all emit $^3F_3 \rightarrow {}^3H_4$, while $^1G_4 + {}^3H_5$ pair produces only one Pr ion which can emit from the $^1G_4 \rightarrow {}^3H_5$ transition. This is another reason to expect more intense $^3F_3 \rightarrow {}^3H_4$ emissions than $^1G_4 \rightarrow {}^3H_5$ emissions.

For $Al_{0.30}Ga_{0.70}As$:Pr, the BE energy will be slightly less than 1.94 eV. The best energetically matched pair is $^1G_4 + {}^3F_2$, however, as stated earlier, this is an unlikely process because the excitation from $^3H_4$ to $^3F_2$ appears to be a very weak transition at best. The next best energetic matches are the same as those for $Al_{0.15}Ga_{0.85}As$, but with a greater energy difference. Thus, similar emissions to $Al_{0.15}Ga_{0.85}As$ are expected, but substantially reduced in intensity, just as have been observed. This same effect occurs with $Al_{0.50}Ga_{0.50}As$, with even greater reduction in the emission intensities as is also seen.

The exact solution to the issue of energy conservation in the BE energy absorption process by the Pr ions may not be exclusively either of the two preceding models. It seems likely that both of these processes occur to some degree, since neither seems to be a completely satisfying model for this BE energy recombination step.

Lack of Pr Luminescence in Si. No luminescence from Pr was seen in Si hosts and this may result from any number of potential quenching effects which have been identified in this study. First, the relation of Pr to silicon is fundamentally different from that of III-V materials since silicon is a group IV elements. Thus, trivalent Pr in a substitutional site is presumed to behave as an acceptor-like impurity. Pr luminescent centers are believed to be substitutional and isoelectronic in the $Al_xGa_{1-x}As$ hosts, while Pr may be neither in silicon. Also the low temperature bandgap of silicon

(1.17 eV) is much less than that of any other host semiconductor tested in this study (1.52 to 2.07 eV), along with being indirect (although weak Pr emissions from the indirect gap $Al_{0.5}Ga_{0.5}As$ host were detected). This low bandgap is, in fact, less than the $^1G_4$ excited state of Pr^{3+} (~1.2 eV) eliminating the possibility of pumping the ground-state 4f electron to this level. Under the dual-resonance model for Pr excitation, there is only one energy pair containing $^3F_3$ and one pair containing $^3F_4$ which have an energy less than the recombination energy of a bound exciton in silicon, i.e., the excitation of $^3F_3+^3H_5$ (1.038 eV) or $^3F_4+^3H_5$ (1.092 eV). Additionally, only p- and n-type silicon host materials were tested. The study of Pr-implanted in to n- and p-type $Al_xGa_{1-x}As$ hosts has shown evidence that, in general, impurities have a strong quenching effect on Pr luminescence. Finally, the excitation laser penetration depth is not well matched to the Pr implantation depths in Si, as was noted earlier. It seems that Pr is not well suited for use as a luminescent material in silicon, although it is not possible from the evidence in this study to positively discriminate between these possible reasons.

Comparison with Er and Yb Excitation Models. Extensive research has been conducted on emissions from both Er and Yb in semiconductors and well-developed excitation mechanism models were put forward. These models do differ from those presented here for Pr, and none has presented a dual-resonance model involving simultaneous excitation of two RE particles. In general, the availability of DLTS data allows more specific details to be part of these processes.

Colon *et al.* have discovered that Er forms at least two hole traps in GaAs (at 35 and 360 meV above the VB) and outlined a very specific set of steps for Er excitation for laser excitation energy greater than and smaller than E_g of the host (Colon *et al.*, 1992b:674). For the above-gap laser excitation, free holes are trapped,

which then form bound excitons whose recombination transfers energy to the Er ion via an Auger energy transfer. For laser excitation less than the bandgap, electrons at the trap are excited to the CB leaving behind a bound hole which subsequently recombines with an electron transferring its energy to the Er 4f-shell. One difference between this work on Er and that presented here for Pr is the existence of deep traps which were not found through temperature dependent PL measurements for Pr, but can not be completely ruled out until DLTS is performed on GaAs:Pr.

Takahei and Taguchi have worked extensively on the Yb in InP, and have shown that Yb forms an acceptor-like electron (AE) trap at about 30 meV below the CB in InP (Takahei and Taguchi, 1992:643). This AE trap level is located close to the CB, but is acceptor-like in that it becomes negatively charged by capturing an electron from the CB. The captured electron was shown to exist outside the Yb 4f shell maintaining the Yb^{3+} ion, thus showing that the AE trap acts as an isoelectronic electron trap. Since the Yb center is isoelectronic, there is no long range coulombic force such as that of typical shallow donors and acceptors. Thus the trapped electron is localized around the Yb site and recombination of this electron with a hole will result in a high transfer rate of the recombination energy via an Auger process to the 4f electron of Yb. Energy conservation in this model by Takahei and Taguchi is invoked simply through the Auger process, presumably through a free carrier. Again, as proposed for Pr, the basic energy source for Yb is trapped electron-hole recombination whether captured separately or as an exciton.

Recommendations

Several extensions of this research effort are possible which would themselves greatly contribute to the increased understanding of Pr luminescence. These include experiments to:

(1) Investigate the dual resonance model of excitation of two Pr ions via further luminescence measurements using different semiconductor hosts with proper bandgap energies. Since the model requires pairs of Pr ions, the intensity of Pr emissions should be proportional to the square of the Pr concentration for low implant doses.

(2) Conduct DLTS and temperature dependent Hall effect measurements on Pr in various hosts to determine deep trap levels associated with Pr in these hosts. This would require higher Pr implantation energies (MeV range) to cause deeper implantation depths to fabricate p-n junctions or Schottky diodes for DLTS measurements.

(3) Conduct SIMS measurements to determine the actual Pr density profile for in the samples used in this study.

(4) Continue work on EL by constructing and optimizing a proper Pr-based diode utilizing well-understood host semiconductors. The most promising semiconductors are low-Al fraction ($x \sim 0.15$) $Al_xGa_{1-x}As$ hosts with low level doped p-n junction. PL tests should be run on any bulk junction material prior to diode device fabrication to verify that the implanted junction material has reasonably strong Pr emissions.

(5) Conduct temperature dependence PL and SEL experiments on Pr-Er dual-doped semiconductors to better understand the processes in these materials. Hopefully a new Pr-Er complex will manifest itself with promising results of strong PL.

(6) Conduct more PL on Si:Pr annealed at lower temperatures than those attempted in this effort (<750 °C).

(7) Compare the band-edge emissions intensity with that of Pr emission as a function of Pr concentration providing some insight into the 4f excitation mechanism.

APPENDIX A: Host Information

Note: all AlGaAs wafers are capped with a layer of 50-200 Å of GaAs to prevent oxidation.

Vendor/Growth	Production Run	Wafer Number(s)	Composition	Layer Thickness	Carrier Dopant	Carrier Type, Density (cm-3)
Epitronics/MOCVD	03-PR-4139	34/3	$Al_{0.15}Ga_{0.85}As$	5000 Å	und	p, < 5E16
Epitronics/MOCVD	03-PR-4145	198/2	$Al_{0.15}Ga_{0.85}As$	5000 Å	und	p, < 5E16
Epitronics/MOCVD	03-PR-4129	167/3	$Al_{0.15}Ga_{0.85}As$	5000 Å	Si	n,1.0E17
Epitronics/MOCVD	03-PR-4129	101/2	$Al_{0.15}Ga_{0.85}As$	5000 Å	Si	n,1.0E17
Epitronics/MOCVD	01-PR-4484	193/3	$Al_{0.15}Ga_{0.85}As$	5000 Å	Zn	p,1.0E17
Epitronics/MOCVD	01-PR-4484	23/2	$Al_{0.15}Ga_{0.85}As$	5000 Å	Zn	p,1.0E17
Epitronics/MOCVD	03-PR-4127	195/2	$Al_{0.30}Ga_{0.70}As$	5000 Å	Si	n,1.0E17
Epitronics/MOCVD	03-PR-4137	30/2	$Al_{0.30}Ga_{0.70}As$	5000 Å	Si	n,1.0E17
Epitronics/MOCVD	01-PR-4490	74/2	$Al_{0.30}Ga_{0.70}As$	5000 Å	Zn	p,1.0E17
Epitronics/MOCVD	01-PR-4490	77/3	$Al_{0.30}Ga_{0.70}As$	5000 Å	Zn	p,1.0E17
Epitronics/MOCVD	02-PR-6570	79/2	$Al_{0.30}Ga_{0.70}As$	5000 Å	und	p, < 5E16
Epitronics/MOCVD	02-PR-6570	80/3	$Al_{0.30}Ga_{0.70}As$	5000 Å	und	p, < 5E16
Epitronics/MOCVD	03-PR-4124	72/2	$Al_{0.50}Ga_{0.50}As$	5000 Å	Si	n,1.0E17
Epitronics/MOCVD	03-PR-4124	182/3	$Al_{0.50}Ga_{0.50}As$	5000 Å	Si	n,1.0E17
Epitronics/MOCVD	01-PR-4508	78/2	$Al_{0.50}Ga_{0.50}As$	5000 Å	Zn	p,1.0E17
Epitronics/MOCVD	01-PR-4513	42/2	$Al_{0.50}Ga_{0.50}As$	5000 Å	Zn	p,1.0E17
Epitronics/MOCVD	02-PR-6573	145/2	$Al_{0.50}Ga_{0.50}As$	5000 Å	und	p, < 5E16
Epitronics/MOCVD	02-PR-6573	86/3	$Al_{0.50}Ga_{0.50}As$	5000 Å	und	p, < 5E16
Epitronics/MOCVD	02-PR-6569	88/2	GaAs epilayer	0.50 μ	und	
Epitronics/MOCVD	02-PR-6569	87/3	GaAs epilayer	0.50 μ	und	
Hitachi/LEC	L4-693	22,37-41,47, 67-71,95,97, 100-102	GaAs substrate	627-636 μ	und	
(WL/ELR)			Silicon		Boron	p
Crysteco / Cz	6462-01-1A		Silicon		Boron	p
Crysteco / Cz	4671-01-1		Silicon		Sb	n

APPENDIX B: Sample Information

Praseodymium Implant Samples

(UES Implants 12/92)

Host Composition,Growth,Vendor,Lot#,Run/Wafer#	Pr,390keV, Dose(cm^{-2})	RTA Temperature (15s) / Sample Identification Code								
		650C	675C	700C	725C	750C	775C	800C	825C	850C
SI-GaAs,LEC,Epitronics/Hitachi,L4-693,#41	None			G04		G03	G00	G01	G02	
SI-GaAs,LEC,Epitronics/Hitachi,L4-693,#41	5E12						G7			
SI-GaAs,LEC,Epitronics/Hitachi,L4-693,#41	1E13			G1		G2	G5	G3	G6	G4
SI-GaAs,LEC,Epitronics/Hitachi,L4-693,#41	5E13						G8			
SI-GaAs,MOCVD,Epitronics,02-PR-6569,87/3	None			GM01		GM02	GM03	GM04		GM05
SI-GaAs,MOCVD,Epitronics,02-PR-6569,87/3	5E12			GM1		GM2	GM3	GM4		GM5
SI-GaAs,MOCVD,Epitronics,02-PR-6569,87/3	1E13			GM6		GM7	GM8	GM9		GM10
SI-GaAs,MOCVD,Epitronics,02-PR-6569,87/3	5E13			GM11		GM12	GM13	GM14		GM15
SI-Al0.14GaAs,MOCVD,Epitronics,02-PR-2332,34/1	5E12 (old)						d1			
SI-Al0.14GaAs,MOCVD,Epitronics,02-PR-2332,34/1	1E13 (old)						d2			
SI-Al0.14GaAs,MOCVD,Epitronics,02-PR-2332,34/1	5E13 (old)						d3			
SI-Al0.15GaAs,MOCVD,Epitronics,03-PR-4139,34/3	None	B01	B04	B02	B05	B03	B06	B07		
SI-Al0.15GaAs,MOCVD,Epitronics,03-PR-4139,34/3	5E12				B14	B8	B9	B10		
SI-Al0.15GaAs,MOCVD,Epitronics,03-PR-4139,34/3	1E13	B1	B4	B2	B5	B3	B6	B7		
SI-Al0.15GaAs,MOCVD,Epitronics,03-PR-4139,34/3	5E13				B15	B11	B12	B13		
n-Al0.15GaAs,MOCVD,Epitronics,03-PR-4129,167/3	None					BN01	BN02	BN03		
n-Al0.15GaAs,MOCVD,Epitronics,03-PR-4129,167/3	5E12					BN1	BN2	BN3		
p-Al0.15GaAs,MOCVD,Epitronics,01-PR-4484,193/3	None					BP01	BP02	BP03		
p-Al0.15GaAs,MOCVD,Epitronics,01-PR-4484,193/3	5E12					BP1	BP2	BP3		
SI-Al0.20GaAs,MOCVD,Epitronics,02-PR-895,83/3	5E12 (old)						e1			
SI-Al0.20GaAs,MOCVD,Epitronics,02-PR-895,83/3	1E13 (old)						e2			
SI-Al0.20GaAs,MOCVD,Epitronics,02-PR-895,83/3	5E13 (old)						e3			
SI-Al0.30GaAs,MOCVD,Epitronics,02-PR-6570,79/2	None	A01	A02	A03	A04	A05		A06		
SI-Al0.30GaAs,MOCVD,Epitronics,02-PR-6570,79/2	5E12				A8					
SI-Al0.30GaAs,MOCVD,Epitronics,02-PR-6570,79/2	1E13	A5	A6	A1	A7	A2		A3		A4
SI-Al0.30GaAs,MOCVD,Epitronics,02-PR-6570,79/2	5E13				A9					
n-Al0.30GaAs,MOCVD,Epitronics,03-PR-4137,30/2	None			AN01	AN02	AN03				
n-Al0.30GaAs,MOCVD,Epitronics,03-PR-4137,30/2	5E13			AN1	AN2	AN3				
p-Al0.30GaAs,MOCVD,Epitronics,01-PR-4490,74/2	None			AP01	AP02	AP03				
p-Al0.30GaAs,MOCVD,Epitronics,01-PR-4490,74/2	5E13			AP1	AP2	AP3				
SI-Al0.50GaAs,MOCVD,Epitronics,02-PR-6573,145/2	None	C01	C04	C02	C05	C03				
SI-Al0.50GaAs,MOCVD,Epitronics,02-PR-6573,145/2	5E12				C6					
SI-Al0.50GaAs,MOCVD,Epitronics,02-PR-6573,145/2	1E13	C1	C4	C2	C5	C3				
SI-Al0.50GaAs,MOCVD,Epitronics,02-PR-6573,145/2	5E13				C7					
n-Al0.50GaAs,MOCVD,Epitronics,03-PR-4124,72/2	None			CN01	CN02	CN03				
n-Al0.50GaAs,MOCVD,Epitronics,03-PR-4124,72/2	5E13			CN1	CN2	CN3				
p-Al0.50GaAs,MOCVD,Epitronics,01-PR-4508,78/2	None			CP01	CP02	CP03				
p-Al0.50GaAs,MOCVD,Epitronics,01-PR-4508,78/2	5E13			CP1	CP2	CP3				
p-Silicon,(WL/ELR)	None					S01		S02		S03
p-Silicon,(WL/ELR)	5E12					S1		S2		S3
p-Silicon,(WL/ELR)	1E13					S5		S6		S7
p-Silicon,(WL/ELR)	5E13					S9		S10		S11

Praseodymium Implant Samples

(UES Implants 2/94)

Host Composition,Growth,Vendor,Lot#,Run/Wafer#	Pr,390keV, Dose(cm^{-2})	RTA Temperature (15s) Sample Identification Code		
		725C	750C	775C
SI-GaAs,LEC,Epitronics/Hitachi,L4-693,#37	1E13			G5a
SI-Al0.15GaAs,MOCVD,Epitronics,03-PR-4145,198/2	1E13			B6a
SI-Al0.30GaAs,MOCVD,Epitronics,02-PR-6570,80/3	1E13	A7a		
SI-Al0.50GaAs,MOCVD,Epitronics,02-PR-6573,86/3	1E13	C5a		
SI-Al0.10GaAs,MOCVD,Epitronics,02-PR-966,23/3	1E13		X10	
SI-Al0.20GaAs,MOCVD,Epitronics,02-PR-895,85/5	1E13		X20	
SI-Al0.25GaAs,MOCVD,Epitronics,02-PR-1038,65/3	1E13		X25	
SI-Al0.30GaAs,MOCVD,Epitronics,02-PR-1034,27/2	1E13		X30	
SI-Al0.35GaAs,MOCVD,Epitronics,02-PR-1039,32/2	1E13		X35	
SI-Al0.40GaAs,MOCVD,Epitronics,02-PR-1037,39/5	1E13		X40	
p-GaAs,MOCVD,Epitronics,3B-PR-840,23/2	None			GMP0
p-GaAs,MOCVD,Epitronics,3B-PR-840,23/2	1E13			GMP1
n-GaAs,MOCVD,Epitronics,02-PR-3727,10/2	None			GMN0
n-GaAs,MOCVD,Epitronics,02-PR-3727,10/2	1E13			GMN1

Host Composition,Growth,Vendor,Lot#,Run/Wafer#	Pr,390keV, Dose(cm^{-2})	RTA Temperature (15s) Sample Identification Code						
		450C	500C	550C	600C	650C	700C	750C
n-Silicon (Sb-doped),Cz,Crysteco,4671-01-1	None	SN01	SN02	SN03	SN04	SN05	SN06	SN07
n-Silicon (Sb-doped),Cz,Crysteco,4671-01-1	1E13	SN1	SN2	SN3	SN4	SN5	SN6	SN7
p-Silicon (B-doped),Cz,Crysteco,6462-01-1A	None	SP01	SP02	SP03	SP04	SP05	SP06	SP07
p-Silicon (B-doped),Cz,Crysteco,6462-01-1A	1E13	SP1	SP2	SP3	SP4	SP5	SP6	SP7

Pr/Er Dual-dope Implant Samples

(UES Implants 12/92 & 11/93)

Host Composition,Growth,Vendor,Lot#,Run/Wafer#	(UES 12/92) Pr,390keV, Dose(cm^{-2})	(UES,11/93) Er,1MeV, Dose(cm^{-2})	RTA Temperature (15s) Sample Identification Code			
			700C	750C	800C	850C
SI-GaAs,LEC,Epitronics/Hitachi,L4-693,#41	None	1E13	GE1	GE2	GE3	GE4
SI-GaAs,LEC,Epitronics/Hitachi,L4-693,#41	None	5E13	GE5	GE6	GE7	GE8
SI-GaAs,LEC,Epitronics/Hitachi,L4-693,#41	1E13	1E13	GD1	GD2	GD3	GD4
SI-GaAs,LEC,Epitronics/Hitachi,L4-693,#41	1E13	5E13	GD5	GD6	GD7	GD8
SI-Al0.15GaAs,MOCVD,Epitronics,03-PR-4139,34/3	None	1E13	BE1	BE2	BE3	BE4
SI-Al0.15GaAs,MOCVD,Epitronics,03-PR-4139,34/3	None	5E13	BE5	BE6	BE7	BE8
SI-Al0.15GaAs,MOCVD,Epitronics,03-PR-4139,34/3	1E13	1E13	BD1	BD2	BD3	BD4
SI-Al0.15GaAs,MOCVD,Epitronics,03-PR-4139,34/3	5E13	5E13	BD5	BD6	BD7	BD8
SI-Al0.30GaAs,MOCVD,Epitronics,02-PR-6570,79/2	None	1E13	AE1	AE2	AE3	AE4
SI-Al0.30GaAs,MOCVD,Epitronics,02-PR-6570,79/2	None	5E13	AE5	AE6	AE7	AE8
SI-Al0.30GaAs,MOCVD,Epitronics,02-PR-6570,79/2	1E13	1E13	AD1	AD2	AD3	AD4
SI-Al0.30GaAs,MOCVD,Epitronics,02-PR-6570,79/2	5E13	5E13	AD5	AD6	AD7	AD8
SI-Al0.50GaAs,MOCVD,Epitronics,02-PR-6573,145/2	None	1E13	CE1	CE2	CE3	CE4
SI-Al0.50GaAs,MOCVD,Epitronics,02-PR-6573,145/2	None	5E13	CE5	CE6	CE7	CE8
SI-Al0.50GaAs,MOCVD,Epitronics,02-PR-6573,145/2	1E13	1E13	CD1	CD2	CD3	CD4
SI-Al0.50GaAs,MOCVD,Epitronics,02-PR-6573,145/2	5E13	5E13	CD5	CD6	CD7	CD8

Pr Codoped Implant Samples

(UES Implants 2/94)

Host Composition,Growth,Vendor,Lot#,Run/Wafer#	Pr,390keV, Dose(cm^{-2})	Codope,Energy,Dose (species,keV,cm^{-2})	RTA Temperature (15s) Sample Identification Code		
			750C	775C	800C
SI-GaAs,MOCVD,Epitronics,02-PR-6569,88/2	1E13	none			GP0
SI-GaAs,MOCVD,Epitronics,02-PR-6569,88/2	none	B,35,1E14			G0B1
SI-GaAs,MOCVD,Epitronics,02-PR-6569,88/2	1E13	B,35,1E14			GPB1
SI-GaAs,MOCVD,Epitronics,02-PR-6569,88/2	none	B,35,1E15			G0B2
SI-GaAs,MOCVD,Epitronics,02-PR-6569,88/2	1E13	B,35,1E15			GPB2
SI-GaAs,MOCVD,Epitronics,02-PR-6569,88/2	none	C,46,1E14			G0C1
SI-GaAs,MOCVD,Epitronics,02-PR-6569,88/2	1E13	C,46,1E14			GPC1
SI-GaAs,MOCVD,Epitronics,02-PR-6569,88/2	none	C,46,1E15			G0C2
SI-GaAs,MOCVD,Epitronics,02-PR-6569,88/2	1E13	C,46,1E15			GPC2
SI-GaAs,MOCVD,Epitronics,02-PR-6569,88/2	none	N,54,1E14			G0N1
SI-GaAs,MOCVD,Epitronics,02-PR-6569,88/2	1E13	N,54,1E14			GPN1
SI-GaAs,MOCVD,Epitronics,02-PR-6569,88/2	none	N,54,1E15			G0N2
SI-GaAs,MOCVD,Epitronics,02-PR-6569,88/2	1E13	N,54,1E15			GPN2
SI-GaAs,MOCVD,Epitronics,02-PR-6569,88/2	none	O,60,1E14			G0O1
SI-GaAs,MOCVD,Epitronics,02-PR-6569,88/2	1E13	O,60,1E14			GPO1
SI-GaAs,MOCVD,Epitronics,02-PR-6569,88/2	none	O,60,1E15			G0O2
SI-GaAs,MOCVD,Epitronics,02-PR-6569,88/2	1E13	O,60,1E15			GPO2
SI-GaAs,MOCVD,Epitronics,02-PR-6569,88/2	none	F,65,1E14			G0F1
SI-GaAs,MOCVD,Epitronics,02-PR-6569,88/2	1E13	F,65,1E14			GPF1
SI-GaAs,MOCVD,Epitronics,02-PR-6569,88/2	none	F,65,1E15			G0F2
SI-GaAs,MOCVD,Epitronics,02-PR-6569,88/2	1E13	F,65,1E15			GPF2
SI-Al0.14GaAs,MOCVD,Epitronics,02-PR-2332,33/2	1E13	none		JP0	
SI-Al0.14GaAs,MOCVD,Epitronics,02-PR-2332,32/2	none	B,35,1E14		J0B1	
SI-Al0.14GaAs,MOCVD,Epitronics,02-PR-2332,32/2	1E13	B,35,1E14		JPB1	
SI-Al0.14GaAs,MOCVD,Epitronics,02-PR-2332,32/2	none	B,35,1E15		J0B2	
SI-Al0.14GaAs,MOCVD,Epitronics,02-PR-2332,32/2	1E13	B,35,1E15		JPB2	
SI-Al0.14GaAs,MOCVD,Epitronics,02-PR-2332,34/1	none	C,46,1E14		J0C1	
SI-Al0.14GaAs,MOCVD,Epitronics,02-PR-2332,34/1	1E13	C,46,1E14		JPC1	
SI-Al0.14GaAs,MOCVD,Epitronics,02-PR-2332,34/1	none	C,46,1E15		J0C2	
SI-Al0.14GaAs,MOCVD,Epitronics,02-PR-2332,34/1	1E13	C,46,1E15		JPC2	
SI-Al0.14GaAs,MOCVD,Epitronics,02-PR-2332,33/2	none	N,54,1E14		J0N1	
SI-Al0.14GaAs,MOCVD,Epitronics,02-PR-2332,33/2	1E13	N,54,1E14		JPN1	
SI-Al0.14GaAs,MOCVD,Epitronics,02-PR-2332,33/2	none	N,54,1E15		J0N2	
SI-Al0.14GaAs,MOCVD,Epitronics,02-PR-2332,33/2	1E13	N,54,1E15		JPN2	
SI-Al0.14GaAs,MOCVD,Epitronics,02-PR-2332,33/2	none	O,60,1E14		J0O1	
SI-Al0.14GaAs,MOCVD,Epitronics,02-PR-2332,33/2	1E13	O,60,1E14		JPO1	
SI-Al0.14GaAs,MOCVD,Epitronics,02-PR-2332,33/2	none	O,60,1E15		J0O2	
SI-Al0.14GaAs,MOCVD,Epitronics,02-PR-2332,33/2	1E13	O,60,1E15		JPO2	
SI-Al0.14GaAs,MOCVD,Epitronics,02-PR-2332,33/2	none	F,65,1E14		J0F1	
SI-Al0.14GaAs,MOCVD,Epitronics,02-PR-2332,33/2	1E13	F,65,1E14		JPF1	
SI-Al0.14GaAs,MOCVD,Epitronics,02-PR-2332,33/2	none	F,65,1E15		J0F2	
SI-Al0.14GaAs,MOCVD,Epitronics,02-PR-2332,33/2	1E13	F,65,1E15		JPF2	

Pr Codoped Implant Samples (cont.)

(UES Implants 2/94)

Host Composition,Growth,Vendor,Lot#,Run/Wafer#	Pr,390keV, Dose(cm^{-2})	Codope,Energy,Dose (species,keV,cm^{-2})	RTA Temperature (15s) Sample Identification Code		
			750C	775C	800C
SI-Al0.25GaAs,MOCVD,Epitronics,02-PR-1038,67/5	1E13	none	KP0		
SI-Al0.25GaAs,MOCVD,Epitronics,02-PR-1038,65/3	none	B,35,1E14	K0B1		
SI-Al0.25GaAs,MOCVD,Epitronics,02-PR-1038,65/3	1E13	B,35,1E14	KPB1		
SI-Al0.25GaAs,MOCVD,Epitronics,02-PR-1038,65/3	none	B,35,1E15	K0B2		
SI-Al0.25GaAs,MOCVD,Epitronics,02-PR-1038,65/3	1E13	B,35,1E15	KPB2		
SI-Al0.25GaAs,MOCVD,Epitronics,02-PR-1038,65/3	none	C,46,1E14	K0C1		
SI-Al0.25GaAs,MOCVD,Epitronics,02-PR-1038,65/3	1E13	C,46,1E14	KPC1		
SI-Al0.25GaAs,MOCVD,Epitronics,02-PR-1038,65/3	none	C,46,1E15	K0C2		
SI-Al0.25GaAs,MOCVD,Epitronics,02-PR-1038,65/3	1E13	C,46,1E15	KPC2		
SI-Al0.25GaAs,MOCVD,Epitronics,02-PR-1038,67/5	none	N,54,1E14	K0N1		
SI-Al0.25GaAs,MOCVD,Epitronics,02-PR-1038,67/5	1E13	N,54,1E14	KPN1		
SI-Al0.25GaAs,MOCVD,Epitronics,02-PR-1038,67/5	none	N,54,1E15	K0N2		
SI-Al0.25GaAs,MOCVD,Epitronics,02-PR-1038,67/5	1E13	N,54,1E15	KPN2		
SI-Al0.25GaAs,MOCVD,Epitronics,02-PR-1038,67/5	none	O,60,1E14	K0O1		
SI-Al0.25GaAs,MOCVD,Epitronics,02-PR-1038,67/5	1E13	O,60,1E14	KPO1		
SI-Al0.25GaAs,MOCVD,Epitronics,02-PR-1038,67/5	none	O,60,1E15	K0O2		
SI-Al0.25GaAs,MOCVD,Epitronics,02-PR-1038,67/5	1E13	O,60,1E15	KPO2		
SI-Al0.25GaAs,MOCVD,Epitronics,02-PR-1038,67/5	none	F,65,1E14	K0F1		
SI-Al0.25GaAs,MOCVD,Epitronics,02-PR-1038,67/5	1E13	F,65,1E14	KPF1		
SI-Al0.25GaAs,MOCVD,Epitronics,02-PR-1038,67/5	none	F,65,1E15	K0F2		
SI-Al0.25GaAs,MOCVD,Epitronics,02-PR-1038,67/5	1E13	F,65,1E15	KPF2		
SI-Al0.15GaAs,MOCVD,Epitronics,03-PR-4145,198/2	none	O,60,1E14		B0O1	
SI-Al0.15GaAs,MOCVD,Epitronics,03-PR-4145,198/2	1E13	O,60,1E14		BPO1	
SI-Al0.15GaAs,MOCVD,Epitronics,03-PR-4145,198/2	none	O,60,1E15		B0O2	
SI-Al0.15GaAs,MOCVD,Epitronics,03-PR-4145,198/2	1E13	O,60,1E15		BPO2	

BIBLIOGRAPHY

Adachi, Sadao. "GaAs, AlAs, and $Al_xGa_{1-x}As$: Material Parameters for Use in Research and Device Applications," Journal of Applied Physics **58**(3): R1-R29 (1 August 1985).

Alferov, Zh. I., V. I. Amosov, D. Z. Garbuzov, Yu. V. Zhilyaev, S. G. Konnikov, P. S. Kop'ev, and V. G. Trofim. "Investigation of the Dependence of Luminescence Emitted by n- and p-type GaP_xAs_{1-x} and $Al_xGa_{1-x}As$ Solid Solutions on their Composition," Soviet Physics-Semiconductors **6**(10): 1620-1625 (April 1973).

Allen, J. W. "Isoelectronic Impurities in Semiconductors: A Survey of Binding Mechanisms," Journal of Physics C: Solid State Physics **4**: 1936-1944 (1971).

Arfken, George. *Mathematical Methods for Physicists, 3ed.* San Diego: Academic Press, 1985.

Aspnes, D. E. and A. A. Studna. "Dielectric Functions and Optical Parameters of Si, Ge, GaP, GaAs, GaSb, InP, InAs, and InSb from 1.5 to 6.0 eV," Physical Review B **27**(2): 985-1009 (15 January 1983).

Aspnes, D. E., S. M. Kelso, R. A. Logan, R. Bhat. "Optical Properties of $Al_xGa_{1-x}As$," Journal of Applied Physics **60**(2): 754-767 (15 July 1986).

Bantien, F., E. Bauser, and J. Weber. "Incorporation of Erbium in GaAs by Liquid-phase Epitaxy," Journal of Applied Physics **61**(8): 2803-2806 (15 April 1987).

Benton, J. L. *et al.* "The Electrical and Defect Properties of Erbium-implanted Silicon," Journal of Applied Physics **70**(5): 2667-2671 (1 September 1991).

Benyattou, T., D. Seghier, G. Guillot, R. Moncorge, P. Galtier, and M. N. Charasse. "Optical Studies of Erbium Excited States in $Ga_{0.55}Al_{0.45}As$," Applied Physics Letters **60**(3): 350-352 (20 January 1992).

Benyattou, T. D. Seghier, G. Guillot, R. Moncorge, P. Galtier, and M. N. Charasse. "Time-resolved Photoluminescence Spectroscopy from Erbium-doped $Ga_{0.55}Al_{0.45}As$," Applied Physics Letters **58**(19): 2132-2134 (13 May 1991).

Bimberg, D., M. Sondergeld, and E. Grobe. "Thermal Dissociation of Excitons Bounds to Neutral Acceptors in High Purity GaAs," Physical Review B **4**(10): 3451-3455 (15 November 1971).

Boer, Karl W. *Survey of Semiconductor Physics Volume II: Barriers, Junctions, Surfaces, and Devices*. New York: Van Nostrand Reinhold, 1992.

Boer, Karl W. *Survey of Semiconductor Physics: Electrons and Other Particles in Bulk Semiconductors*. New York: Van Nostrand Reinhold, 1990.

Brügel, Werner. *An Introduction to Infrared Spectroscopy*. New York: Wiley Inc, 1962.

Casey, Jr., H. C. and M. B. Panish. *Heterostructure Lasers*. New York: Academic Press, 1978.

Coffa, S., F. Priolo, G. Franzò, V. Bellani, A. Carnera, and C. Spinella. "Optical Activation and Excitation Mechanisms of Er Implanted in Si," Physical Review B **48**(16):11782-11788 (15 October 1993-II).

Colon, Captain J. E. *Luminescence Study of Ion-Implanted and MBE-Grown Er-Doped GaAs and $Al_xGa_{1-x}As$*. PhD dissertation. School of Engineering, Air Force Institute of Technology (AU), Wright-Patterson AFB, OH, December 1992a.

Colon, J. E., D. W. Elsaesser, Y. K. Yeo, R. L. Hengehold, and G. S. Pomrenke. "Excitation Mechanism of the Erbium 4f Emissions in GaAs," *Materials Science Forum 83-87*: 671-676 (1992b).

Colon, Jose E., David W. Elsaesser, Yung Kee Yeo, Robert L. Hengehold, and Gernot S. Pomrenke. "Luminescence Study of the Intra-4f Emissions from GaAs:(Er+O) and $Al_xGa_{1-x}As$:(Er+O)," Mat. Res. Soc. Symp. Proc. Vol. **301**: 169-174 (1993a).

Colon, J. E., D. W. Elsaesser, Y. K. Yeo, R. L. Hengehold, and G. S. Pomrenke. "Enhancement of the Er^{3+} Emissions from AlGaAs:Er Codoped with Oxygen," Applied Physics Letters **63**(2): 216-218 (12 July 1993b).

DiBartolo, Baldassare. *Optical Interactions in Solids*. New York: Wiley & Sons, 1968.

Dieke, Gerhard Heinrich. *Spectra and Energy Levels of Rare Earth Ions in Crystals*. New York: Interscience Publishers, 1968.

Dmitriev, A. G., L. F. Zakharenkov, V. A. Kasatkin, V. F. Masterov, and B. E. Samorukov. "Electroluminescence of Ytterbium-doped Indium Phosphide," Soviet Physics-Semiconductors **17**(10): 1201 (October 1983).

Ennen, H., J. Wagner, H. D. Muller, and R. S. Smith. "Photoluminescence Excitation Measurements on GaAs:Er Grown by Molecular-beam Epitaxy," Journal of Applied Physics **61**(10): 4877-4879 (15 May 1987).

Ennen, H., G. Pomrenke, A. Axmann, K. Eisele, W. Haydl, and J. Schneider. "1.54-μm Electroluminescence of Erbium-doped Silicon Grown by Molecular Beam Epitaxy," Applied Physics Letters **46**(4): 381-383 (15 February 1985).

Ennen, H., J. Schneider, G. Pomrenke, and A. Axmann. "1.54-micron Luminescence of Erbium-implanted III-V Semiconductors and Silicon," Applied Physics Letters **43**: 943-945 (15 November 1983).

Erickson, Lynden E., Usman Akano, Ian Mitchel, Nelson Rowell, and Aiguo Wang. "Photoluminescence Spectra of Trivalent Praseodymium Implanted in Semi-insulating GaAs," Journal of Applied Physics **74**(4): 2347-2353 (15 August 1993).

Favennec, P. N., H. L'Haridon, D. Moutonnet, M. Salvi, and M. Gauneau. "Optical Activation of Er^{3+} Implanted in Silicon by Oxygen Impurities," Japanese Journal of Applied Physics **29**(4): L524-L526 (April 1990).

Favennec, P. N., H. L'Haridon, D. Moutonnet, M. Salvi, M. Gauneau, and A. C. Papadopoulo. "Implantation of Erbium Elements in GaAs and Related Compounds," *Inst. Phys Conf. Ser. No. 106: Chapter 5, Paper presented at Int. Symp. GaAs and Related Compounds, Karuizawa, Japan, 1989*: 330-338.

Gippius, A. A., V. S. Vavilov, V. V. Ushakov, V. M. Konnov, N. A. Rzakuliev, S. A. Kazarian, A. A. Shirokove, and V. N. Jakimkin. "Defects and Optically Active Transition and Rare Earth Elements in III-V and II-VI Compounds and Diamond," *Materials Science Forum Volumes 10-12*: 1195-1200 (1986).

Haydl, W. H., H. D. Müller, H. Ennen, W. Körber, and K. W. Benz. "Ytterbium-doped InP Light-emitting Diode at 1.0 μm," Applied Physics Letters **46**(9): 870-872 (1 May 1985).

Hecht, Eugene, and Alfred Zajac. *Optics*. Reading, Mass.:Addison-Wesley, 1979.

Isshiki, H, H. Kobayashi, S. Yugo, T. Kimura, and T. Ikoma. "1.54 μm Electroluminescence by Electron Impact Excitation of Er Atoms Doped in InP," Japanese Journal of Applied Physics **30**(2B): L225-L227 (February 1991).

Kasatkin, V. A. "Instability of Low-Symmetry Yb^{3+} and Pr^{3+} Luminescence Centers in Gallium Phosphide," Soviet Physics-Semiconductors 19(10): 1174-1175 (October 1985).

Kasatkin, V. A., F. P. Kesamanly, and B. E. Samorukov. "Photoluminescence of Heat-treated Gallium Phosphide Doped with Praseodymium and Ytterbium," Soviet Physics-Semiconductors 15(3): 352 (March 1981).

Klein, P. B., F. G. Moore, and H. B. Dietrich. "Spectroscopic Investigation of the Er Site in GaAs:Er," *Materials Science Forum Vol. 83-87*: 665-670 (1992).

Klein, P. B., F. G. Moore, and H. B. Dietrich. "Photoluminescence and Magnetic Resonance Studies of Er^{3+} in MeV Implanted GaAs," Applied Physics Letters 58: 502 (1991).

Klein, P. B., F. G. Moore, and H. B. Dietrich. "1.54μm Electroluminescence in MeV Ion Implanted Er-doped GaAs," Electronics Letters 26: 1299-1300 (1990).

Klein, P. B., and G. S. Pomrenke. "Photoluminescence Decay of 1.54 μm Er^{3+} Emission in Si and III-V Semiconductors," Electronics Letters 24: 1503-1504 (1988).

Knox, Robert S., and Albert Gold. *Symmetry in the Solid State*. New York: W. A. Benjamin, Inc., 1964.

Korber, W. and A. Hangleiter. "Excitation and Decay Mechanisms of the intra-4f Luminescence of Yb^{3+} in Epitaxial InP:Yb layers," Applied Physics Letters 52: 114-116 (11 January 1988).

Kourkoutas, C. D., J. Novac, M. Kuliffiyova, G. J. Papioannou, P. Kordos, and V. Ioannou-Sougleridis. "Transport Properties of Praseodymium Doped p-Type $In_{0.53}Ga_{0.47}As$ Layers," Solid State Communications 78(6): 543-546 (1991).

Kozanecki, A., M. Chan, C. Jeynes, B. Sealy, and K. Homewood. "Lattice Location of Erbium Implanted into GaAs," Solid State Communications 78(8): 763-766 (1991).

Lai, M. Z. and L. B. Chang. "Characterization of Praseodymium-doped InGaP Epilayer Grown by Liquid Phase Epitaxy," Journal of Applied Physics 72(4): 1312-1315 (15 August 1992).

Lambert, B., A. Le Corre, Y. Toudic, C. Lhomer, G. Grandpierre, and M. Gauneau. "Electrical and Optical Properties of Rare Earth Dopants (Yb, Er) in n-type III-V (InP) Semiconductors," Journal of Physics: Condensed Matter **2**: 479-483 (1990).

Langer, Dietrich W., Yabo Li, Xiao M Fang, and Victoria Coon. "MOCVD Growth and Properties of Erbium Doped GaAs," Mat. Res. Soc. Symp. Proc. Vol. **301**: 15-20 (1993).

Lightowlers, E. C. "Photoluminescence Assessment of MBE Silicon," Semiconductor Science and Technology **5**: 1161-1167 (1990).

Lozykowski, H. J. "Kinetics of Luminescence of Isoelectronic Rare-Earch Ions in III-V Semiconductors," Physcial Review B **48**(24):17758-17769 (15 December 1993).

Masterov, V. F. and L. F. Zakharenkov. "Rare-earth Elements in III-V Semiconductors (Review)," Soviet Physics-Semiconductors **24**(4): 383-396 (April 1990).

McKelvey, J. P. *Solid State and Semiconductor Physics*. Malabar, Fl: Krieger Publishing Co., 1984.

Michel, J., J. L. Benton, R. F. Ferrante, D. C. Jacobson, D. J. Eaglesham, E. A. Fitzgerald, Y.-H. Xie, J. M. Poate, and L. C. Kimerling. "Impurity Enhancement of the 1.54-μm Er^{3+} Luminescence in Silicon," Journal of Applied Physics **70**(5): 2672-2678 (1 September 1991).

Miya, R., Y. Terunuma, T. Hosaka, and T. Miyashita. "Ultimate Low-loss Single-mode Fibre at 1.55μm," Electronics Letters, **15**: 106-108 (15 February 1979).

Muller, H. D., H. Ennen, J. Schneider and A. Axmann. "Photoluminescence of Neodymium-implanted Gallium Phosphide and Gallium Arsenide," Journal of Applied Physics **59**: 2210-2212 (15 March 1986).

Nakagome, H., K. Uwai, and K. Takahei. "Extremely Sharp Erbium-related Intra-4f-shell Photoluminescence of Erbium-doped GaAs Grown by Metalorganic Chemical Vapor Deposition," Applied Physics Letters **53**(18): 1726-1728 (31 October 1988).

Pankove, J. I., ed. *Electroluminescence*. Berlin: Springer-Verlag, 1977.

Pankove, Jacques I. *Optical Processes in Semiconductors*. New York: Dover, 1971.

Pantelides, Sokrates T. "The Electronic Structure of Impurities and other Point Defects in Semiconductors," Reviews of Modern Physics **50**: 797-858 (October 1978).

Pomrenke, G. S., E. Silkowski, J. Colon, D. J. Topp, Y. K. Yeo, and R. L. Hengehold. "Luminescence of Thulium in III-V Semiconductors and Silicon," Journal of Applied Physics **71**(4): 1919-1926 (15 February 1992).

Pomrenke, G. S., R. L. Hengehold, and Yung Kee Yeo. "Lanthanide (Yb, Er, Tm, Pr, Ho) and Actinide (U) Activated Luminescence in III-V Semiconductors," European Journal of Solid State Inorganic Chemistry **28**: 159-162 (1991a).

Pomrenke, G. S., Y. K. Yeo, and R. L. Hengehold. "Near IR Emissions from Er, Tm, and Pr Implanted GaAs and AlGaAs," Mat. Res. Soc. Symp. Proc. Vol. **216**: 415-420 (1991b).

Pomrenke, G. S., R. L. Hengehold, and Y. K. Yeo. "Excitation Mechanism of Rare-Earth Emissions (Yb, Tm, Er, Pr) in GaAs and InP," Gallium Arsenide and Related Compounds 1989, Institute of Physics Conference Series Number **106**: 339-344 (1990).

Pomrenke, Major Gernot S. *Luminescence of Lanthanides and Actinides Implanted into Binary III-V Semiconductors and AlGaAs*. PhD dissertation. School of Engineering, Air Force Institute of Technology (AU), Wright-Patterson AFB, OH, December 1989.

Pomrenke, Gernot S., H. Ennen, and W. Haydl. "Photoluminescence Optimization and Characteristics of the Rare-earth Element Erbium Implanted in GaAs, InP, and GaP," Journal of Applied Physics **59**(2): 601-610 (15 January 1986).

Poole, I, K. E. Singer, and A. R. Peaker. "Growth and Structural Characterization of Molecular Beam Epitaxial Erbium-doped GaAs," Journal of Crystal Growth **121**: 121-131 (1992).

Prather, John L. *Atomic Energy Levels in Crystals*. National Bureau of Standards Monograph 19 (February 24, 1961).

Reisfeld, Renata and Christian K. Jorgensen. *Lasers and Excited States of Rare Earths*. Berlin: Springer-Verlag, 1977.

Roland, A., A. Le Corre, P. N. Favennec, M. Gauneau, B. Lambert, D. Lecrosnier, H. L'Haridon, D. Moutonnet, and C. Rochaix. "Erbium-doped GaAs Light-Emitting Diode at 1.54μm," Electronics Letters **24**: 956-957 (July 1988).

Rzakuliev, N. A., V. M. Konnov, V. N. Yakimkin, V. V. Ushakov, A. A. Gippius, J. Oswald, and J. Pastrnak. "Luminescence of Pr, Nd and Yb Ions Implanted in GaAs and GaP," Czech. Journal of Physics B **38**: 1288-1293 (1988).

Smith, R. S., H. D. Muller, H. Ennen, P. Wennekers, and M. Maier. "Erbium Doping of Molecular Beam Epitaxial GaAs," Applied Physics Letters **50**(1): 49-51 (5 January 1987).

Solomon, J. S., G. S. Pomrenke, R. L. Hengehold, and Y. K. Yeo. "SIMS and Photoluminescence Studies of Rare Earth Implants in InP," *Proceedings of the Seventh International Conference on Secondary Ion Mass Spectroscopy (SIMS VII)*. 571-574. Chichester: John Wiley & Sons, 1989.

Stradling, R. A. and P. C. Klipstein. *Growth and Characterization of Semiconductors*. Bristol: Adam Hilger, 1990.

Sturge, M. D. "Optical Absorption of Gallium Arsenide between 0.6 and 2.75 eV," Physical Review **127**(3): 768-773 (August 1, 1962).

Sze, S. M. *Semiconductor Devices, Physics and Technology*. New York: John Wiley & Sons, 1985.

Taguchi, Akihito, Hiroshi Nakagome, and Kenichiro Takahei. "Optical and Electrical Properties of Ytterbium-doped GaAs grown by Metalorganic Chemical Vapor Deposition," Journal of Applied Physics **58**(7): 3390-3393 (1 October 1990).

Takahei, K. and H. Nakagome. "Room-temperature Observation of Intra-4f-shell Photoluminescence of Nd^{3+} Ions Doped in GaP by Metalorganic Chemical Vapor Deposition," Inst. Phys. Conf. Ser. **106**: 913 (1989).

Takahei, K. and A. Taguchi. "Energy Transfer in Rare-earth-doped III-V Semiconductors," *Materials Science Forum 83-87*: 641-652 (1992).

Taniguchi, M., H. Nakagome, and K. Takahei. "Luminescence Intensity and Lifetime Dependences on Temperature for Nd-doped GaP and GaAs," Applied Physics Letters **58**(25): 2930-2931 (24 June 1991).

Thonke, K., K. Pressel, G. Bohnert, A. Stapor, J. Weber, M. Moser, A. Molassioti, A. Hangleiter, and F. Scholz. "On Excitation and Decay Mechanisms of the Yb^{3+} Luminescence in InP," Semiconductors Science and Technology 5: 1124-1131 (1990).

Tsang, W. T., and R. A. Logan. "Observation of Enhanced Single Longitudinal Mode Operation in 1.5-μm GaInAsP Erbium-doped Semiconductor Injection Lasers," Applied Physics Letters 49(25): 1686-1688 (22 December 1986).

Tsang, W. T., and R. A. Logan. "A New High-power, Narrow-beam Transverse-mode Stabilized Semiconductor Laser at 1.5 μm: the Heteroepitaxial Ridge-overgrown Laser," Applied Physics Letters 45(10): 1025-1027 (15 November 1984).

Ushakov, V. V., A. A. Gippius, V. A. Dravin, and A. V. Spitsyn. "Luminescence of a Rare-earth (Erbium) Impurity in Gallium Arsenide and Phosphide," Soviet Physics-Semiconductors 16(6): 723 (June 1982).

Uwai, K., H. Nakagome, and K. Takahei. "1.54 μm Emission from Er-doped GaAs and InP Grown by Metalorganic Chemical Vapor Deposition," *Extended Abstracts of the 19th Conference on Solid State Devices and Materials, Tokyo, Japan*: 87-90 (1987).

van der Ziel, J. P., M. G. Oberg, and R. A. Logan. "Single Longitudinal Mode Operation of Er-doped 1.5-μm InGaAsP Lasers," Applied Physics Letters 50(19): 1313-1315 (11 May 1987).

Weast, Robert C., ed. *Handbook of Chemistry and Physics 65th Ed.* CRC Press: Cleveland, 1984.

Whitney, Peter S., K, Uwai, H. Nakagome, and K. Takahei. "Erbium-doped GaAs Light-emitting Diodes Emitting Erbium f-shell Luminescence at 1.54μm," Electronics Letters 24(12): 740-741 (June 1988a).

Whitney, Peter S., Kunihikc Uwai, Hiroshi Nakagome, and Ke'ichiro Takahei. "Electrical Properties of Ytterbium-doped InP Grown by Metalorganic Chemical Vapor Deposition," Applied Physics Letters 52(21): 2074-2076 (21 November 1988b).

Wu, M., E. Chen, T. Chin, and Y. Tu. "Erbium Doping in InGaAsP Grown by Liquid-phase Epitaxy," Journal of Applied Physics 71(1): 456-461 (1 January 1992).

Yoshida, A., and T. Asakura. "A Simple Technique for Quickly Measuring the Spot Size of Gaussian Laser Beams," Optics and Laser Technology: 273-274 (December 1976).

Zhao, X., K. Hirakawa, and T. Ikoma. "Diffusion and Photoluminescence of Erbium in GaAs and InP," *Inst. Phys. Conf. Ser. No. 96: Chapter 5, Paper Presented at Int. Symp. GaAs and Related Compounds, Atlanta, Georgia, 1988*: 277-282.

VITA

Major Paul L. Thee was born on 6 October 1960 in Grand Rapids, Michigan. He graduated from Lake Washington High School in Kirkland, Washington, in 1978 and attended the University of Washington from which he received a Bachelor of Science in Physics degree in 1982. Upon graduation, he received a regular commission in the USAF through the ROTC program. As his first assignment, he served as a physicist working on computational models of warheads in the Bombs and Warheads Branch of the Air Force Armament Laboratory at Eglin AFB, Florida, until entering the School of Engineering, Air Force Institute of Technology, in May 1985. He graduated with a Masters Degree in Engineering Physics and was assigned to Headquarters, Air Force Technical Applications Center as NURAD program manager in 1986. He went on to become Resource Manager for the Nuclear Technology Directorate in 1988. In June 1991, he returned to AFIT to continue his education in the doctoral program and was promoted to the rank of major two years below-the-zone.

Permanent Address: 5829-112th PL NE
Kirkland, Washington 98033

REPORT DOCUMENTATION PAGE

Form Approved
OMB No. 0704-0188

1. AGENCY USE ONLY (Leave blank)	2. REPORT DATE	3. REPORT TYPE AND DATES COVERED
	June 1994	Doctoral Dissertation

4. TITLE AND SUBTITLE
The Excitation Mechanism of Praseodymium-doped Semiconductors

5. FUNDING NUMBERS

6. AUTHOR(S)
Paul L. Thee, Major, USAF

7. PERFORMING ORGANIZATION NAME(S) AND ADDRESS(ES)
Air Force Institute of Technology
WPAFB, OH 45433-6583

8. PERFORMING ORGANIZATION REPORT NUMBER
AFIT/DS/ENP/94-01

9. SPONSORING/MONITORING AGENCY NAME(S) AND ADDRESS(ES)
AFOSR/NE (Bldg 410)
Bolling AFB
Washington, D.C. 20332-6448
Attn: LtCol Gernot Pomrenke

10. SPONSORING/MONITORING AGENCY REPORT NUMBER

11. SUPPLEMENTARY NOTES

12a. DISTRIBUTION/AVAILABILITY STATEMENT
APPROVED FOR PUBLIC RELEASE; DISTRIBUTION UNLIMITED

12b. DISTRIBUTION CODE

13. ABSTRACT *(Maximum 200 words)*

This study on praseodymium (Pr) luminescence in $Al_xGa_{1-x}As$ was conducted to enhance the understanding of the excitation mechanism. Pr was implanted at 390 keV with doses from 5×10^{12} to $5\times10^{13}/cm^2$ into $Al_xGa_{1-x}As$ (x=0.0 to 0.50) wafers which were annealed using the rapid thermal annealing (RTA) method. Low temperature photoluminescence (PL) was conducted using an Ar-ion laser and Ge detector. PL emissions of Pr from all hosts include peaks near 1.3 and 1.6 μm which are assigned to the intra-4f transitions of $^1G_4\rightarrow{}^3H_5$ and $^3F_3\rightarrow{}^3H_4$, respectively. The intensity of PL emissions depends strongly on the Al mole fraction. Selective excitation luminescence experiments revealed that the Pr-related PL intensity is quenched when the excitation laser energy is decreased below the host free exciton energy. Temperature dependent PL studies revealed activation energies corresponding to bound exciton dissociation from the Pr ions. Coimplantation of Pr with Er, B, C, N, O, and F all proved to quench the Pr luminescence. An excitation model proposes that Pr luminescence can occur when the Pr forms bound excitons and absorbs the recombination energy.

14. SUBJECT TERMS
Photoluminescence, Rare Earth Elements, Praseodymium, Gallium Arsenide, Aluminum Gallium Arsenide, Selective Excitation Luminescence, Excitation Mechanism

15. NUMBER OF PAGES
169

16. PRICE CODE

17. SECURITY CLASSIFICATION OF REPORT	18. SECURITY CLASSIFICATION OF THIS PAGE	19. SECURITY CLASSIFICATION OF ABSTRACT	20. LIMITATION OF ABSTRACT
Unclassified	Unclassified	Unclassified	UL